Establishing the Effect of Vibration and Postural Constraint Loading on the Progression of Intervertebral Disc Herniation

by

Justin Paul Yates

A thesis

presented to the University of Waterloo

in fulfillment of the

thesis requirement for the degree of

Master of Science

in

Kinesiology

Waterloo, Ontario, Canada, 2009

Authors Declaration

I hereby declare that I am the sole author of this thesis. This is a true copy of the thesis, including any required final revisions, as accepted by my examiners.

I understand that my thesis may be made electronically available to the public.

Justin Yates

Abstract

A strong epidemiological link has been established between the reporting of low back pain, and the development of low back disorders to exposures of vibration in an occupational setting. Specifically, intervertebral disc herniations as a form of low back disorders have been indicated as a possible injury development pathway due to seated occupational vibration exposures. However, very little experimental evidence exists corroborating the strong epidemiological link between intervertebral disc herniations and vibration exposures using basic scientific approaches. The purpose of the current investigation was to provide some basic experimental evidence of the epidemiological link between intervertebral disc damage (herniation) and exposure to vibration.

Partial intervertebral disc herniations were created in a population of in-vitro porcine functional spinal units using a well established herniation protocol of repetitive flexion/extension motions under modest compressive forces. After herniation initiation, functional spinal units were exposed to 8 different vibration and postural constraint loading protocols consisting of two postural conditions (full flexion and neutral) and 4 vibration loading conditions (whole-body vibration, shock loading, static compressive loads, and whole-body vibration in addition to shock loading) to assess the effects of vibration and posture on functional spinal unit damage progression. There were three main outcome variables that were assessed and used to quantify damage progression; average stiffness changes, herniation distance progression (distance of tracking changes), and specimen height changes, while cumulative loading factors were considered. Additionally the concordances between two types of contrast enhanced medical imaging (Computed Tomography and Discograms) were qualified to a dissection 'gold standard', and an attempt was made to classify disc damage progression via three categorical variables.

Concordance to a dissection ‘gold standard’ was higher for the Computed Tomography medical imaging approach than for the Discograms. The categorical criteria used to qualify disc damage progression were insufficiently sensitive to detect damage progressions illustrated through dissection and medical imaging techniques. The partial herniation loading protocol was quantified to be more damaging overall to the functional spinal units compared to the vibration and postural constraint loading protocols. However, the combination of load (vibration) and posture (postural constraint) did provided sufficient mechanical insult to the functional spinal units to progress damage to the intervertebral discs beyond the level illustrated via the partial herniation loading protocol. Vibration loading exposures alone were found to alter specimen height changes and distance of tracking changes, however posture alone had no significant effects on these variables. Neither posture nor vibration loading conditions had any meaningful significant effects on average stiffness changes.

It appeared that the combination of load (vibration) and posture (postural constraint) loading protocols provided sufficient mechanical insult to intervertebral discs to exacerbate pre-existing disc herniations. However, load (vibration) loading alone appeared to be more influential in the exacerbation of disc damage than did posture (postural constraints) alone. The current investigation was successful in establishing some basic scientific evidence to further the vibration to disc herniation epidemiological link.

Acknowledgments

I would like to thank my advisor Dr. Stuart McGill for his patience, insight and continual guidance in this research, and his professional and personnel guidance that will undoubtedly serve me well in the future. Thank you to my committee members Dr. Jack Callaghan and Dr. Lora Giangregorio whose expertise were instrumental in the completion of this research. Thank you to Dr. Stephan Milosavljevic for providing the detailed vibration exposures sustained by the occupation farmers and for his advice during the development of this investigation. I would also like to thank my parents, Doug and Donna, and friends for their constant love and support in everything that I do. Special thanks must go to Annali Leeson, who withstood my day to day grumbling over the last two years and without whose support I never would have made it. Last but not least, I wish to thank CRE-MSD for funding this research and NSERC for laboratory funding and equipment maintenance.

Table of Contents

List of Acronyms

LBD – low back disorder
LBP – low back pain
NP – nucleus pulposus
AF – annulus fibrosus
WBV – whole body vibration
IVD – intervertebral disc
FSU – functional spinal unit

List of Tables and Table Captions

List of Illustrations and Illustration Captions

Chapter 1: Introduction

1.1.The Scope of the Problem:

The term low back disorder (LBD) has become an overused generic term to classify many disorders of the lumbar spine. LBDs are a non-specific term given to a wide range of injuries and pathologies including sciatic pain, transient low back pain (LBP), disc protrusions and herniations (Bovenzi et al. 1994), damage to the boney vertebral elements of the spine, endplate fractures, and annular fibre damage (Wilkstrom et al. 1994), as well as stiffness, pain, or aching sensations in the low back (Bovenzi and Stacchini 2002). Countless investigators have illuminated factors linked to LBP. Factors of note are prolonged sitting, driving, and postural constraints (Kittusamy and Buchholz 2004; Waters et al. 2007), exposure to mechanical shock and whole-body vibration (WBV) (Videman et al. 1990; Bovenzi et al. 1994; Troup 1978), heavy lifting and repetitive motions (Deyo et al. 1990; Wilkstrom et al. 1994) and non neutral spinal postures in addition to twisting motions (Deyo et al. 1990).

Vibration exposures as the result of occupational activities are wide spread. Bovenzi and Hulshof (1999) estimated that 4 -7 % of all employees in Canada and some European countries are exposed to potentially harmful WBV. Several investigations have illustrated common occupations in which WBV magnitudes and durations which are likely to be detrimental to health (specifically spinal health) commonly occur including; tractor operation and farming activities (Waters at al. 2007; Mansfield 2005; Sandover 1998; Milosavljevic et al. 2008a), operators and passengers of commercial transit equipment (Mansfield 2005; Dupuis and Zerlett 1987;), and construction workers (Brinckmann et al. 1998; Kittusamy and Buchholz 2004, Dupuis and Zerlett 1987). The exact mechanism by which WBV leads to mechanical damage in the lumbar spine is yet to be fully understood (Mansfield 2005). Mechanical shock loading is likely to occur in many situations in conjunction with WBV. Shock loads have been identified in the operation of occupational farming equipment and tractors (Waters et al. 2007, Milosavljevic et al. 2008b), in the operation of road vehicles (Mansfield, 2005, Dupuis et al. 1991) and military equipment (Dupuis and Zerlett 1987) over rough terrain. Mechanical shock loading and the associated impacts on the human musculoskeletal system (in particular the lumbar spine) have been insufficiently investigated as noted by Dupuis et al. (1991) and it was stated by Waters et al. (2007) that an urgent need exists to assess the effects of mechanical shock loading on spinal tissues. Troup (1978) indicated that mechanical shock or impact, particularity after long term exposures to WBV, postural stress, and muscular effort (factors common to many industrial and agricultural tasks) holds the potential to cause significant injury to spinal structures.

Numerous epidemiological investigations have linked vibration exposure to injury in the lumbar spine. Vibration exposure has been linked to LBP (Bovenzi et al. 1994, 2002; Mayton et al. 2007; Dupuis and Zerlett 1987), intervertebral disc (IVD) herniations (Kelsey and Hardy 1975; Bovenzi and Hulshof 1999), ruptures of the annulus fibrosus (Videman et al. 1990), early degeneration of the lumbar spine (Bovenzi and Hulshof 1999; Kittusamy and Buchholz 2004), and sciatic pain and chronic episodes of LBP (Bovenzi et al 1994). Although there is a strong epidemiological link between vibration exposures and lumbar spine injury (including IVD herniations), basic scientific evidence to corroborate this link is lacking.

IVD herniation is a specific condition that can lead to LBP as noted by Kelsey and Hardy (1975); Bovenzi et al. (1994) and Mayton et al. (2007). LBP can occur in relation to the factors thought to lead to general LBP disorder including; prolonged sitting, driving, and postural constraints (Kittusamy and Buchholz 2004; Waters et al. 2007), exposure to mechanical shock and whole-body vibration (Videman et al. 1990; Bovenzi et al. 1994; Troup 1978), heavy lifting and repetitive motions (Deyo et al. 1990; Wilkstrom et al. 1994) and non neutral spinal postures in addition to twisting motions (Deyo et al. 1990). Marras (2000) estimated that 11 – 13 million people in the United States of America experience an episode of LBP in a given year, while workers compensation claims were estimated to be as high a 100 billion annually. LBDs account for 16-19% of all workers compensation claims, but 33- 41% of the total cost for all compensatable claims. (Webster and Snook 1994; Spengler et al. 1986). It has been estimated by Deyo et al. (1990) that 2 billion of the 13 billion dollars spent in the United States as a result of LBP was a result of herniated discs and that recurrent incidence of disc herniations were extremely high, resulting in large recurring costs. It is evident that LBDs represent a disproportionately high percentage of total costs of worker compensation claims. The costs of LBP (including IVD herniations) are staggering, and further investigations into causal factors of these injuries and possible treatment interventions are warranted.

Given the large cost of treating IVD herniations, and the epidemiological link between vibration exposures and disc herniations we were motivated to investigate the effects of vibration and postural constraint loading on the IVD herniation process. The goal of this investigation was to provide basic scientific evidence to support the epidemiological link between vibration exposures and disc damage, with the hope of identifying specific risk factors for intervention to reduce IVD herniations in occupations exposed to vibration.

1.2.Purpose:

The purpose of this investigation was to provide basic scientific evidence to corroborate the large body of epidemiological literature that has linked vibration exposure, and postural factors to IVD herniations. To accomplish this purpose, a population of porcine functional spinal units (FSUs) was subjected to a well established herniation protocol (Callaghan and McGill

2001; Drake et al. 2005; Aultman et al. 2005; Drake and Callaghan 2009; Tampier et al. 2007) to induce partial IVD herniations. Following partial herniation development, vibration and postural loading protocols were implemented to simulate occupational exposure to vibration. Two postures (full flexion and neutral) and 4 vibration loading conditions (WBV, shock, static, and WBV in combination with shock) were tested to investigate which postural and vibration factors would exacerbate existing IVD damage. IVD damage exacerbation was quantified by three main outcome variables; average stiffness changes, herniation progression changes (distance of tracking changes), and specimen height loss changes. Concordance between the medical imaging types of Computed Tomography (CT) and discograms were qualified to a 'gold standard' dissection technique, and categorical variables were used to qualitatively describe the disc damage caused by the vibration and postural constraints.

1.3. Specific Investigation Hypothesises:

1. Vibration exposures will exacerbate existing IVD tracking changes produced by a partial herniation protocol; the combination of WBV and shock will lead to the largest IVD tracking changes, followed by less IVD tracking changes due to WBV and then minimal IVD tracking changes due to shock alone. Static loading is not expected to change the level IVD tracking changes.

2. Vibration exposures will influence average stiffness changes during loading. Increases in average stiffness will rank as follows in descending order; WBV and shock, WBV, shock, static loading.

3. Vibration exposures will influence specimen height changes during loading. Specimen height decreases will rank as follows in descending order; WBV and shock, WBV, shock, static loading.

4. Posture will influence the parameters of IVD tracking changes (increase), average stiffness changes (increase) and specimen height changes (increase) within the vibration exposures; fully flexed postures are hypothesized to lead to larger changes in these parameters than neutral postures.

5. The partial herniation loading protocol will be more damaging to the IVD than then vibration and postural constraint loading protocols and will lead to larger relative increases in average stiffness, IVD tracking changes, and specimen height lost from established baselines

6. Concordance will be high between medical imaging and a 'gold standard' dissection technique. However, Computed Tomography image concordance will be higher than discogram image concordance.

7. IVD damage level classification will increase due to the vibration and postural constraint loading protocols.

Chapter 2: Literature Review

2.1. General Anatomy of the Spine

The human spine consists of 24 boney vertebrae not including the fused sacrum and coccyx segments at the most caudal aspects of the vertebral column. In general, the vertebrae of the spine become larger in size as they progress from the cranial cervical spine to the mid level thoracic vertebrae and finally to the caudal lumbar vertebrae. There are 7 cervical vertebrae (C1-C7), 12 thoracic vertebrae (T1-T12), and 5 lumbar vertebrae (L1-L5) in the normal human spine; these vertebrae act as a site for both muscular and ligamentous attachments, protect the spinal cord, and act to restrict movements and support the body's weight (Moore and Dalley 1999). With the exception of the fused caudal vertebrae (sacrum and coccyx) and the atlas and axis (C1-C2) of the cervical spine, all vertebrae are composed of the same basic structures (although the size and shape of these structures varies at the different levels of the spine) including the spinous process, 2 transverse processes, 4 articular processes (2 superior and 2 inferior that form the facet joints), the vertebral body (consisting of the epiphyseal ring and the vertebral body), the vertebral arch (consisting of the lamina and pedicle), and the vertebral foramen (Moore and Dalley 1999). The locations of these structures and their general functions are illustrated in Figure 1.

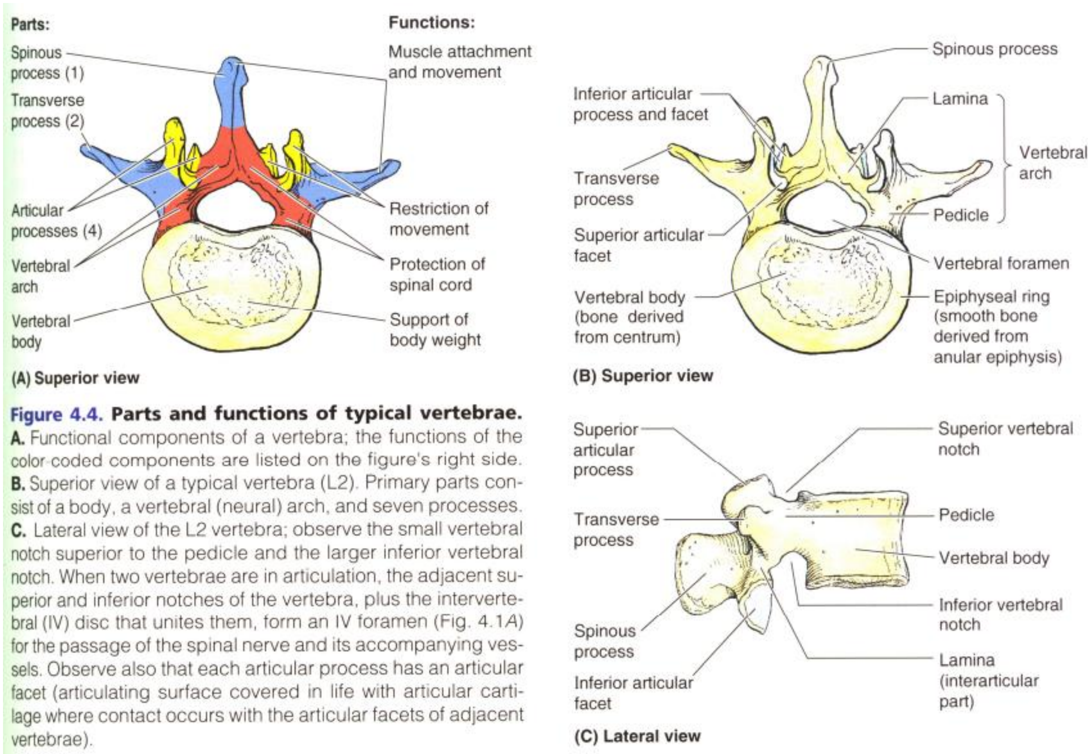

Figure 1: Illustration of the gross boney anatomy of the general human vertebrae. Part A and Part B indicate the location in addition to the major function of the different parts of the vertebral boney structure from the superior orientation. Part C indicates the location of the various vertebral structures in the sagital orientation. Image obtained from Moore and Dalley (1999) Clinically Orientated Anatomy 4th edition, Figure 4.4 on pg 437.

2.2. Lumbar Spine Anatomy

Specifically, the vertebra of the lumbar spine increase in size from the cranial (L1) to the caudal (L5) vertebrae as illustrated in Figure 2. The lumbar spine differs from the cervical and thoracic spines in several characteristics; of note are larger vertebral bodies, vertebral foramen that are larger than those of the thoracic vertebrae but smaller than those of the cervical vertebrae, longer more slender transverse processes, and the existence of shorter spinous processes that are thicker and more broad (Moore and Dalley 1999).

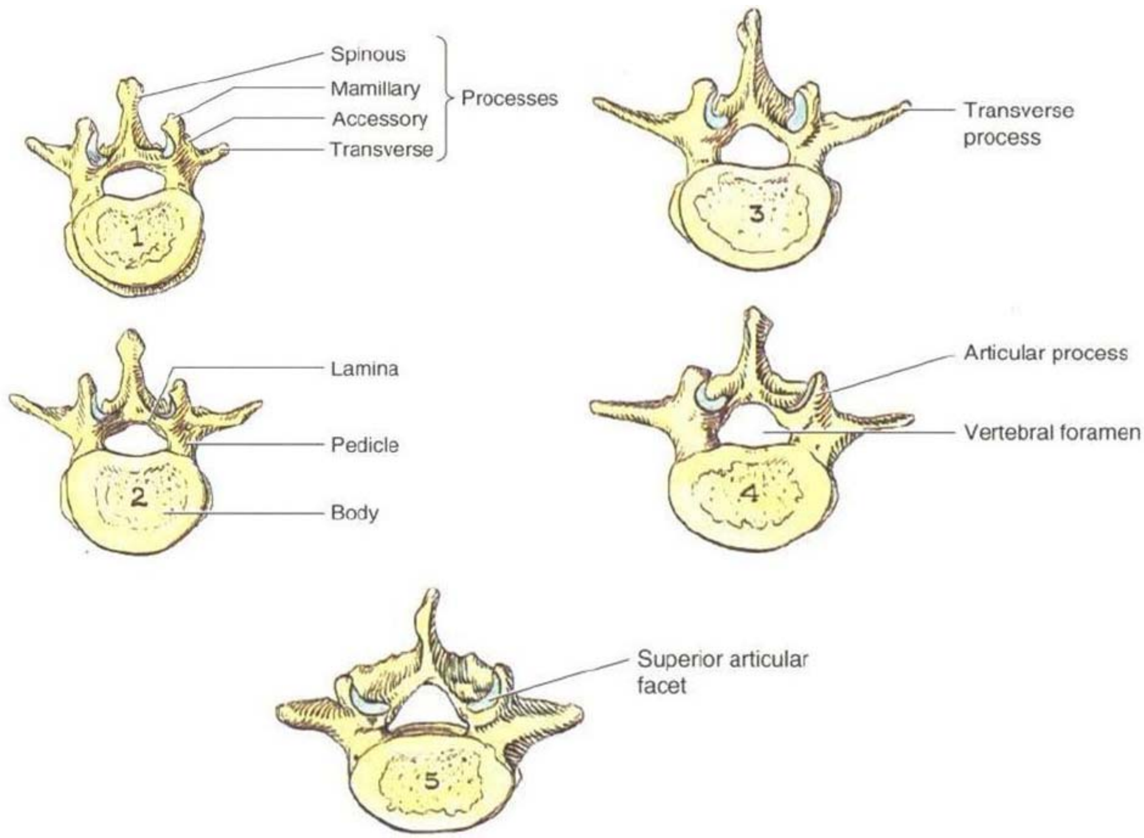

Figure 2: Illustration of the vertebral anatomy of the human lumbar spine. Note the Increasing size of the lumbar vertebrae as they progress from the cranial (L1) to the caudal (L5) segments, particularly the increasing size of the vertebral body. Also note the alteration in the shape of the 4 boney processes (transverse, spinous, accessory, mamillary) as the lumbar vertebrae progress caudally. Image obtained from Moore and Dalley (1999) Clinically Orientated Anatomy 4th edition, Figure 4.8 on pg 442.

The shape of the IVD within the lumbar spine in not constant, rather the IVD shape has been noted to closely match the shape of the vertebral end plate to which it is attached and to vary widely between individuals and within individuals (Farfan 1973). There are three common shapes to the IVD of the lumbar spine (Figure 3). Farfan (1973) noted that re-entrant posterior outline discs are more common in the upper lumbar spine, and that flattened posterior outline and rounded posterior outline shapes of the IVD are more common in the lower lumbar spine. He also noted that the L3-L4 level was the most common site for the transition from one shape of IVD to another within the individuals investigated.

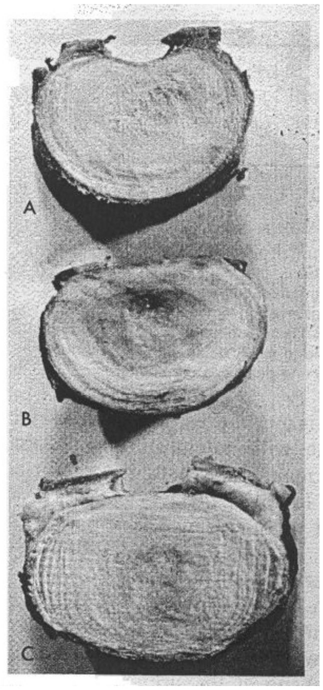

Figure 3: Illustration of the three most common shapes of the IVD in the lumbar spine. (A) Re-entrant posterior outline noted to be more common in the upper lumbar spine. (B) Flattened posterior outline and (C) rounded posterior outline, noted to be more common in the lower lumbar spine. Image obtained from Farfan (1973) Mechanical Disorders of the Low Back, Figure 2-18 pg 25.

2.3. Intervertebral Joint Anatomy; A Sub-Section of the Lumbar Spine

The intervertebral joint is a sub section of the spine that contains all structures linking two adjacent vertebrae, but permits motion at the joint while simultaneously holding the joint firmly together (Farfan, 1973). There are a few basic parts to each intervertebral joint including the IVD (consisting of the annulus fibrosus (AF), the nucleus pulposus (NP), and the superior and inferior endplates) the superior and inferior vertebral bodies, the superior and inferior facet joints, and the ligaments that attach the joint together (consisting of the posterior longitudinal ligament, the anterior longitudinal ligament, the supraspinous ligament, the interspinous ligament, the intratransverse ligaments and the ligamentum flavum). Employing the definition of an intervertebral joint proposed by Farfan (1973), it can be illustrated that the lumbar spine contains 4 such structures; the L1-L2, L2-L3, L3-L4, and the L4-L5 intervertebral joints.

2.3.1. The Intervertebral Disc

The IVD is thought to be composed of fibro cartilage (Eyre and Muir 1976; 1975) consisting of three structures, (1) the vertebral endplates forming the superior and inferior boarder of the IVD, (2) the gelatinous NP at the centre of the IVD, (3) and the AF (inner and outer) layers that surround the NP and contain it in the IVD in the horizontal direction (Figure 4). The outer AF is rigidly attached to the vertebral endplates, while the inner AF that surrounds the NP is less rigidly attached to the vertebral endplates (Farfan 1973). Also of note is the observation that the posterior AF is often thinner than the anterior AF (Adams et al. 1985, Moore and Dalley 1999, Tampier 2006).

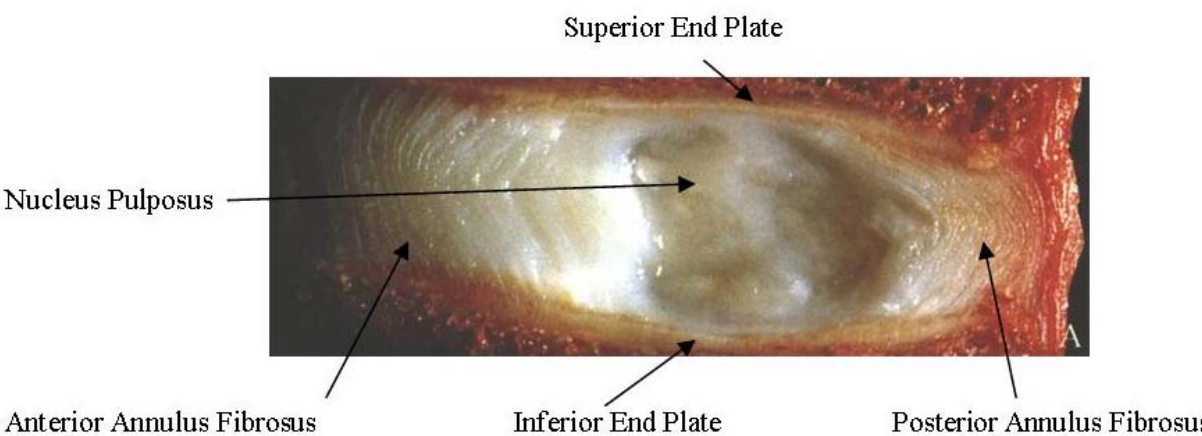

Figure 4: Sagittal view of the structures that compose the intervertebral disc. Note that both the posterior and anterior annulus fibrosus contain inner and outer layers. However, these layers are difficult to distinguish and are not labelled on this illustration. Image obtained from Adams, Bogduk, Burton, Dolan (2002) The Biomechanics of Back Pain, Plate 1.

2.3.2. The Nucleus Pulposus (NP)

The NP is commonly believed to be the mechanical shock absorber of the spine (Moore and Dalley 1999). However, since the NP has been illustrated to be an incompressible fluid, this statement seems questionable (McGill, 2003; Farfan 1973). Work by Farfan (1973) first implied that the vertebral body of the IVD were responsible for the shock absorption characteristics present in the spine based on fluid flow parameters in the IVD, while McGill (2007) echoed the idea of the vertebral body acting as the shock absorber of the spine, but through an endplate bulging mechanism. Type II collagen fibres and proteoglycans are common in the NP, resulting in the hydrostatic nature found in the IVD (Eyre and Muir 1975, 1976). The NP is the largest avascular, non-innervated structure in the human body (Farfan, 1973).

2.3.3 .The Annulus Fibrosus (AF)

The AF is comprised of two distinct layers, the inner AF, and the outer AF. The inner AF has a structural composition closer to that of the NP in that it has a high concentration of type II collagen fibres (Eyre and Muir 1975, 1976). The inner AF is believed to resist compressive loading (Hayes et al. 2001), and is not as rigidly attached to the endplate as the outer AF (Farfan 1973). The Outer AF is composed of mostly type I collagen fibres (Eyre and Muir 1975, 1976), and is rigidly attached to the endplates (Farfan 1973). Hayes et al. (2001) noted that the type I collagen fibres found in the outer AF are effective at resisting tensile forces. The layers of the AF consist of distinct bundles of fibres termed lamellae. The orientation of the lamellae fibres changes from layer to layer, but their angles are approximately the same from the vertical between all layers. The lamellae layers have be reported to alternate between 45-60 degrees from the vertical compressive axis by Tampier (2006), while Farfan (1973) noted the lamellae angles to alternate between 48 – 73 degrees (Figure 5).

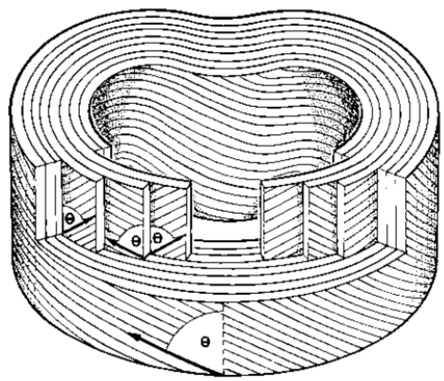

Figure 5: An illustration of the consecutive layers of the lamellae fibres present in the annulus fibrosus. Note that the angle of the fibres are approximately the same between layers, but the orientation of the fibres are opposite between layers. The above illustration was found in Bogduk, Twomey, (1991) Clinical Anatomy of the Lumbar Spine pg 13.

2.4. Review of Intervertebral Disc Herniation

2.4.1. Definitions; The Herniation Process and Complete versus Partial Herniation

Early work by Adams and Hutton (1982) indicated that the process of IVD prolapse, defined as the displacement of the NP, could occur as a sudden event with high compressive loads and with the IVD in a hyperflexion position. However, later work by Adams and Hutton (1985) indicated that disc prolapse could also occur in a gradual progression through radial fissures as the NP leaked its way through the AF towards the exterior of the IVD. The progressive nature of disc herniations has been noted by several other investigators (Callaghan and McGill 2001; Tampier et al. 2007; Adams et al. 2000). Radial tears in the AF leading to ruptures of the fibres of the AF were believed to allow the progression of the NP between the layers of the AF (Figure 6) in the herniation process as indicated by Adams and Hutton (1985), Adams et al. (2000), Osti et al. (1992) and Gordon et al. (1991).

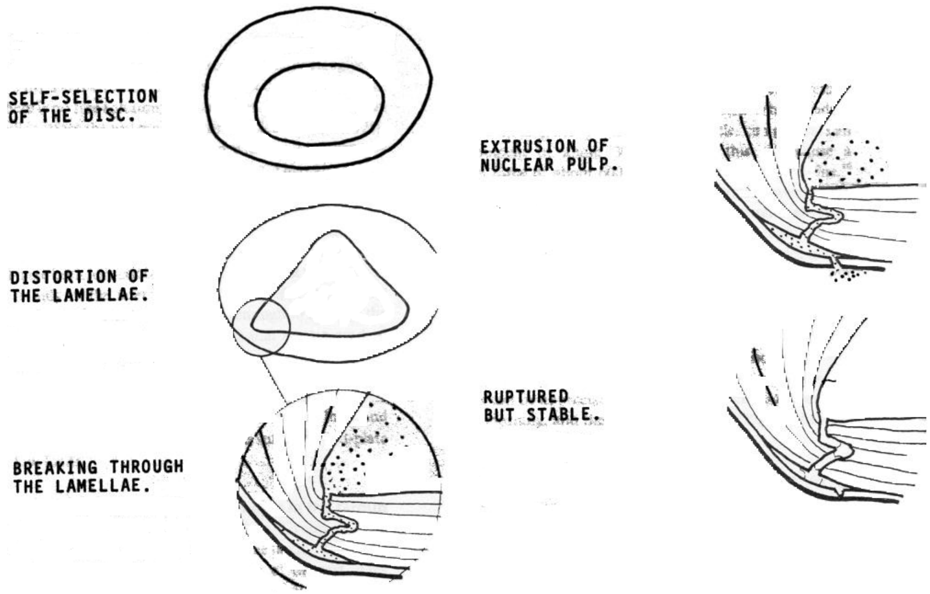

Figure 6: Diagram of a radial tears forming in the annulus fibrosus as a result of distortion of the lamellae bundles, leading to ruptures of the fibres of the annulus and the extrusion of nucleus pulposus material. Image obtained from Adams and Hutton (1985) Gradual Disc Prolapse, Figure 11 pg 530.

However more recent work by Tampier et al. (2007) has brought the belief of NP progressing through ruptured AF fibres into question. Through dissection, histochemical and radiologic techniques they were unable to identify any ruptures or failures in the fibres of the AF in herniated porcine IVDs. Instead, they illustrated that the NP material initiated its migration through the AF by forming small clefts in the inner AF at the areas of highest stress concentration (Figure 7). Once the NP material moved through these initial clefts, spreading between the AF layers was observed until sufficient pressure was accumulated and the next cleft (weak spot) was found in the subsequent layer of the AF. These processes continued progressively during the herniation process.

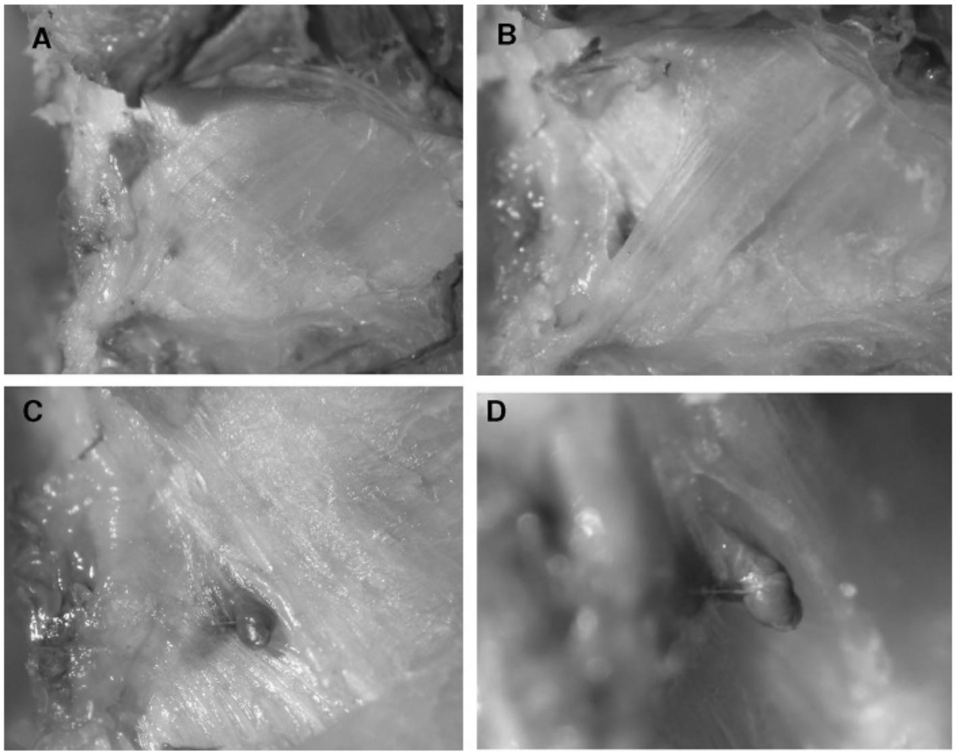

Figure 7: Illustration of the nucleus pulposus progression between annular layers via cleft formation. Note that no ruptures of the annulus fibrosus fibres were found. (A) – (D) illustrate the removal of successive layer of lamellae to reveal first the cleft formation, and then the stained nucleus material progressing through the cleft. Image taken from Tampier et al. (2007) Progressive Disc Herniation: An Investigation of the Mechanism Using Radiologic, Histochemical, and Microscopic Dissection Techniques on a Porcine Model, Figure 4 pg 2872.

IVD herniation has been defined by Fardon and Milette (2001) as the localized displacement of disc material that has progressed beyond the limits of the IVD space. Herniated material can consist of NP material, cartilage, bone, annular tissue, or a combination of these tissue types. The disc space was defined as the area of the IVD boarded cranially and caudally, by the endplates and peripherally by the outer edges of the vertebral ring apophyses (Fardon and Milette, 2001). Although well defined, this definition of IVD herniation can only indentify those discs where the herniation has progressed through the outer layers of the AF, and cannot be employed to define herniations where material is still contained by at least some of the AF layers. The term partial herniation has been employed by Tampier et al. (2007) to define herniations where the progression of the NP has initiated but has only reached the level of the inner or middle AF fibres. Tampier et al's. (2007) definition of partial herniation defines the displacement of NP material into the AF fibres, but still contained in the definition of disc space proposed by Fardon and Milette (2001).

Many investigators have attempted to reproduce IVD herniations under various loading conditions. Moderately successful attempts employed non-neutral spine postures in conjunction with axial loading were conducted by Adams and Hutton (1985) and Gordon et al. (1991). More reliable techniques were developed by Callaghan and McGill (2001) employing repetitive non-neutral flexion/extension motions in addition to modest axial load and have been used by several other investigators to reliably produce IVD herniation (Aultman et al. 2005; Drake et al. 2005; Tampier et a. 2007, Scannell and McGill 2009). Together, these investigations suggest that the IVD herniation can be produced with the combination of non-neutral spine posture and repetitive loading.

2.4.2. Investigations Regarding Intervertebral Disc Herniation

The process of IVD herniation has been studied by employing two separate forms of in vitro material. Cadaver material has been used by many investigators (Adams et al. 2000, 1985; Osti et al. 1992; Gordon et al. 1991; Brinckmann and Porter 1994), while animal spine models employing porcine (Callaghan and McGill 2001; Drake et al. 2005; Aultman et al. 2005; Tampier et al, 2007; Parkinson and Callaghan 2009, Drake and Callaghan 2009; Scannell and McGill 2009), ovine (Osti et al. 1990), and rat (Takenaka et al. 1987) materials have also been used. Furthermore, computer modelling techniques have been used to investigate the disc herniation processes by Goel et al. (1995) and Li and Wang (2006).

2.4.2.1. Investigations into Disc Herniation Employing Cadaver Material

Work done by several investigators had indicated that combined loading in axial compression and non neural spinal postures can create IVD herniation in in-vitro cadaver tissues (Adams and Hutton 1985; Adams et al. 2000; Gordon et al. 1991). Adams and Hutton (1985) tested cadaver motion segments in varied cyclic axial compressive loading and postural constraints. Of all the loading combinations (axial compression and posture) they investigated only cyclic compression (40 cycles per min) in fully flexed postures with axial compressive magnitudes ranging from 500 – 4000 N illustrated gradual disc prolapse. Of the 29 motion segments exposed to 500 – 4000 N to cyclic compression and flexed postural constraints, 5 specimens sustained gradual disc prolapse indicated through radiologic and dissection techniques. Combined complex loading was also employed by Gordon et al. (1991) to reliably create IVD herniation in cadaver motion segments. Cyclic compression (1334 N) at a rate of 1.5 Hz in flexion (7 degrees from neutral) and rotation (less than 3 degrees) produced annular damage in 14 out of 14 motion segments tested. Annular protrusions were produced in 10 motion segments, while nuclear extrusions resulted in the other 4 motion segments.

Precursors to IVD degeneration were indicated by Adams et al. (2000) in an investigation that exposed 38 cadaver motion segments to complex loading (axial compressive load and postural deviations from neutral) parameters. Notable annular damage was produced in 27 out of the 38 motion segments; 9 discs illustrated extreme outward budging of the annulus, 2 discs illustrated complete radial tears, 15 discs illustrated inwardly collapsing annulus fibres, and 1 disc illustrating posterior migration of the NP. While Brinckmann and Porter (1994) added evidence to the hypothesis that a degenerative change (the degenerative cascade) could have occurred prior to an IVD herniation. Using 20 cadaver motion segments Brinckmann and Porter

(1994) measured the disc bulges that were created from axial load (1 – 2 KN) and illustrated no asymmetry of the disc contour or any localized radial bulges associated with disc protrusion. A surgical procedure was performed that lead to a radial fissure of the AF sparing the last 1 mm of this material at the periphery. Under load, it was shown that the disc would migrate into the radial fissure creating a bulge. Fragments in the NP were then created in the IVDs by inserting small pieces of annular fibres from a different segment of the same spine. Disc bulges were increased in size after the fragments were created, and loads (0.9 – 6.1 KN) in combination with flexion of less than 10 degrees resulted in the rupturing of the disc budge and prolapse of the extruded fragments through complete annular tears. Initiating surgical damage decreased the validity of this investigation as clean, sharp cuts are unlikely to occur in vivo. However, this investigation served as a proof of principal that gradual disc prolapse is preceded by degeneration and that the formation of radial annular fissures and the occurrence of annular fragments in the NP could exacerbate existing damage.

Common morphological changes (rim lesions, circumferential tears in the annulus, and radial annular tears) to the IVDs of cadaver lumbar spines were indicated through radiologic, histochemical, and dissection techniques (Osti et al. 1992). Radial tears associated with degeneration of the NP were found almost exclusively in the posterior AF and were most common in the lower lumbar segments, making the lower lumbar segments most likely to incur damage from accumulated in-vivo loading (Osti et al. 1992). Clinical data confirms that the lower lumbar spine is the most common area for herniation type damage in the lumbar spine, as Deyo et al (1990) indicated that 95 % of lumbar herniations occur at the L4/L5 and L5/S1 levels.

A possible mechanism for the IVD herniation damage illustrated through complex loading parameters was proposed by Adams et al. (1994), in an investigation where they loaded 18 cadaver motion segments to assess the strength of the lumbar IVD in anterior bending. On average failure of the motion segments occurred at 18.3 (3.7) degrees flexion, with 33.0 (12.8) Nm of bending moment and a compressive force of 446 (140) N. They indicated that vertical tensile failures of the lamellae bundles of the posterior annulus were present after the hyperflexion injury. Fatigue damage was accumulated in the posterior AF from the repeated movements up to the elastic limit of flexion. This investigation concluded that disc failure in bending occurred through overstretching of the AF in the vertical direction and that in vivo, the posterior elements of the motion segments may not provide adequate resistance to flexion to protect the posterior AF tissues from severe damage.

2.4.2.2. Conclusions from Investigations Employing Cadaver Materials

Complex loading in axial compression and none neutral spine postures will produce IVD damage, herniation, and gradual disc prolapse (Adams and Hutton 1985; Adams et al. 2000; Gordon et al. 1991), and damage thought to be precursors to IVD herniations (Adams et al. 2000; Brinckmann and Porter 1994). Common morphological changes (indicating IVD damage) to those seen after mechanical testing of cadaver motion segments were observed in a population of cadaver motion segments harvested after death, without in-vitro mechanical testing applied (Osti et al. 1992). In-vivo accumulation of damage to the spinal segments is most likely to result in herniation damage – or precursors to herniation damage – at the L4/L5 and L5/S1 lumbar joints (Deyo et al. 1990; Osti et al. 1992). Finally, overstretching of the AF in the vertical direction may be a damage generation pathway as a result of repeated loading and non neutral posture and in-vivo, the posterior elements of the motion segments may not provide adequate resistance to flexion to protect the posterior AF tissues from severe damage (Adams et al. 1994).

2.4.2.3. Investigations into Disc Herniation Employing Animal Material

Work done by several investigators had indicated that loading in axial compression with repeated flexion/extension motions can create IVD herniation in in-vitro animal tissues (Callaghan and McGill 2001; Aultman et al. 2005; Scannell and McGill 2009, Tampier et al. 2007). Callaghan and McGill (2001) employed an effective porcine cervical spine model to create gradual IVD herniations. Using the combination of cyclic flexion and extension movements at a rate of 1 Hz (maximum 86,400 cycles), and axial compressive loading ranging from 260, 867, and 1472 N they were able to reliably produce IVD herniations. As the number of repetitive flexion/extension cycles and the axial load on the specimens increased, the porcine spines were more likely to have herniated, and to herniate in less time; under 260 N of compression only 1 out of 5 specimens herniated, under 867 N of compression 10 out of 12 specimens herniated, and under 1472 N of compression 8 out of 9 specimens herniated. All herniations that were produced occurred in the posterior / posterior lateral direction, and through radiologic imaging they were able to track the progressive nature of the IVD herniation process (Callaghan and McGill, 2001).

Further evidence was added to the theory that IVD herniation is a progressive process by Tampier et al. (2007) and Parkinson and Callaghan (2009). Porcine spines were loaded for 12 hours or until failure occurred via a compressive waveform from 300 N of load up to (10, 30, 50, 70) % of the predicted normalized max tolerance values. Results from this investigation indicated that the spines were at greater risk of herniation when the loads were lower (below

30% estimate compressive tolerance) and at greater risk of fracture (endplate and vertebrae) when the loads when higher, assuming that the loading was carried out until failure (Parkinson and Callaghan 2009). Therefore, spines were more likely to herniate from prolonged low magnitude progressive loading, than from larger more acute loading. The mechanism of progressive IVD herniation were investigated by Tampier et al. (2007), employing the methods described by Callaghan and McGill (2001) and using dissection, histochemical and radiographic (x-rays) techniques. They loaded 16 porcine motion segments under 1472 N of compressive load and cyclic flexion (15 degrees) – extension (2 degrees) with a range of cycles from 4400 – 14400 cycles in an attempt to detect herniations at various stages of progression. Radiological imaging (x-rays) were taken in an attempt to track the progression of the herniations, while microscopic and histochemical techniques were employed to attempt to track the pathway taken by the NP in the herniation process. The investigation produced 8 complete herniations without nuclear extrusion, 4 partial herniations, and 4 specimens with no detectable damage. Microscopic dissection techniques indicated NP material had reached the level of the posterior longitudinal ligament in all 8 of the full herniations, while NP material was found between the inner and middle AF layers in the 4 partial herniations. Communication of the NP from layer to layer in the AF was found to have occurred due to clefts that were formed in the annular layers. Spreading of the adjacent fibres was illustrated, while no failure or ruptures of the AF fibres were indicated. Histochemical analysis illustrated NP material inside the lamellae bundles in the posterior AF (forming pockets filled with nuclear material) in the 4 partial herniations, and in 8 specimens with full herniations the lamellae structure was disrupted and the NP was found between the external AF layer and the posterior longitudinal ligament. None of the herniations detected were found to progress in a straight line. This investigation strengthened the hypothesis that IVD herniation is a progressive injury process. The results indicated that the NP progresses towards the posterior / posterior lateral aspect of AF through clefts formed in a non-linear manner through the layers of the AF, and that delamination of the AF occurs within the layers of lamellae.

Using similar methods to Callaghan and McGill (2001), IVD herniations have been indicated to occur with substantially fewer cycles of flexion/extension under approximately the same compressive force than previously thought. IVD herniations were created under approximately 1.5 KN of axial load in as few as 5400 – 10800 cycles of flexion/extension by Scannell and McGill (2009), and in as few as 4400 – 14400 by Tampier et al. (2007). The axis of bending was found to influence the pathway of NP progression via a focused direction of herniation in 16 porcine motion segments subjected to 6000 cycles of repeated flexion/extension at 30 degrees of axial rotation (Aultman et al. 2005). Lesions to the periphery of ovine spinal segments in-vivo were found to lead to degenerative changes that were likely at the time of dissection (sacrifice) to lead to full or frank IVD herniations and NP migrations. While the occurrence of radial clefts (tears in the AF) were found to increase with the length of time elapsed between surgery and sacrifice with further migration of the NP relating to the size of the radial cleft formation (Osti et al. 1990).

The affects of axial torque on the process of IVD herniation were examined by Drake et al. (2005). Eighteen porcine motion segments were exposed to 6000 cycles of flexion/extension under 1472 N of compressive load. Axial torque (5 Nm) was applied to 9 of the motion segments while the other 9 motion segments had no axial torque applied. All specimens exhibited delamination of the AF post loading protocol as illustrated by dissection techniques. The group with applied axial torque illustrated earlier onset of IVD herniation, higher incidence of facet fracture and a higher energy dissipation. The results of this investigation indicated that axial torque will accelerate the degenerative process of the porcine spine under repetitive flexion/extension loading. The effects of axial twist on the herniation process were examined by Drake et al. (2009). Eight motion segments were subjected to repetitive flexion/extension under 1.5 KN of load, while another 8 motion segments were flexed and axially twisted to the left. Loading occurred in blocks of 1000 cycles until herniation or a maximum of 10,000 cycles. The combination of flexion and axial twist was found to produce fewer herniations (5 herniations out of 8 with 1 facet fracture and 2 specimens with no damage) than the flexion/extension motions alone (8 out of 8 herniations). However, loading (twisting) in non neutral postures (flexion) did lead to damage.

None neutral spine postures were further indicated by Takenaka et al. (1987) to produce damage to rat IVD in the form of acute hyperflexion herniations. Gradual disc prolapse does not occur as a single causal event, but is a cumulative injury (Callaghan and McGill, 2001; Tampier et al. 2007). Therefore the methods used by Takenaka et al. (1987) are not directly applicable to the gradual herniation process. However what is important to note was that herniations (although acute in nature) were produced through non-neutral spinal postures, and that non-neutral postures are present in investigations that have been successful at producing IVD herniations (Aultman et al. 2005; Adams et al. 2000. 1985; Gordon et al. 1991; Callaghan and McGill 2001; Brinckmann and Porter 1994). Therefore, it appears that non-neutral spinal postures can be damaging to the IVD given the right loading conditions.

2.4.2.4. Conclusions from Investigations Employing Animal Materials

The combination of axial compressive loading and repeated flexion/extension motions can create IVD herniations in in-vitro animal tissues (Callaghan and McGill 2001; Aultman et al. 2005; Scannell and McGill 2009, Tampier et al. 2007). Increasing the number of flexion/extension cycles, or the amount of axial compressive load will increase the extent of herniation damage, and decrease the time to herniation initiation (Callaghan and McGill 2001). Animal tissues (porcine) have been shown to incur herniation damage in a few as 4400 – 14400 cycles of flexion/extension under modest axial compressive load (Tampier et al. 2007). The IVD herniation process in in-vitro animal tissue is likely cumulative and progressive in nature (Callaghan and McGill 2001; Tampier et al. 2007; Parkinson and Callaghan 2009), and can be influenced by the bending axis in flexion motions (Aultman et al. 2005), existing structural damage (Osti et al. 1990), static axial torque (Drake et al. 2005) and twisting torque (Drake and Callaghan 2009).

2.5. Radiological Evidence of Intervertebral Disc Herniations

Many investigators have employed radiological techniques (specifically x-rays and discograms) in attempts to identify and to track the progression of IVD herniations with varying decreases of success (Adams et al. 2000; Callaghan and McGill 2001; Tsai et al. 1998; Drake et al. 2005; Gordon et al. 1991; Tampier et al. 2007). Gordon et al. (1991) were able to produce 14 cadaver motion segments with either annular protrusions or nuclear extrusions and noted that Magnetic Resonance Imaging (MRI) images were able to detect NP migration in 11 out of 14 segments (correlation between gross dissection and MRI images of 69%). Using x-ray imaging compared to gross dissection they indicated that in 7 out of 14 segments x-rays failed completely to indicate any damage, while in the other 7 out of 14 segments, x-rays indicate damage of a severity substantially less then what was found post dissection. Tampier et al. (2007) also indicated the difficulty in identifying IVD herniations using radiologic (discogram) techniques compared to their microscopic gold standard; only 4 out of 8 complete herniations were correctly identified through x-ray measures. Partial herniations were even more difficult to identify correctly through x-ray imaging as only 1 out of 4 of partial herniations were correctly identified. Difficulty in the identification of disc herniations using radiographs alone was also indicated by Deyo et al. (1990), and they recommended that more complex techniques should be employed (CT, MRI, and myelography) to accurately identify IVD herniations. Bernard (1990) illustrated that contrast enhanced CT imaging in conjunction with discography could increase the useful clinical diagnostic information and was influential on the selection of treatment for individuals with IVD herniations. CT discography has been indicated to correctly predict the type of disc herniation (protruded, extruded, sequestered, or internally disrupted) in-vivo (Bernard 1990). A normal IVD CT discogram and a pathological CT discogram (radial fissure leading to herniation progression) are illustrated in Figure 8. MRI images were shown to be effective at identifying IVD herniations and spinal canal dimension (a factor predictive of sciatic pain in response to IVD herniation) by Carragee and Kim (1997).

With the above investigations in mind, it appears that radiographs (discograms) alone may be insufficient to effectively diagnose IVD herniations as illustrated through in-vitro investigations. More complex imaging techniques (CT and MRI images) in addition to simple radiographs and discograms will increase the efficacy in the detection of IVD herniations; as illustrated though clinical research and basic scientific investigations.

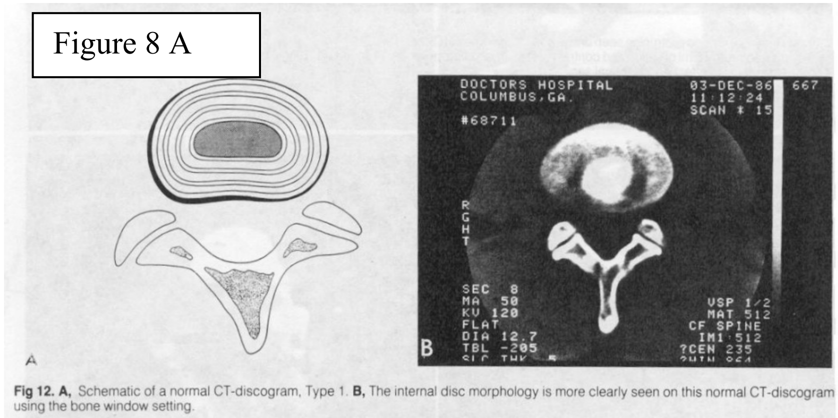

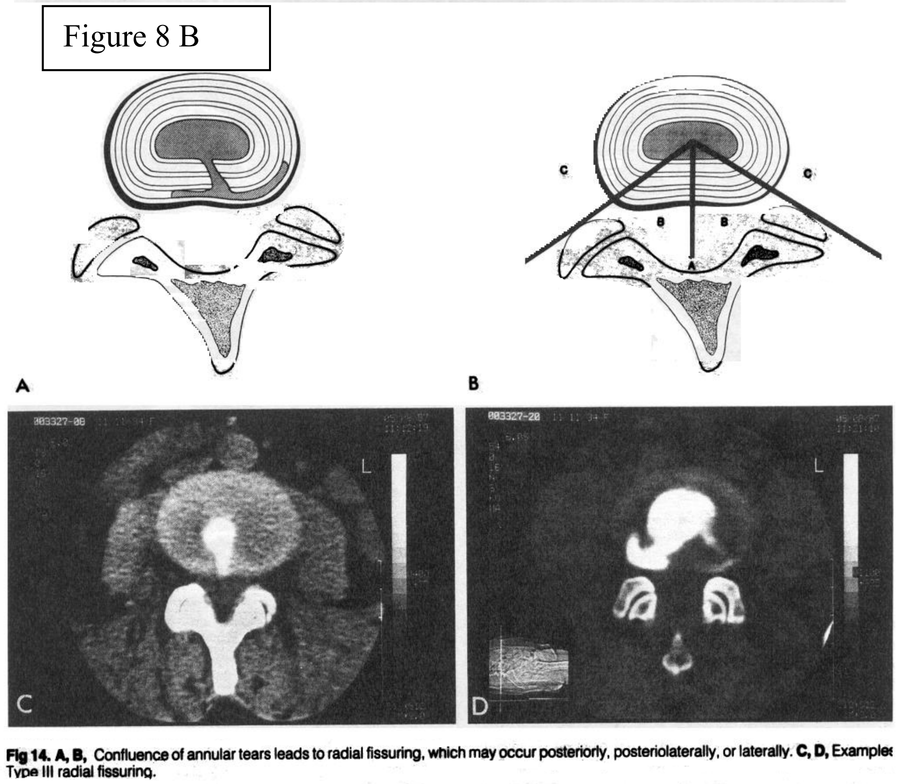

Figure 8: (A) schematic diagram and CT discogram of a normal IVD. Note the defined border of the nucleus pulposus. (B) Schematic diagram and CT discogram of pathologic IVDs (posterior and posterior lateral herniations). Images taken from Bernard (1990) Lumbar Discography Followed by Computed Tomography; Refining the Diagnosis of Low-Back Pain, Figures 12 (A and B) and Figures 14 (A and B).

2.6. Medical Imaging Review

All medical imaging techniques require some form of energy to produce accurate images. This energy must be capable of penetrating the tissues of the patients or specimens that are intended to be imaged; otherwise accurate images are not produced. This section on medical imaging will focus on two separate modalities, those of Screen Film Radiography and Computed Tomography (CT) medical imaging techniques. Both these medical imaging techniques use energy in the form of the electromagnetic spectrum of light that is outside that of visible light to produce images. The energy produced during CT and Screen Film Radiography must interact (absorption, attenuation, scattering) with the tissues of the object that is intended to be imaged, for useful information to be provided via these procedures (Bushberg et al. 2002).

The electromagnetic energy (in the form of x-rays) are produced by an x-ray emitter (often referred to as an x-ray tube) on one side to the object to be imaged, and an x-ray detector is placed on the other side of the object to detect the x-rays. Generally short duration pulses of x-rays are emitted from the x-ray emitter, pass through the object being imaged, and some of the x-rays pass through the object and reach the detector where a radiologic image is formed. The attenuation properties (by which x-rays are removed as they pass through matter) of different tissues (bone, fat, muscle, and air) that comprise the patient or specimen to be imaged are very different. These different attenuation properties result in the largely heterogeneous distribution of x-rays that leave from the object of interest. Essentially, the radiologic image that is produced on the detector is a picture of the x-ray distribution as a result of x-rays passing through the patient or specimen and onto the detector (Bushberg et al. 2002).

The contrast of medical imaging techniques can be defined as the difference in the gray scale of the image that is produced (Bushberg et al. 2002). X-ray contrast in both Screen Film

Radiography and CT is directly proportional to the differences in tissue composition (Attenuation factors), that effect the absorption coefficients of the x-rays. Spatial resolution is the ability to see small details in the produced image. The larger the spatial resolutions of the acquired image, the smaller the area of interest that can be identified. The collimation will adjust the size and shape of the x-ray field that emerges from the emitter, and will influence the radiologic image that is produced by altering the contrast through changing the properties of the x-ray beam (Bushberg et al. 2002).

2.6.1. Screen Film Radiologic Imaging

Screen Film Radiology is a form of projection radiology used to acquire a two dimensional image of a patients or specimens three dimensional anatomy. Screen Film Radiology results in substantial amounts of information compression in the acquired image, as the structures and anatomy of the entire patient or specimen area of interest are compressed and illustrated in one single image. Screen Film Radiology results in an image that is essentially the superimposition of the radiographic shadows that result from x-rays passing from the emitter, through the object of interest (and are attenuated to varying degrees), and onto the detector (the screen film that records the altered distribution of the x-rays (Bushberg et al. 2002). The screen film consists of a cassette with a photosensitive film inside it. The cassette blocks ambient light from prematurely exposing the film until it is exposed to x-ray radiation at the time of image acquisition. The resolution of a Screen Film Radiographic image is measured in pixels. An illustration of the general equipment setup commonly used in Screen Film Radiology can be found in Figure 9. One major disadvantage to Screen Film Radiology is that by using only one radiologic image, the exact position of a particular structure alone the straight line trajectory of the x-ray beam is not known (Bushberg et al. 2002).

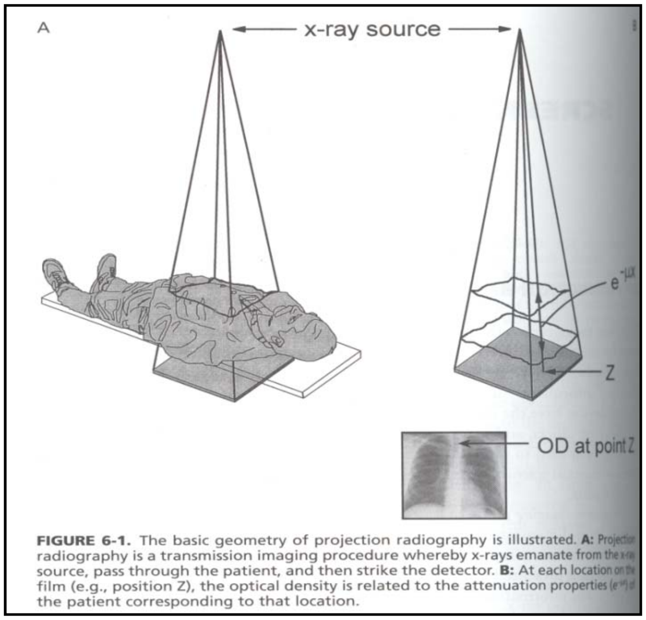

Figure 9: Illustration of the general equipment setup commonly used in the Screen Film Radiology procedure. Note the position of the x-ray emitter, the positioning of the object of interest (object to be imaged), and the position of the screen film inside the cassette (indicated by the shaded square in the figure. The above illustration was found in Bushberg et al. (2002) the Essential Physics of Medical Imaging, Second Edition pg 146.

2.6.2 Computed Tomography Medical Imaging

Computed Tomographic medical imaging procedures use the same x-ray technology (regarding x-ray beam emission) as used in the Screen Film Radiology techniques, however the detector is not a screen-film in a cassette but rather a fixed detector within the CT equipment. CT medical imaging techniques acquire images by passing an x-ray beam through the object of interest at a varying numbers of angles by rotating the x-ray emitter and detector around the object of interest. The x-ray emitter and detector are usually housed in a gantry (Figure 10). Complex computer algorithms are used to synthesize the numerous images obtained at the various angles into a tomographic (picture of a slice) image. Multiple transverse images can be produced resulting in stacks of single slice images. CT image resolution is measured with the unit of voxel size (essentially a three dimensional pixel) that have the two dimensional width and height of the standard pixel, but also include a third dimension representing the slice thickness. By including the third dimension, CT medical imaging procedures are able to negate the problem of image information compression that is common in the Screen Film Radiology techniques.

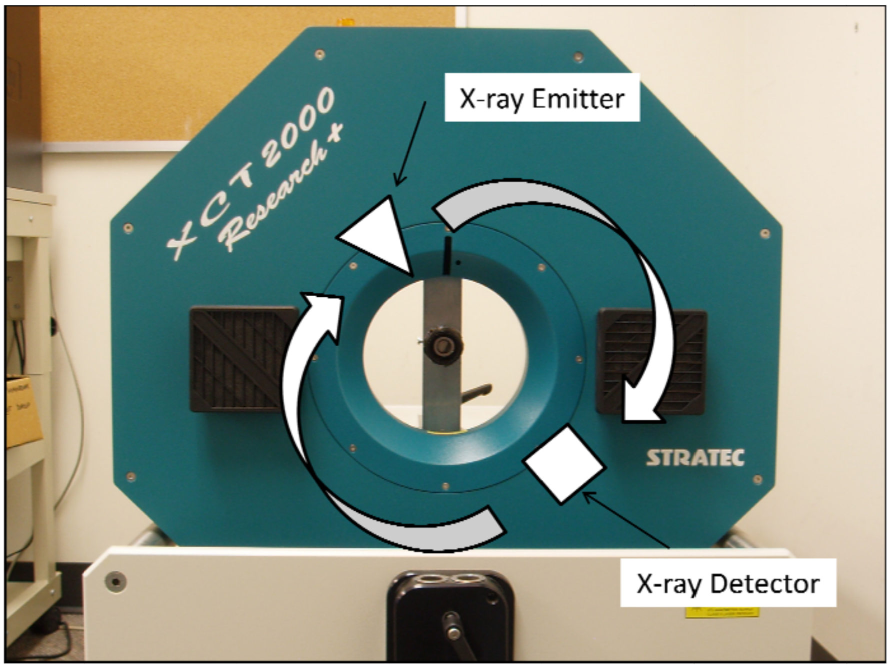

Figure 10: An example of a CT system gantry containing the x-ray detector and emitter. The x-ray detector and emitter are free to rotate inside the gantry. One rotation of the detector and emitter inside the gantry results in a portion of the information being obtained for that particular slice. The number of rotations of the gantry required to reconstruct a CT slice varies by machine.

There are several imaging quality issues that can occur when using CT medical imaging. After passing through a given thickness of the object of interests tissue (soft tissue, bone, and air), the lower energy x-rays are attenuated to a larger degree than the higher energy x-rays. The differential x-ray beam attenuation results in a shift in the energy spectrum of the x-rays towards higher energy components once the x-rays reach the detector. The average energy of the x-ray beam increases due to this higher energy spectrum shift; the average energy of the x-ray beam becomes “harder”. The hardening of the x-ray beam is known as “beam hardening”, and can result in substantial artifacts in the CT images (Figure 11 A). If the patient moves during the image acquisition process in CT imaging motion artefact can occur. This results in a blurred image with a drastic reduction in image resolution and contrast (Figure 11 B). Finally, partial volume errors can occur in CT image acquisition when different types of tissue (example; bone and soft tissue) occur in the same voxel. Partial volume errors result in the pixel being unable to represent either bone or soft tissue in the example. Therefore, the pixel becomes a weighted average of the tissue types contain within it. Partial volume effects are usually quite visible in CT imaging and can be identified before the lead to erroneous identification of potentially pathologic structures or conditions (Figure 12).

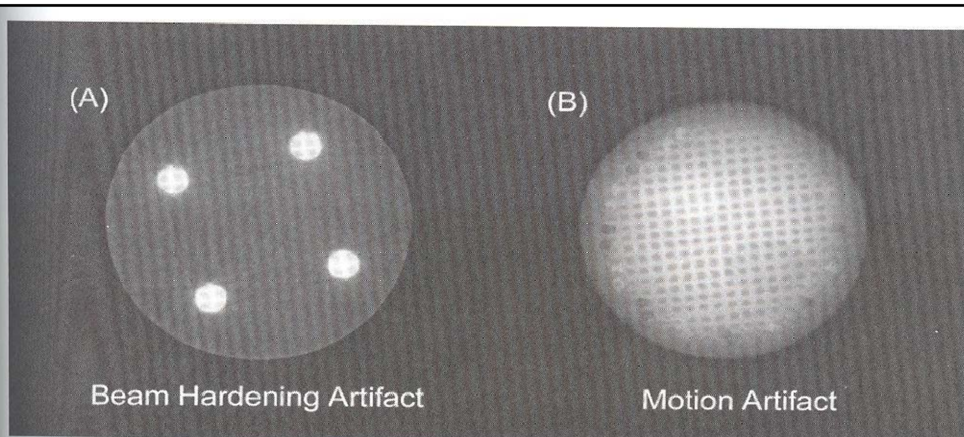

FIGURE 13-40. A: A beam-hardening artifact caused by four calcium-filled cylinders is illustrated. **B:** Artifacts due to motion are shown.

Figure 11: Illustrations of beam hardening artifacts (A) and motion artifacts (B) that can occur in Computed Tomographic medical imaging procedures. These artifacts can reduce image resolution and contrast. The above illustration was found in Bushberg et al. (2002) the Essential Physics of Medical Imaging, Second Edition pg 371.

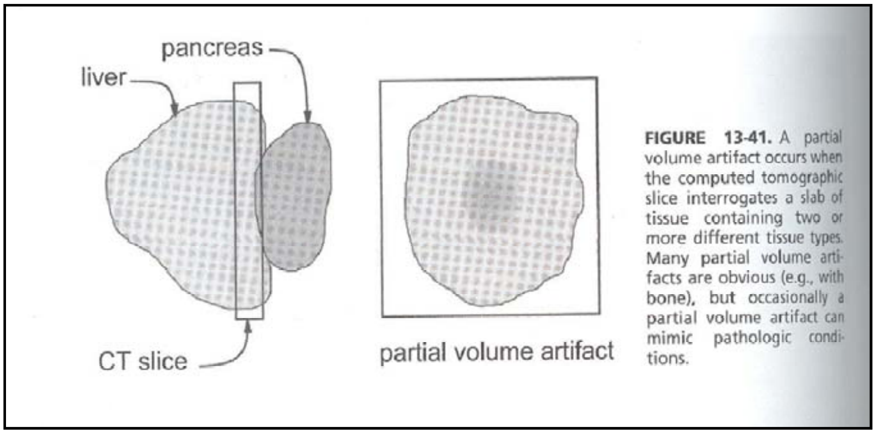

Figure 12: Illustrations of partial volume artifacts that can occur in Computed Tomographic medical imaging procedures. These artifacts can reduce image resolution and contrast, as well as lead to erroneous identifications of pathologic structures. The above illustration was found in Bushberg et al. (2002) the Essential Physics of Medical Imaging, Second Edition pg 371.

2.7. Quantifying the Direction of Intervertebral Disc Herniation

The anatomic direction taken by the NP as it passes through the layers of the AF in the progressive herniation process has been well investigated. In vitro cadaver work has directly indicated the posterior / posterior lateral area of the IVD to be the most common direction for disc herniations to progress (Adams et al. 1985, 2000; Gordon et al. 1991; Osti et al. 1992; Tsai et al. 1998). In vitro animal models have also directly indicated the posterior / posterior lateral aspect of the AF to be the most susceptible as the site for disc herniation (Callaghan and McGill 2001; Aultman et al. 2005; Tampier et al. 2007; Drake et al. 2005). Work done by Adams et al. (1996) and McNally et al. (1992) has indirectly indicated that the posterior / posterior lateral aspects of the IVD are most susceptible to injury. Their work employed stress profilimitry on cadaver IVDs to measure the stress concentration within each motion segment. Collectively this work has indicated that the posterior AF is the area of highest stress concentration within the IVD, and that pressure in the NP will rise rapidly as the limit of flexion is approached. The work of Adams et al. (1996) and McNally et al. (1992) documenting stress concentration in cadaver

IVDs using stress profilometry was extended by Edwards et al. (2001) when they were able to identify the posterior lateral area of the AF to contain the largest stress concentrations in three separate postures; neutral posture, 5 degrees of flexion, and 5 degrees of extension. A finite element model using geometry from CT scans of the human L3 – L4 joint indicated that interlaminar shear stress likely to cause delamination were highest under load in the posterior lateral aspects of the AF, and that increased magnitudes of load lead to larger disc bulges in the posterior / posterior lateral directions (Goel et al. 1995). Larger disc bulges in the posterior direction (on both the right and left side) were also indicated by Li and Wang (2006) in their finite element model of the lumbar spine based on CT and MRI images. They indicated that these larger disc bulges could lead to the acceleration of the degenerative process in the posterior direction likely to be the pre-cursor to gradual IVD herniation.

2.8. Motion Segment Stiffness Changes Related to Intervertebral Disc Degeneration

Employing their disc herniation model, Callaghan and McGill (2001) illustrated that porcine motion segment joint angular stiffness in repetitive flexion/extension motions increased in relation to increased loading time and increased loading magnitudes. They also linked increased joint angular stiffness values to increased damage found post dissection in their specimens. The addition of axial torque to the disc herniation model was found to further increase joint angular stiffness in flexion/extension motions, while a similar relationship to that found by Callaghan and McGill (2001) between increasing load exposure time and loading magnitude was further suggested (Drake et al. 2005). Increased stiffness values in flexion/ extension using cadaver motion segments were correlated to an increased severity of annular damage, likely to be caused by repetitive motions in vivo, and were hypothesized to be the results of fluid loss and NP degeneration (Thompson et al. 2000). An in vivo investigation by Ekstrom et al. (1996) employing pulsatile loads on porcine specimens added further evidence to the notion that stiffness increased as a result of prolonged loading (however, stiffness was in the axial direction). These authors also noted that the first 15 minutes of load illustrated the most significant stiffness increases. Axial stiffness was further found to increase in compressive loading of cadaver motion segments by Rostedt et al. (1998).

It appears that disc damage (herniations and annular deformations) as the result of repetitive flexion /extension and axial force loading protocols will affect the joint angular stiffness of cadaver and porcine motion segments. Specifically, higher loading magnitudes and longer loading times will lead to the most dramatic increase in joint angular stiffness. Direct compressive axial loading will also increase stiffness (axial stiffness) of motion segments, and illustrated a similar relationship as flexion/extension motions in that increased magnitudes and loading durations resulted in further stiffness increases. Therefore, joint angular stiffness and axial stiffness appear to be related to load magnitude and repetitive motion exposures.

2.9. Cumulative Loading and FSU Damage

Cumulative spinal loading has been implicated as a risk factor for the reporting of general LBP (Kumar 1990). Cumulative loading documents the time varying exposures that a worker (or specific anatomical structures or tissues) are subjected to. Cumulative loading is intending to assess the probability of injury and pain reporting in the tissues or workers that are exposed to repetitive loading by directly quantify the loading exposures. A common method of calculating cumulative loading is to sum the area under a force-time curve for a given loading exposure, using the mathematical procedure of integration. The cumulative load experienced for a tissue or worker can then be extrapolated to a given exposure time, usually an 8 hour shift (shift exposures) that a worker would experience. (Callaghan 2005). Exposures as a result of cumulative loading are influenced by the magnitude of the force (loading), the repetition rate, posture, and the exposure time (Parkinson and Callaghan 2007 b). Callaghan (2005) noted that the rate of loading exposure in cumulative loading is of the utmost importance, as loading rate can substantially alter the cumulative loads experienced.

The theory behind cumulative loading exposure relates to tissue repair rates. A tissue will become damaged or fail at a force less than its maximum strength (acute load failure point), if the tissue is repeatedly exposed to forces below the maximum strength for a sufficient amount of time, providing the loading rate overtakes the rate of tissue repair (Callaghan 2005). Biological repair process are absent in investigations that employ in-vitro specimens and tissues. As a result loading times for investigations using in-vitro specimens or tissues are usually kept short (Parkinson and Callaghan 2007a, 2007b; Drake et al. 2005; Tampier et al. 2007; Callaghan and McGill 2001), with the intent of negating tissue repair processes that could occur in-vivo.
By loading porcine specimens at 3 different maximum compressive tolerances (50%, 70%, and 90%) and with 5 different loading durations (0%, 50%, 100%, 200%, 1000%) of a 2 second duty cycle, the insertion of static loading periods in an in-vitro cumulative loading investigation illustrated that periods of static rest were not sufficient to reduce the risk of injury in compression (Parkinson and Callaghan 2007a). However load magnitudes did alter the cumulative load tolerated by the spines with failures at 5-8 MNs depending on the magnitude of loading; the lower the percentage maximum compressive force, the higher the overall cumulative load tolerated by the specimens. Overall all, loading magnitude was illustrated to have effects on

survival rate, cumulative loading exposure, number of cycles to failure, height lost, and survival time in in-vitro porcine specimens (Parkinson and Callaghan 2007a).

Prolonged compressive loading in in-vitro spinal segments has been illustrated to lead to injuries, and tissue failures at sub-maximal compressive levels (Liu et al. 1983; Parkinson and Callaghan 2007a, 2007b, 2009). By combining the previous work of other investigators, Callaghan (2002) as cited in Callaghan (2005), was able to demonstrate that a non-linear relationship existed between loading magnitude and cycles to failure. Higher loading magnitudes (percentage of maximum strength) had a greater risk of injury in fewer loading cycles than did lower loading magnitudes. Recent work by Parkinson and Callaghan (2007b) using the porcine model and cyclic loading protocols has indicated that weighting factors should be used in the calculation of cumulative loading exposures. These weighing factors would allow higher loading magnitudes (shown to produce injury in fewer cycles) to be weighted more heavily in the calculation of cumulative load than lower loading magnitudes. Results indicated that all loads less than 37.5% of the maximum predicted strength should be assigned a weighing factor of 1 and that the weighting factor would increase exponentially as loads increased towards 100 % predicted maximum strength. Parkinson and Callaghan (2009) cyclically loaded 50 porcine FSUs at varying peak loads (10, 30, 50, 70, 90) % of predicted maximum strength and in two postures (flexion and neutral). They indicated that significantly greater cumulative compression was sustained before failure when loads were below 30 % maximum strength values, and that spines were at an increased risk of disc herniation with loads below 30 % maximum strength and at an increased risk for vertebral fracture with loads over 30% maximum strength. Flexion was not able to alter injury pathways from disc herniation to fracture type injury with loading at or above 50 % maximum strength (Parkinson and Callaghan 2009). However, dynamic flexion motions have been indicated to reduce the cumulative compression that can be sustained before failure in porcine FSUs (Parkinson and Callaghan 2007a, 2007b). Prolonged sub-maximal axial compression with repeated flexion/extension motions have been indicated to reliably produce IVD herniations in porcine in-vitro motion segments (Callaghan and McGill 2001). The same body of work has illustrated that there is a lack of a single cumulative loading failure threshold, and indicated that IVD herniation appeared to be a progressive process (Figure 13).

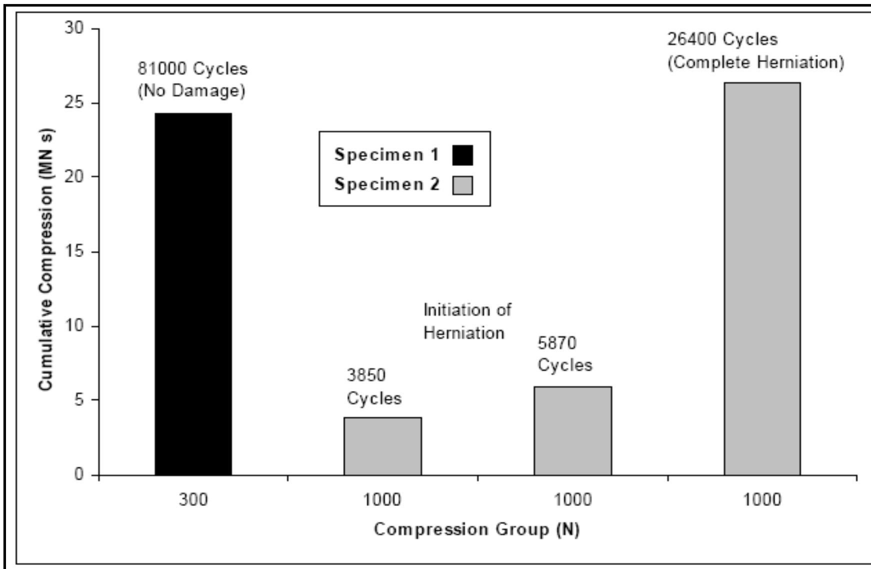

Figure 7 Cumulative compression for two in-vitro spine specimens tested in combined flexion/extension motion with static compression. Specimen 1 (300N) exhibited no injury. The three columns representing specimen 2 (1000N) demonstrate the development of initiation of an injury and complete intervertebral disc herniation (based on data from Callaghan & McGill, 2001).

Figure 13: Graph illustrating that porcine IVD failure can occur through herniation type damage in a progressive nature, and that failure is dependent on the loading magnitude and number of cycles applied to the specimens. The above illustration was found in Callaghan (2005). Cumulative Spine Loading: From Basic Science to Application. In W. Karwowski, & W. S. Marras (Eds.), The Occupational Ergonomics Handbook pg 13.

2.10. Justification of the Porcine Model

The porcine cervical spine model has been shown to be reliable for the production of IVD herniations (Callaghan and McGill 2001). Porcine spines are obtained from a homogeneous population that allows for the control of age, weight, degeneration level, diet, activity level, and genetic makeup of material. This level of control would be nearly impossible to obtain while employing cadaver materials in herniation testing. Cadaver material that could be obtained would likely come from elderly individuals, or younger individuals that incurred severe trauma; as such these materials are likely to be degenerated or damaged. Degenerated IVDs have been shown to be more resistant to herniation then younger degeneration free IVDs (Adams 2000, Goel et al. 1995) As a result, many of the obtainable cadaver spines would be unlikely to herniate. Porcine cervical spines have been illustrated to be a good approximation of the human lumbar spine in functional, geometric, and anatomical parameters (Yingling et al. 1999, Oxland et al. 1991), and are generally not degenerated resulting in an increased likely hood of herniation. Specifically, similarities noted between porcine cervical and human lumbar vertebral include; similar facet joint orientation, ligamentous structure, comparable stiffness values and injury modalities in shear and compression (Yingling et al. 1999). Oxland et al. (1991) noted porcine cervical spines to have similar posterior interspinous and supraspinous ligament consistency, facet orientation, and similar shape of the vertebral body and posterior spinous processes when compared to human lumbar spinal segments. Porcine cervical spines are smaller in scale then human lumbar spines, and possess anterior processes not present in the human spine. However, these anterior processes are unlikely to bear significant load, or play a significant mechanical role (Yingling et al. 1999).

As noted by Drake et al. (2005) and Callaghan and McGill (2001), in vivo spinal tissue has the ability to regenerate and repair damage sustained, processes that are absent in vitro. However, the synthesis of proteoglycans and the process of collagen repair have been shown to take well over two weeks (Urban et al. 2004). In testing (in vitro or in vivo) that spans the course of a day; it is unlikely that repair process would have sufficient time to regenerate damage inflicted on the IVD. Rest / sleep cycles however, would be present in vivo and have been implied to be a repair process for the IVD through rehydration effects (Callaghan and McGill 2001), and cannot to effectively mimicked in vitro. The rehydration that would occur due to a rest / sleep cycle may increase the risk of herniation through increased water content in the IVD (Adams and Muir 1976) and the resulting increase in hydraulic behaviour.

The freezing process has been shown to affect porcine FSUs, but only in loading at ultimate compressive strength (Callaghan and McGill 1995). The rapid freezing process does not alter the mechanical properties of the AF (Galante 1967), the compressive elastic properties of the IVD (Callaghan and McGill 1995) or the creep and elastic response of human lumbar disks (Dhillon et al. 2001). The freezing process results in increased hydration in the IVD upon thawing; these effects can be effectively reversed with the use of a pre-load protocol of 300 N of axial force for 15 minutes (Adams and Dolan 1995) and this protocol has been commonly applied (Adams et al. 2000; Callaghan and McGill 2001; Gunning et al. 2001).

2.11. Definitions of Whole Body Vibration and Mechanical Shock Loading

Vibration in general has been defined as mechanical movements that oscillate around a fixed point (Mansfield, 2005). WBV has been defined as vibration that affects the whole of the person under exposure, and is often noted to be transferred through backrests, floors surfaces, handles of vibrating equipments, and seat surfaces to individuals (Mansfield, 2005). Waters et al. (2007) have defined WBV as a continuous steady state vibration often generated by the vehicles power supply source and by its general operating characteristics. Mechanical shock loading has been defined as a series of transient shock events generated by travel over rough terrain and or obstacles (Waters et al. 2007), while Mansfield (2005) defined transient or shock motions as non-periodic motion directly caused by high acceleration magnitudes or events. Mechanical shock loading has been termed high acceleration events or repeated shock (Sandover 1998), or jarring jolting exposures (Mayton et al. 2007). However, for the purpose of this investigation the term mechanical shock will be used to define these events, as a recent literature review found this term to occur most frequently (Waters et al. 2007) and to comply with the language used by ISO 2631-5:2000(E); a standard often used to evaluate health risks of a seated person under exposures to vibration containing multiple shocks. Increased doses of vibration exposure (WBV, mechanical shock, or both in combination) are related to increased risk of adverse health effects (ISO 2631-5).

Vibration exposures have been indicated as a significant risk factor for injury to the lumbar spine, and specifically the IVD (ISO 2631-5). People are generally most sensitive to WBV that occurs in the lower frequency ranges, usually 1-20 Hz. The lumbar spine appears to be most sensitive to vibrations at the lumbar spine's resonate or natural frequency. Resonance can be defined as the frequency at which the response of the system (lumbar spine) will be maximized (or exceed the input) when compared to the stimulus (acceleration caused by vibration) resulting in the maximum force/displacement transfer from the stimulus to the system. The resonant behaviour of the lumbar spine has been illustrated to occur around 4-5 Hz (Mansfield, 2005; Sandover and Dupuis 1987; Seidel et al. 1986; Dupuis and Zerlett 1987; Fritz 1998; Pankoke et al. 2001). WBV exposure has been found to occur at the resonant frequency of the lumbar spine (4-5 Hz) in many occupational tasks including; ATV operation (Milosavljevic 2008 Personal Communication), agricultural machine operators (Waters et al. 2007), construction equipment operators (Kittusamy and Buchholz 2004), and coal mining operators

(Brinckmann et al. 1998). Therefore, WBV at or near the resonant or natural frequency of the human lumbar spine will lead to increased injury risk due to high force/displacement transfers.

Mechanical shock loading in combination with WBV has been indicated to increase the risk of injury to the lumbar spine through an increased vibration dose exposure (ISO 2631-5), and has been indicated by Troup (1978) to pose a significant risk to the lumbar spine, especially after long-term exposure to WBV. Dupuis et al. (1991) indicated that vibration exposures where mechanical shocks are present are more detrimental than vibration exposures where mechanical shocks are absent. Specifically they found that the strain effects produced on the lumbar spine were greater in vibration that included mechanical shock loading, than in vibration that excluded it. In occupations were WBV exposure occurs, mechanical shock loading is likely. Therefore, investigations examining WBV should not ignore the potentially detrimental health effects of mechanical shock loading.

2.12. Studies Relating Vibration Exposure to Low Back Injury

There are strong epidemiological links between vibration exposure (both WBV and mechanical shock loading) and injury to the lumbar spine. General injuries to the lumbar spine will be considered including; general LBP, lumbar syndrome symptom generation, and early degeneration of the lumbar spine. Investigations that have linked posture and vibration stresses to lumbar disc herniation as a specific injury mechanism will be considered separately, and in greater detail.

2.12.1. General Injury

Vibration exposure has been found to increase the risk of LBP (Bovenzi 1994; 2002; Wilkstrom et al. 1994; Mayton et al. 2007; Kittusamy and Buchholz 2004; Troup 1978). Bovenzi et al. (1994) conducted a study on 1155 tractor drivers exposed to WBV and postural stress and compared the LBP in this group to a control group of office workers not exposed to WBV. Exposure to WBV was quantified through the use of the 1985 ISO standards (ISO 2631 – 1) and measured via frequency weighted accelerations and total vibration dose. LBP was assessed through the Nordic Questionnaire to assess LBP. The authors indicated that tractor drivers had a threefold increase in risk of LBP compared to the office workers, and that a significant association existed between cumulative vibration exposure (as measured through total vibration dose) and LBP. Also noted was that sciatic pain and chronic episodes of LBP were associated with vibration exposure. As total vibration dose increased, LBP increased in the tractor drivers. A recent literature review by Bovenzi et al. (2002) of epidemiological studies on the relation between vibration exposure and LBP from 1986 – 1997 further illustrated the idea that LBP was more common in drivers of vehicles that were exposed to vibration then in control subjects without vibration exposure. The most commonly reported symptom as a result of WBV was found to be general LBP, and the occurrence of LBP appeared to increase with increased exposures to WBV (Wilkstrom et al. 1994). In a cross-sectional study Dupuis and Zerlett (1987) compared 352 operators of earth-moving machines exposed to WBV to 315 workers not exposed to WBV. They reported similar findings to Bovenzi et al. (1994, 2002); the group exposed to WBV reported higher discomfort in the lumbar spine after a shift than did the control group. Specifically they indicated that lumbar syndrome reports (symptoms associated with degenerative conditions of the lumbar spine) were significantly higher in the WBV exposure group (83%), then in the control group (53%) not exposed to WBV. Mayton et al. (2007) investigated farm tractor operation and the associated musculoskeletal disorder symptoms in 43 occupational farmers, and quantified various acceleration magnitudes experienced on several difference sizes and classes of farm tractors. Unfortunately they did not relate the dose of measured vibration exposures to incidence of LBP, but it was reported that 38% of the farmers questioned had experienced LBP that was recurrent over the last year. Early degeneration of the lumbar spine was found to be related to WBV and non-neutral body postures, including static prolonged sitting, in a cohort of construction workers (Kittusamy and Buchholz, 2004). While Troup (1978) indicated that vibratory stress in the form of WBV, mechanical shock or these loads in combination and postural stress were major causes of LBP, adding further evidence to the theory that vibration exposures can lead to LBP.

There appears to be a strong link between vibration exposure (WBV and mechanical shock loading) and increased incidence and reporting of general LBP. Further investigations into the exact mechanical insult resulting from vibration stresses in the lumbar spine are required to enhance the understanding of the link between vibration exposures and general LBP.

2.12.2. Disc Herniation as a Specific Mechanism of Injury

One of the first investigations to illustrate a link between WBV, sitting and IVD herniations was conducted by Kelsey and Hardy (1975). Their epidemiological study employed participants with probable disc herniations and age and sex matched controls without evidence of IVD damage. The diagnosis of disc herniations was confirmed from a combination of radiological examinations, questionnaires, and medical history. Their results indicated that operating a motor vehicle for a substantial portion of a working shift lead to an increased relative risk of 2.75 for a lumbar disc herniation. Truck driving males were found to be 5 times more likely to develop an acute lumbar disc herniation than males that did not drive truck for a living. It appeared that sitting was also associated with the increased risk for lumbar disc herniations. However, relative risks for sitting while driving were twice as high as sitting alone; indicating that sitting was not the sole causal factor in the increased risk of herniation to the lumbar discs. Prolonged driving experience and exposure to WBV were also found to lead to an excess risk of lumbar disc herniations in a cohort of port machine operators investigated by Bovenzi et al. (2002). They were able to quantify the vibration dose that port machine operators were exposed to by employing the ISO 2631-1 (1985 and 1997) standards and calculating the cumulative vibration exposure experienced by the operators. They illustrated that prevalence ratios of disc damage (95 % confidence interval) increased as the cumulative vibration exposure increased, further illustrating the idea that risk of injury to the lumbar spine increases as vibration dose increases. A large literature review conducted of epidemiological studies linking lumbar spine injury to WBV also indicated that occupational exposure to vibration in a seated posture was associated with lumbar IVD herniations (Bovenzi and Hulshof 1999). Further evidence was provided to link occupational exposure to WBV and disc degeneration and herniation by Virtanen et al. (2007), when they illustrated that a cohort of train engineers had a greater incidence of disc degeneration than did matched cohorts of paper mill operators not exposed to WBV.

Evidence is mounting that those occupations that involve prolonged sitting and operation of vehicles that expose individuals to vibration stress will increase the likelihood of IVD damage, specifically IVD herniation. Unfortunately, experimental investigations into the relationship between vibration exposure dose and disc damage have yet to be conducted, therefore limiting our understanding of the vibration herniation relationship suggested by the epidemiological literature.

2.13. Investigations Linking Vibration Exposure to Injury Mechanisms

Although the investigations discussed below are experimental in nature, they were all unable to elucidate a direct link between vibration exposure and IVD injury. However, these investigations suggest several injury mechanisms likely to occur in-vivo in response to WBV. Videman et al. (1990) conducted an investigation where they subjected 86 cadaver lumbar spines to discography techniques, and conducted detailed surveys of the family members of the deceased to gather information on the type of occupational task performed by the cadaver material donors in vivo. They noted that 50 % of the donors that were engaged in occupation driving reported back pain, and the discography and dissection techniques indicated that annular rupture (likely precursors to NP migration and disc herniation) were found most frequently in those exposed to occupational driving. Of the donors that had preformed heavy work in-vivo, 54% reported back pain, and moderate to severe endplate fractures were the most common injury mechanism found through dissection and discography. From these results, it appears that driving occupations (exposed to postural constraints and vibration) were more likely to experience soft tissue IVD damage, while heavy work occupations were more likely to experience fractures in the IVD (in the area of the endplate). Contrary to this, Sandover (1983) indicated dynamic compressive loading (as would occur in vibration exposure) has the potential to create fatigue induced micro fractures – repetitive loading has been shown to decrease the fatigue life of many engineering materials (Beer et al, 2004) – leading to callus formations on the endplates of the IVD associated with decreased nutrition and IVD degeneration. They also noted that dynamic shear, bending and rotational loads could lead to fatigue induced breakdown of the annular lamellae and result in further degeneration of the IVD, and perhaps IVD prolapse. Regardless of the loading parameters, mechanical vibration loading could lead to changes in the end-plate and annular tissues and is a plausible explanation for IVD degeneration.

Tissues of the IVD, except for the outer annulus, depend on diffusion for nutrient supply (Farfan 1973), and reduced nutrition to the IVD is likely to lead to cell death and early disc degeneration (Urban et al. 2004). Decreased nutrition to the IVD as a result of vibration has been indicated by several investigations and had been hypothesized to lead to accelerated degeneration of IVD (Hirano et al. 1988; Urban et al. 2004).

Motion segment height reductions are a common structural change associated with IVD degeneration (Adams et al. 2002), while larger height changes have been illustrated with increasing damage severity; as indicated by increased stiffness reductions at more progressed stages of IVD herniation in the data reported by Callaghan and McGill (2001). Spinal height changes as a result of vibration were investigated in vivo by Sullivan and McGill (1990). They subjected 5 participants to vertical vibrations of 2mm/s^2 at 5Hz for a 30 min exposure time in a sitting posture. Their results indicated that during the 30 minutes vibration exposure, significantly more spinal height was lost than in the control condition of static sitting. However, spinal height measures in the late afternoon after vibration exposure indicated less height loss then when no vibration exposure was given. This implied that short term vibration would increase spinal height post exposure when compared to static compression and was termed the rebound effect of vibration by the authors. Hirano et al. (1987) found a similar trend; 30 minutes of short term vibration significantly decreased the IVD height and water content of their rabbit specimens in-vivo, but long term vibration (18 – 42 hours) with rest cycles (every 6 hours) resulted in fewer water content decreases and height loss. Ekstrom et al. (1996) added further evidence that vibration exposures could lead to injury mechanisms using disc displacement measures of in-vivo porcine specimens exposed to pulsatile loads at 5 Hz for 1 hour. They indicated disc height losses over the exposure period, and a trend towards increasing dynamic stiffness as the exposure period progress; particularity in the first 15 minutes of loading. The inflammatory response of the IVD tissues to vibration was hypothesized to lead to mechanical insult causing dilation of blood vessels and increased loss of fluid from IVD to surrounding tissues, while increasing the permeability of the vessel walls to proteins. This could result in the accumulation of inflammatory proteins in the IVD, leading to swelling and increased osmotic pressure, resulting in increased disc height. (Sullivan and McGill 1990). Vertebral height, sagital plane displacement and disc height comparisons between vibration exposed workers and a cohort of workers not exposed to vibration in the mining and steel industry was conducted by Brinckmann et al. (1998). They indicated that disc height lost was highly dependent of the magnitude of vibration exposure, and seat damping characteristics. They illustrated that the higher the vibration exposure (larger accelerations over longer periods) produced increased disc height lost, and seats with poorer damping characteristics resulted in increased disc height loss.

In summary, vibration exposure has the potential to influence IVD degeneration and herniation. The immediate short term decreased disc height changes in response to vibration (Sullivan and McGill 1990; Hirano et al. 1987; Ekstrom et al. 1996) may be indicative of increased mechanical stress (at least when compared to static compression alone), and could indicate more damage to the soft tissues of the IVD. Alternatively, this reduced IVD height in response to vibration may indicate fatigue induced micro trauma. In addition, the “rebound effect of vibration” as indicated by Sullivan and McGill (1990) could potentially increase the susceptibility of the IVD to herniation through increasing the hydraulic pressure and behaviours of the disc.

2.14. Quantification of Acceleration Caused by Vibration Exposure

Previously, the parameter of Root-Mean-Square (r.m.s) has been used to assess the effects of vibration exposure on individuals (Mansfield 2005,). Since by definition vibration is a movement that will oscillate about some fixed point (usually the mass of the object), the average values of any vibration signal will theoretically be zero (if we assume no translation of the vibration signal). Therefore, the average of a vibration signal is unlikely to indicate the true exposures and magnitudes of the input signal, as theoretically these values would sum to zero. Mathematically, the r.m.s parameter would solve this problem of taking the average of a signal with a mean of zero. The parameter of r.m.s. has the units of acceleration (m/s^2) and commonly includes a frequency weighting factor. Root-Mean-Square values are calculated mathematically as follows; where $a_{w.r.m.s}$ is the frequency weighted r.m.s., *T* is the measurement duration and a_w (t) is the frequency weighted acceleration at time *t* (Mansfield 2005).

$$a_{w.r.m.s} = \sqrt{\frac{1}{T}\int_{o}^{T} a_w^2 \ (t) dt}$$

The ISO standards are the most common standards that can be applied to the collection and quantification of vibration data. The ISO 2631-1 (1997) standards are commonly used for the assessment of health risks caused by WBV, and use the parameter of Vibration Dose Value (VDV) which is frequency weighted in the X,Y,Z directions. The VDV is used to calculate the daily VDV by extrapolating to the vibration exposure time (Mansfield 2005). Appendix A illustrates an example of the daily VDV calculation done by Milosavljevic et al. (2008a).

In order to assess vibration that contains multiple shocks, the r.m.s parameter should not be used as it is relatively insensitive to multiple shocks because their influence decays as the measurement time increases. In contrast the parameter of VDV does not decay and continually compiles exposures over time with each shock. The difference between these parameters is well illustrated in Figure 14. Vibration exposure that contains multiple shocks should be assessed using the ISO 2631 -5 (2004) guidelines. These standards suggest the calculation of an acceleration dose (D_k) that can be summed for the course of a day, thus representing the average daily dose (D_{kd}). Using D_{kd}, the daily equivalent static compression dose (S_{ed}) is calculated which is used in the calculation of Factor R (the ratio of static compression dose to ultimate strength of the lumbar spine) to assess the health risks of the vibration exposures (ISO 2631 -5 (2004)). Appendix B illustrates an example of the calculations required for the ISO 2631 – 5 (2004) standards to be implemented (Milosavljevic et al. 2008 b).

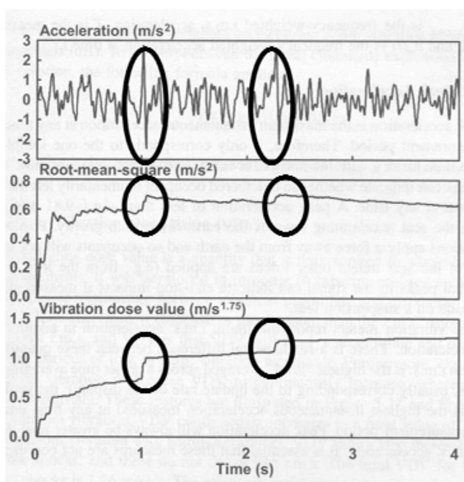

Figure 14: A comparison of acceleration quantification using the running r.m.s parameter and the VDV measurement (ISO 2631-1) for a random vibration signal that contains multiple shocks (indicated by ovals in the figure). Note how the r.m.s parameter decays after the shock exposures, and the VDV does not illustrate this decay. Image taken from Mansfield (2005) Human Response to Vibration, Figure 5.12 pg 113.

2.15. Justification of ATV Vibration Data

Several investigators have quantified vibration exposure in occupation tasks. The operation of agricultural tractors has been illustrated to cause WBV with rms accelerations of 0.7 – 4.3 m/s^2 and mechanical shock loading with peak vibrations ranging from 8.5 – 53.2 m/s^2 while employing the older ISO 2631 – 1 (1985) standards (Sandover 1998). While Mayton et al. (2007) have indicated that typical farming equipment operation exposes drivers to mechanical shocks ranging from 11.3 – 33.7 m/s^2. Mining load-haul drivers have been illustrated to be exposed to WBV in the range of r.m.s. from 0.6-2.5 m/s^2, with some impacts (mechanical shocks) in the magnitude of 3.8 – 20 m/s^2 using the ISO 2631 – 1 (1997) standards (Village et al. 1989). While the operation of heavy construction equipment has indicated WBV r.m.s. exposures of 0.2-0.75 m/s^2 for car operation, 0.5 – 2.4 m/s^2 while driving wheeled loaders, and 0.7 – 1.4 m/s^2 for operating heavy trucks on site (Dupuis and Zerlett 1987). A large review of vibration exposures summarized the magnitude of vibration exposure common to vehicle operation in an occupational setting, indicating un-weighted mechanical shock maximums in the order of 20 m/s^2 were not uncommon (Sandover 1998).

Occupational All-Terrain Vehicle (ATV) riding has been shown to expose operators to un-weighted WBV with magnitudes ranging from 0.011 – 2.37 m/s^2, and mechanical shock loading in the magnitude of 15 – 20 m/s^2 were not uncommon (Milosavljevic 2008 personnel communication). The WBV produced by ATV riding is a close approximation of WBV exposures reported above by several investigators in occupational driving tasks (Sandover 1998; Dupuis and Zerlett 1987; Village et al. 1989) (Table 1). Furthermore, the mechanical shock loading reported for ATV riding coincides well with the accelerations noted by (Sandover 1998) to be common in occupational driving tasks. Therefore, it appears that occupational ATV vibration exposures to both WBV and shock are close approximations of vibrations exposures caused by many occupational driving tasks.

Table 1: Summary of the similarity between occupation ATV vibration exposures and other equipment operation vibration exposures reported in the literature.

Author	Vehicle	WBV (m/s^2)	Mechanical Shock (m/s^2)
Sandover (1998)	Agricultural Tractors	0.7 – 4.3 (m/s^2)	8.5 – 53.2 (m/s^2) 20 (m/s^2) common
Mayton et al. (2007)	Farming Equipment	2.8 -3.3 (m/s^2)	11.3 – 33.7 (m/s^2)
Village et al. (1989)	Mining Equipment	0.6 – 2.5 (m/s^2)	3.8 – 20 (m/s^2)
Milosavljevic et al. (2008a, 2008b, Personnel communication)	Agricultural Equipment (ATV)	2.37 (m/s^2) common (90 min exposures)	upwards of 10 (m/s^2) common 18.35(m/s^2) maximum 2000 shock / day

An Investigation conducted by Milosavljevic et al. (2008a) employed the ISO-2631 – 1 (1997) standards to assess WBV risks using the Vibration Dose Value (VDV) parameter instead of r.m.s. un-weighted accelerations common in the previous investigations. Appendix A contains the methods used by Milosavljevic et al. (2008a) to calculate VDV in accordance with the ISO 2631 – 1 (1997) standards. The VDV calculations employed weighting factors to the time domain of a signal to modify them to represent the human response to vibration, rather than the mechanical characteristics of the vibrating system, allowing for a more accurate indication of relative risk due to vibration exposure (Mansfield, 2005). The ISO 2631 – 1 (1997) contains an action limit (AL) of 9.1 $m/s^{1.75}$, and a maximal permissible limit (MPL) of 21.0 $m/s^{1.75}$ as noted by Milosavljevic et al. (2008a). These exposures were quickly reached by the 20 occupational ATV drivers average vibration exposures; the AL was reached after 8.0 minutes of ATV use, and the MPL was reached after 220.0 minutes (3.7 hours) of ATV use. Note that seasonal variation regarding ATV daily riding times existed ranging from 1.6 (1.0) hours to 2.3 (1.3) hours. And Mansfield (2005) noted that VDV values between the AL and MPL will likely lead to injury. Therefore, occupational ATV riding possess a risk to operator's health based on their exposure to WBV.

The more recent ISO 2631 – 5 (2004) standards that where designed to assess vibration containing multiple mechanical shocks were also applied by Milosavljevic et al. (2008b) to the sample of 12 occupational ATV drivers. The ISO 2631 – 5 (2004) calculates a factor R, the magnitude of which is used to calculate the risk of adverse health effects due to the vibration exposure containing multiple shocks (Details of how these calculation are preformed can be found in Appendix B). R values < 0.8 indicate a low probability of adverse health effects, while R values over 1.2 indicate a high probability of adverse health effects (ISO 2631 – 5). None of the 12 occupational ATV drivers exceeded the lower limit of 0.8 for factor R, indicating a low probability of adverse health effects due to mechanical shock (Milosavljevic et al. 2008b). However, the authors noted that 12 subjects maybe insufficient to capture the full effect of mechanical shock in ATV riding. Even though a low probability of adverse health effects were indicated, mechanical shocks should not be ignored as shock vibration exposures have been noted to pose a significant health risk, particularity to the lumbar spine (Waters et al. 2007; Troup 1978).

Several authors have employed biomechanical models to convert representative accelerations of seated persons exposed to vibration to compressive forces at various IVD level (Fritz 2000, Hinz et al. 1993, Verver et al. 2003). A biomechanical model was developed by Fritz (2000) employing 16 ridged bodies to represent the upper body and arms in a sitting posture (on a ridged seat) in conjunction with frequency dependent transfer function to calculate the forces acting on the L3-L4 vertebral joint. Fritz's (2000) model was exposed to vibrations with a frequency range of 0 – 30 Hz and maximum accelerations of 0.1 – 0.5 G (approximately 0.98 - 4.91 m/s^2). The result was a maximum compressive force of the seated models at the L3-L4 lumbar spinal level of 634N. Work by Hinz et al. (1993) using a biomechanical model employing the effective mass of a human body above the L3-L4 lumbar spinal level was implemented to determine the compressive loads at the L3 – L4 segment while sitting on a rigid seat. The frequency ranges used in the model were 0.5 - 7 Hz with a maximum acceleration of 0.3 G (approximately 2.94 m/s^2). The resulting maximum compressive forces at the L3 – L4 spinal segments in response to the model inputs were 657 N. Verver et al. (2003) used a numerical human and seat biomechanical model to estimate compressive forces due to vertical vibrations at the L3-L4 lumbar spinal level. Vibration exposures ranged in frequency from 0.5 – 15 Hz, had r.m.s accelerations of 2.35 m/s^2, and a peak maximum acceleration of 0.4 G (approximately 3.92 m/s^2). Two different seat configurations were used in the model; rigid seat and standard car seat (containing damping characteristics). Maximum compressive forces at the L3-L4 segments were 581 N and 852 N for the rigid and standard car seats respectively. Since the maximum acceleration due to WBV while riding ATVs in an occupational manner are known to be 2.37 m/s^2 (approximately 0.24 G) and the maximum accelerations in the above biomechanical models ranged from 0.1 – 0.5 G (Verver et al. 2003; Fritz 2000; and Hinz et al. 1993), these models can be used to approximate forces at the L3-L4 level due to WBV ATV exposures.

In summary, ATV riding has been illustrated to pose a significant risk to the heath of operators based on vibration exposures using the VDV parameter as indicated by the ISO 2631 –

1 (1997). Factor R from the ISO 2631 – 5 (2004) indicated little risk, but likely underestimated mechanical shock duration exposures due to the short collection periods and potentially unrepresentative terrain during the collection process. Vibration magnitudes obtained from ATV operations were in close agreement with magnitudes reported in relevant literature regarding occupational driving vibration exposure. As such ATV vibration exposures can be related to other driving tasks. Substantial data regarding accelerations caused by ATV operation were made available by Dr. Milosavljevic and Dr. Allan Carmen (Milosavljevic et al. 2008a, 2008b; personnel communication) allowing us to accurately define the exposure times to WBV and their magnitudes, in addition to mechanical shock parameters. The biomechanical models of Verver et al. (2003), Fritz (2000), and Hinz et al. (1993) used similar frequency ranges and maximum acceleration forces (G) to the occupational ATV operation data. As such these models provide insight into the approximate compressive forces acting on the lower lumbar spine due to occupational WBV ATV exposures.

2.16. Using Vertical Z Vibration to Simulate Whole-Body Vibration and Mechanical Shock Loading

In practice WBV and mechanical shock loading will occur in three directions; anterior posterior (x), lateral (y) and vertical (z). However, many investigation into vibration loading have used only vertical (z) direction vibration to simulate exposures (Dupuis et al. 1991; Sullivan and McGill 1990; Seidel et al 1986; Tasi et al 1998). The use of only vertical forces to simulate WBV and shock loading exposure often occurs due to equipment restrictions; notably the capability to generate single axis forces only. Unfortunately, it has been noted that vertical vibration alone should not be used to simulate WBV and shock loading (Mansfield 2005) as it will neglect loading in the anterior, posterior and lateral direction that have potential to cause tissue damage.

2.17. Muscular Activity in Response to Vibrations

Muscular activity (as measured via EMG) in response to vibration exposure has been shown to have a lag time between vibration exposure and muscular response. Mechanical shock exposures were illustrated to cause increased EMG activity, and were hypothesized to increase the intradiscal pressure of the IVD leading to increased loading of the tissue (Dupuis et al. 1991). Muscular activity was also shown to increase the compressive loads on the spine during vibration (Seidel et al. 1986) and to enhance strain on the IVD tissues during vibration. Seidel et al. (1986) also noted that muscle activation during vibration exposure was not optimal for protection of the spinal tissues. However, during vibration exposures in prolonged relaxed sitting in a bent forward posture, EMG activity was illustrated to almost complete disappear from the back muscles (Seidel et al. 1988). Wikstrom et al. (1994) noted in their review article that this lack of EMG activity in response to vibration exposures could potentially be harmful as it would lead to a destabilization of the spinal column, thus increasing the risk of injury to this structure.

It appears that either muscle activation, or the lack of muscle activation in response to vibration will be detrimental to spinal health. Increased muscle activation in response to vibration will lead to larger compressive forces on the spine and will increase the risk of injury. Additionally, if prolonged vibration exposure leads to reduced muscle activation, the stability of the spine will be compromised and injury will again be more likely to occur. Alternatively, both of the above scenarios regarding muscle activation and vibration exposure could occur (increased compressive loads, followed by reduced stability), resulting in further injury risks.

2.18. Summary of the Literature Review

The major points that can be taken from the literature review are briefly summarized below. These major points were considered in the design of this investigation as detailed in Chapter 3 (Methods) of this work.

1. The most effective methods to create in-vitro gradual IVD herniations employ the combination of deviated spinal postures and modest compressive loading in a repetitive loading scenario.
2. Considering previous studies regarding IVD herniations several key points can be noted;
    a. Spinal segments that show little to no degeneration are most likely to herniate. Generally, using animal models allows for control over the extent of degeneration (or lack thereof) present in the spinal segments. As a result investigations that have employed animal models have generally been effective at creating gradual IVD herniations.
    b. Radiologic (discogram) medical images have historically not been as effective in detecting IVD herniations. However more complex medical imaging techniques such as Computed Tomography (CT) or Magnetic Resonance Imaging (MRI) have had greater success in detecting IVD herniations.
    c. FSU flexion/extension stiffness and axial height loss will increase as a function of IVD degeneration.
    d. IVD herniations most often occur in the posterior, posterior-lateral direction.
3. Exposures as a result of cumulative loading are influenced by the magnitude of the force (loading), the repetition rate, posture, and the exposure time. Also, there is a lack of a single cumulative loading failure threshold for IVD herniations.

4. Vibration exposures have been identified to cause a significant injury risk to the lumbar spine and are most often quantified via the ISO 2631-1 and ISO 2631-5 standards
5. Epidemiological evidence is mounting that IVD herniations are related to vibration exposures. However, basic scientific investigations into this relationship are lacking.
6. Vibration exposures (simulated with low frequency cyclic loading) have been shown to lead to axial height and stiffness changes in spinal segments
7. Vibration exposures experienced during occupational ATV operation are representative of vibration exposures experienced by many other occupations.

Chapter 3: Methods

3.1. Study Design Overview

Pilot work using the vibration exposures and postural considerations identical to those that will be used in the current investigation have indicated that these exposures alone - even over an extended period of time – would not lead to detectable IVD herniations. Damage to the motion segments (end plate fractures) did occur with mechanical shock loading out of physiological loading ranges during the pilot testing. But mechanical shock loading in these magnitudes will not be performed for the current investigation. From these pilot investigations, it was concluded that it was unlikely that exposures to vibration and postural constraints would initiate the herniation process in the amount of time suitable for in-vitro porcine motion segment testing. However, vibration and postural constraint loading was still hypothesized to exacerbate the IVD herniation process. Therefore, motion segments were exposed to a partial herniation loading protocol to cause herniation initiation comparable to what might occur as the result of the manual materials handling tasks commonly done in the daily activities of occupational farmers and other occupations. Following this, the motion segments were exposed to the vibration and postural constraint loading meant to simulate ATV riding (thought to exacerbate herniation damage). Note in Figure 15: Experimental Methods each section heading is numbered to correspond with the methods section while the numbers in superscript parenthesis indicate the numbers of the procedure in cases where more than 1 procedure was performed; an example would be the repeated passive tests, or repeated preload procedures.

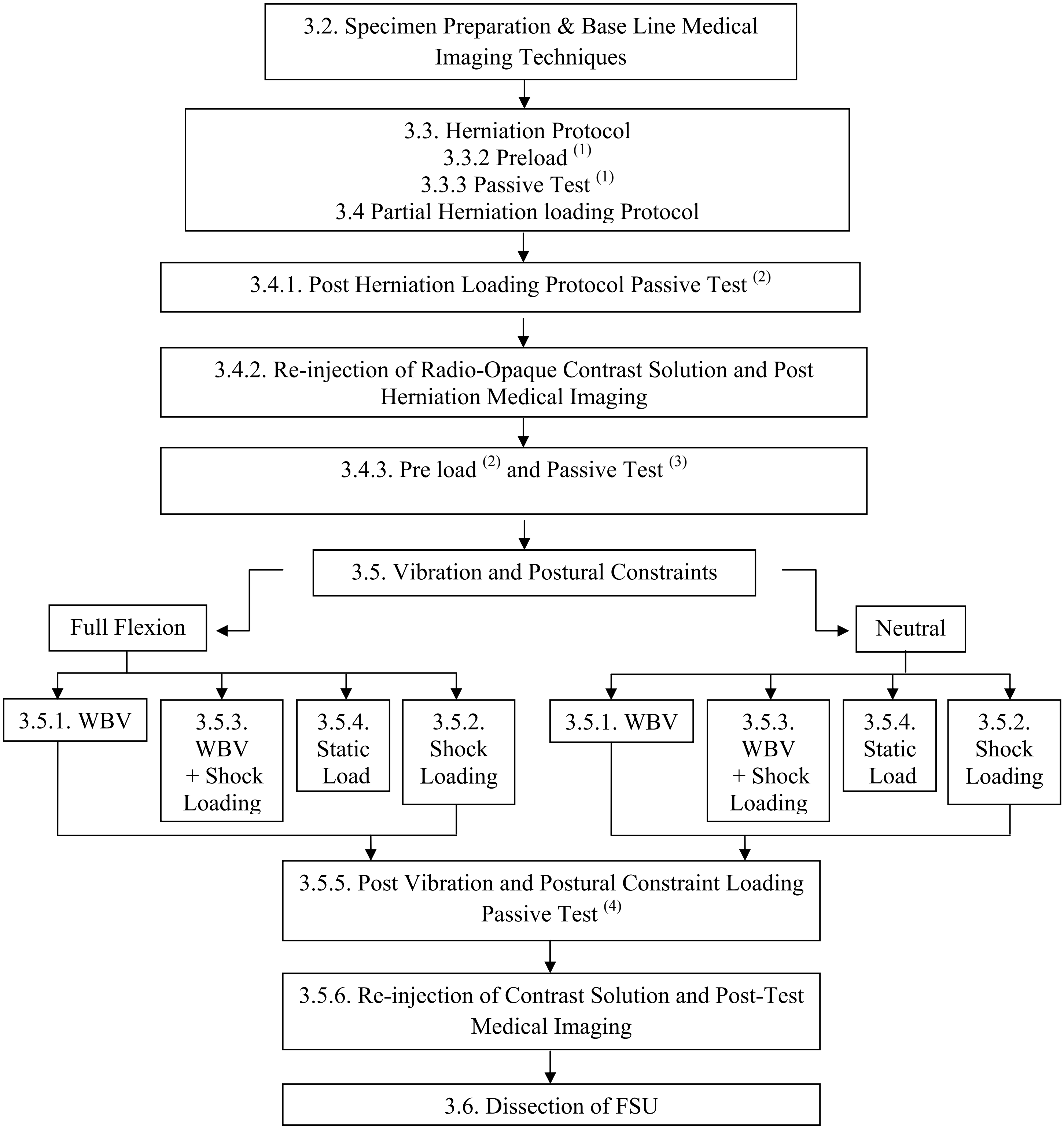

Figure 15: Experimental Methods

3.2. Specimen Preparation and Baseline Medical Imaging Measures

A porcine cervical spine model was employed for this investigation. Work by several researchers has indicated that porcine cervical spines are a close approximation to the human lumbar spine in anatomical, functional, and biomechanical characteristics (Yingling et al. 1999; Oxland et al. 1991). In addition, the porcine model offers the distinct advantage of providing a homogeneous population of specimens that control for age (mean age 6 months), weight (mean weight 80 Kg), genetic makeup, diet, and activity level. It has been noted by McGill (2007) and Dolan (1995) that degenerated intervertebral discs (IVD) are unlikely to herniate as they lack the required hydraulic pressure to force the NP through the layer of the AF, due in part to the loss of IVD height (and the associated loss of NP volume) linked to the degeneration process. The porcine cervical spines employed by this investigation were screened using the scale proposed by Galante (1967) to assess the level of degeneration in the IVD. Only specimens that meet the grade 1 criteria were used by this investigation, thus ensuring the specimen sample represented a non-degenerated cohort of porcine spines, which had a higher potential to incur IVD herniation.

In total 32 porcine spines were obtained from a common source (local abattoir) for this investigation, and were frozen to -20°C in doubled polyethylene bags and stored prior to the testing procedures. The frozen spines were thawed for 14-16 hours prior to the testing procedures at room temperature (23°C). Porcine spines were then dissected into two functional spinal units (FSU) per spine resulting in a C3-C4 and C5-C6 segments. Note that a FSU was defined for this investigation as two vertebral bodies and the intervening IVD. Both the C3-C4 and C5-C6 FSUs were used for this investigation, resulting in a total specimen population of N = 64 with N=32 C3-C4 FSUs and N=32 C5-C6 FSUs. The entire specimen population (N=64) was exposed to the partial herniation loading protocol as described in more detail below. However for post herniation loading exposures, each FSU was randomly assigned to one of the 8 possible vibration and posture constraint loading scenarios (1 - Neutral Posture and WBV, 2 - Neutral Posture and Shock 3 - Neutral Posture and WBV with the addition of Shock Loading, 4 - Neutral Posture and Static Compressive Load, 5 - Full Flexion and WBV, 6 - Full Flexion and Shock 7 - Full Flexion and WBV with the addition of Shock Loading, 8 - Full Flexion and Static Compressive Load) resulting in N=8 FSUs in each vibration and posture loading group with N = 4 of each of the C3-C4 and C5-C6 FSUs in each group.

The musculature surrounding each FSU was carefully trimmed away leaving only the osteo-ligamentous structures intact. Finally, the superior and inferior portions of the anterior processes were trimmed and the exposed superior and inferior facet joints of the FSU were removed to allow for fixation of the FSU to two custom built cups (made of high density polymer to facilitate the use of CT imaging). The area of the endplate at the level of the IVD was estimated via an established method involving the calculation of the area of the superior and inferior exposed endplates using the formula of an ellipse ($\pi/4 * A * B$), where A is the length of the exposed endplate in the anterior-posterior direction, and B is the length of the endplate in the medial-lateral direction. The average of the superior and inferior exposed endplate was used to represent the endplate area at the level of the undisrupted IVD (Callaghan and McGill, 2001, 1995; Parkinson et al. 2005; Yingling et al. 1999).

Specimens were then fixated into the custom fabricated cups with an outer aluminum ring and a high density inner plastic portion that was removable through a series of screws. The fixation procedure employed two large aggressively threaded screws and heavy gauge zip ties with a length of 203mm, a width of 3.6mm, and rated to hold 40lb of pressure (commonly used to secure pipe fittings). High density plastic cups and plastic zip ties were used to facilitate the use of the CT scanner, as metal objects that pass through the x-ray beam during the imaging procedure would negatively affect the machines detector, in addition to decreasing the resolution of the images by creating beam hardening artifacts in the CT images. One screw was placed into each of the superior and inferior exposed endplate of the FSU, thus securing the superior and inferior aspects of the FSU to the cups. These screws passed through the back of the cups and into the exposed endplates, resulting in the depth of penetration into the FSU being controlled (never exceeded 10 mm in depth). The zip ties were wrapped bilaterally around the anterior process and lamina of both the superior and inferior vertebra of the FSU, pulled tight through the holes in the cups and tied off on the posterior of the cups (8 ties per specimen). To further secure the FSU to the cups, non-exothermic dental plaster (Denstone ®, Miles, South Bend, IN, USA) was poured around the FSU and covered the inferior portion of the inferior vertebrae, and the superior portion of the superior vertebral. Figure 16 presents a digital photograph of the fixation procedure and a digital x-rays (discogram) of a FSU fixated to the custom cups.

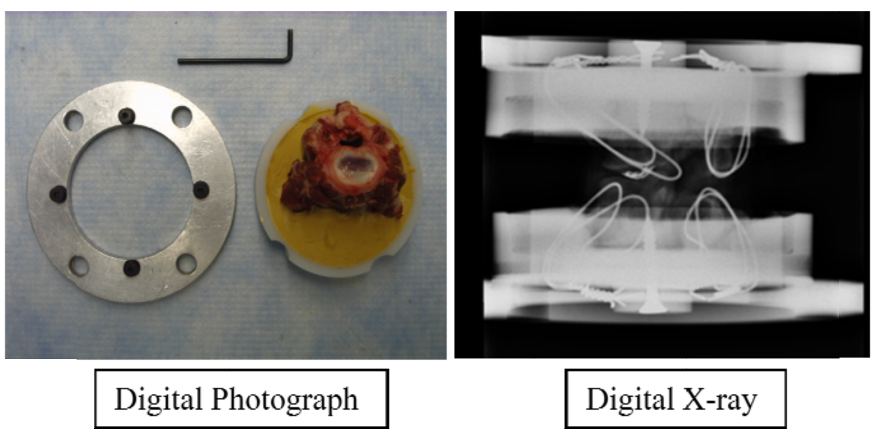

Figure 16: Digital photograph and digital x-ray (discogram) image of the FSU fixated in the custom cups. Note the digital photograph illustrates a specimen fixated into the inner removable high density plastic cup and the outer aluminum ring is also illustrated. Also note the concave surface of the inner ring, used to hold the dental plaster. On the digital x-ray note that 8 metal wires are visible in place of the zip ties used to hold the FSU to the cups to facilitate the visualization of where the zip ties would be. Additionally note the large aggressively threaded screws placed in each of the superior and inferior vertebrae.

To facilitate the tracking of the NP as it herniated through and between the layers of the AF a custom mixture of solution was injected into the IVD of each FSU through the anterior wall of the AF using a 21 gauge needle after each specimen was fixated to the cups. The custom solution contained a total volume 0.55ml, composed of 0.4 ml of a radio-opaque contrast solution (Omnipaque ™ – General Electric Company, USA) used to identify IVD herniation via medical imaging techniques (digital x-rays and CT) and 0.15 ml of a custom blue dye mixture (Coomassie Brilliant Blue G-mix: 0.25% dye, 2.5% MeOH, 97.25% distilled water) used to identify herniations post FSU dissection procedures after the testing protocols. This solution was injected until pressure was felt on the plunger of the needle. This resulted in some FSUs that were not able to receive the full 0.55 ml of solution. However, injection was ceased when pressure built up on the plunger to ensure the IVD was only minimally altered with respect to its fluid volume.

Post dissection, fixation and contrast solution injection, the FSU underwent pre-test medical imaging techniques to establish a baseline position of the NP in the IVD and to ensure specimens were not exhibiting any pre-existing damage. Pre-test imaging techniques consisting of sagittal plane film discograms and transverse CT scans in series. Sagittal plane film discograms were obtained of the FSU mounted in the plastic portion of the cups via a Mercury Modular X-Ray machine using the following setting (exposure time = 0.05 s, radiation exposure = 85 Kilovolts) and were viewed using a Kodak Direct View CR500 (Carestream, Toronto, Canada) viewing apparatus in a high quality DICOM format. To ensure each of the individual specimens was in the same position in relation to the x-ray beam emitter during subsequent x-rays and custom jig was fabricated to control rotation and X, Y positioning of the specimens mounted in the cups. Each x-ray cassette and the lower surface of the x-ray cabinet were marked.

This allowed each cassette to be placed in the same position (X and Y directions) within the cabinet, while the marks on each cassette allowed each specimen (set into the custom jig) to be placed in the same position (X and Y direction) on the cassette. The custom wooden jig prevented rotations of the specimens within the standardized X and Y positions. Only the bottom portion of the wooden jig had a standardized marked position on the cassette. This ensured each specimen could be imaged with the degree of lordosis it was fixated to the cups in (Figure 17).

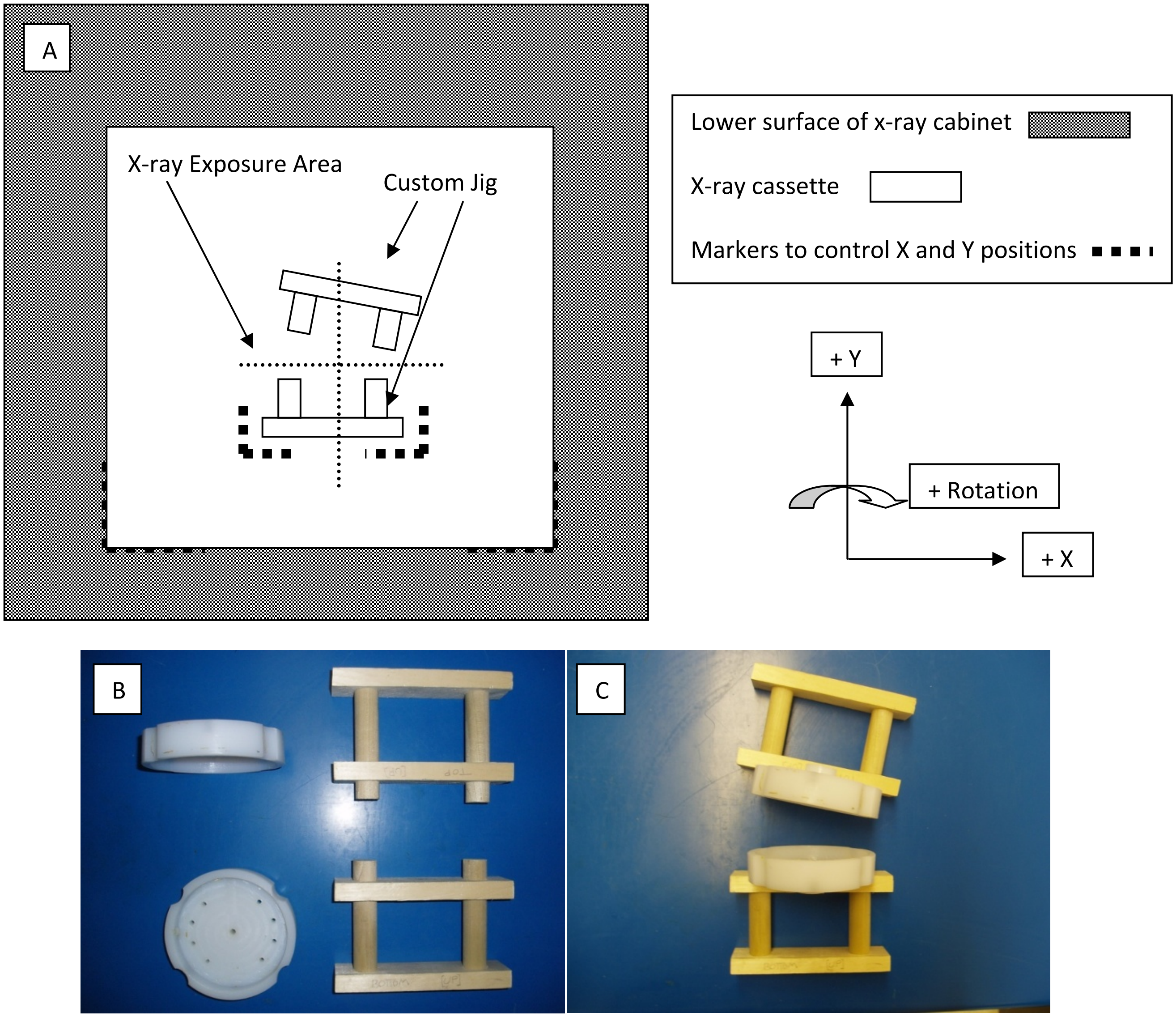

Figure 17: A – stylized representation of how the X and Y position orientations were controlled. Note the x-ray cassette in its position on the lower surface of the x-ray cabinet, and the stylized custom wooden jig in its position on the x-ray cassette. B – Digital photograph of the plastic portion of the cups where the spine would be mounted and the wooden jig. C – Digital photograph of the plastic cups resting on the wooden jig to control for rotation of the specimens mounted within the cups.

Previous work has indicated that sagittal discogram images alone were not ideal to detect IVD herniations (Tampier et al. 2007; Gordon et al. 1991; Deyo et al. 1990). Therefore CT images were also obtained of the FSU in an attempt to increase the efficacy of the identification of the IVD herniations. Pre-test CT images were produced using a pQCT Scanner (XCT 2000 Research Plus, Stratec Medizintechnik GmbH, Germany) illustrated in Fig 18, and consisted of serial transverse slices of the FSU from the inferior endplate to the superior endplate to capture the entire height of the IVD. Each serial transverse slice consisted of 15 images taken at 12 degree increments within the gantry of the XCT 2000 system. A custom jig was fabricated to hold the plastic portion of the cups inside the opening in the gantry of the CT scanner during the medical imaging procedure. The scout view scan (scan speed of 40 mm/sec) was used to determine the approximate position of the IVD (visible through the radio-opaque injection) in each specimen. CT images were obtained of each specimen while fixated in the plastic portion of the cups. Pilot testing indicated that 8 serial transverse slices at a thickness of 1.1 mm were sufficient to achieve imaging for the entire IVD, and that a voxel size of 0.2 mm produced high quality images in a reasonable amount of time with a scan speed of 10mm/s. CT images were viewed and converted into jpeg format using a public domain NIH Image program, Image J (developed at the U.S. National Institutes of Health and available on the internet at http://rsb.info.gov/nih-image/.)

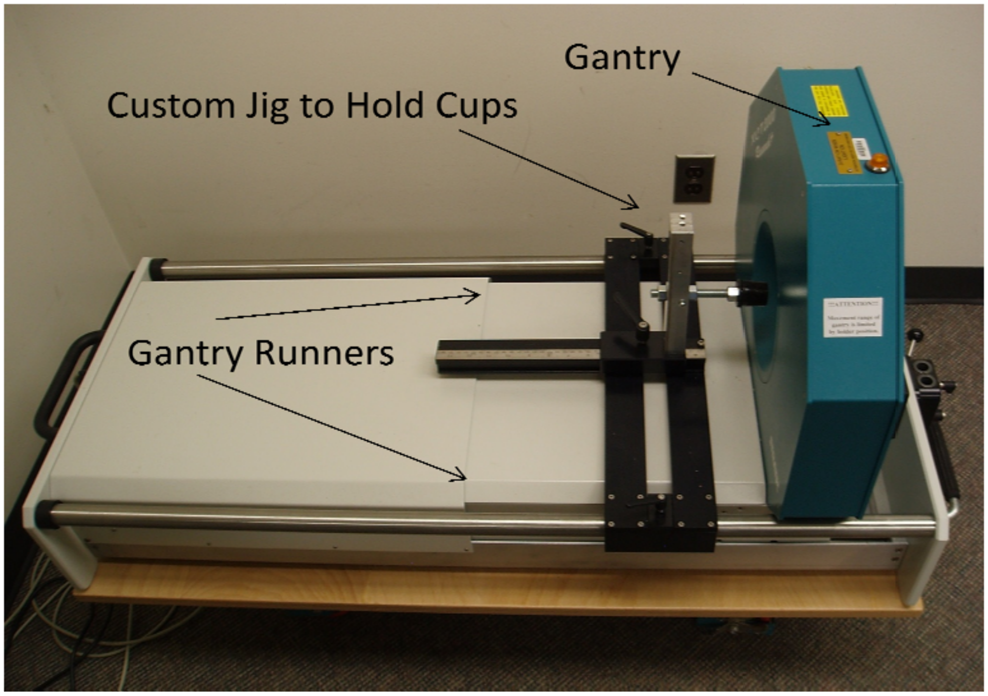

Fig 18: Illustration of the XCT Research Plus Computed Tomography scanner. Note the position of the gantry where the x-ray emitter and detectors are located, and the custom jig used to hold the cups containing the specimens during the image acquisition procedure. The gantry can slide along the runners indicated in the illustration to move along the specimens.

3.3. Herniation Protocol

3.3.1. Description of Equipment

Following the dissection of each porcine spine into two FSUs, the injection of the contrast solution, fixation of the FSU to the cups, and the pre-test medical image stage the FSUs were put through a well established IVD herniation protocol. The herniation protocol was developed by and shown to reliably produce IVD herniations in the porcine spine model by Callaghan and McGill (2001) and had been employed by other investigators (Aultman et al. 2005; Drake et al. 2005; Tampier et al. 2007). Briefly, a servo hydraulic dynamic testing system (Instron Canada, model 8511, Burlington, Ont., Canada) delivered axial compressive loading to the FSU fixated in the cups. Congruently a custom servomotor system (model BNR3018D, Cleveland Machine Controls, Billerica, MA, USA) and a 40:1 planetary gear head (model 34PL0400, Applied Motion Products, Watsonville, CA, USA) was used to deliver flexion and extension torques and was controlled by a software package (Galil Motion Control, Mountain View, CA, USA). Figure 19 illustrates the servo hydraulic dynamic testing system and the custom servomotor and their orientation to each other in addition to indicating which direction they apply loading and forces to the FSUs.

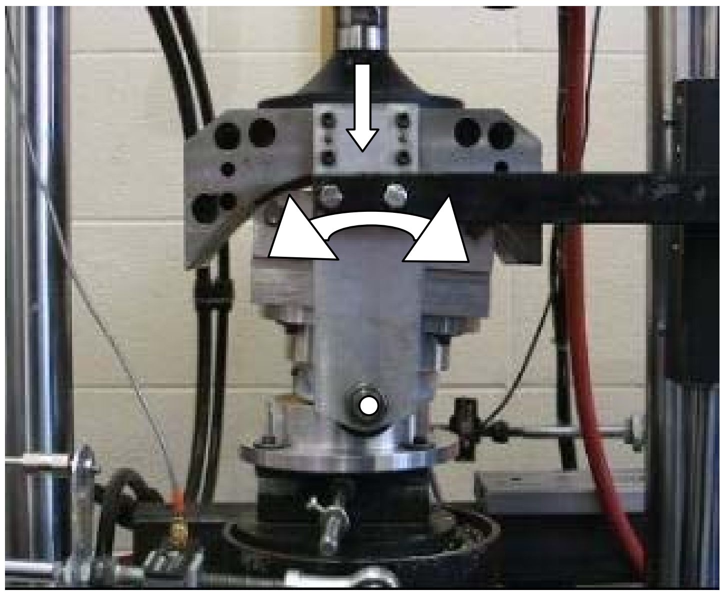

Figure 19: Digital photograph of the servo hydraulic testing system (Instron) and the servomotor. Note at the top of the photograph is the ram used to apply the axial compressive load to the FSU by the Instron. The servomotor is located directly behind the FSU mounted in the cups and attached at the level indicated with the white circle to the carriage used to bring the FSU through cycles of flexion and extension. Arrows on the photograph indicate the direction of load applied by the Instron ram and the anatomical motions of flexion and extension as a result of the moments produced by the servomotor system.

3.3.2. Preload (1)

The first step in the herniation loading protocol was to reverse the effects of swelling that occurred in the FSU post-mortem. This was accomplished by applied a 0.3KN axial compressive load using the Instron for a period of 15 min, during the initial preload phase [preload (1)] the servomotor system was programmed to find the position of zero torque about the flexion/extension axis. This position was taken as the neutral position of the FSU and corresponded to a position of elastic equilibrium for each specimen. Angular displacement (deg), axial compressive load (N), torque (Nm), and vertical position (mm) were A/D converted and sampled at a rate of 15 Hz throughout the preload procedure. The measurement of vertical position (mm) post preload procedure was used as the baseline to assess the specimen height changes that occurred throughout the partial herniation loading procedure in this investigation.

3.3.3. Passive Test [(1)]

Following the preload protocol, each FSU was subjected to a passive test procedure. The axial load placed on the FSU was increased to 1.5 KN and this force was applied by the Instron as in the preload. The servomotor system generated flexion and extension torques at a rate of 0.5°/s that resulted in the FSU being taken through the anatomical motions of flexion and extension. The profile of the torque versus angular rotation was plotted during the passive test at a sampling rate of 15 Hz. This profile was used to determine the point where the torque versus angular position curve deviated from linear into an exponential relationship for the motions of flexion and extension (Figure 20). Five repeats of the passive test were preformed to levels of angular rotations and torques just above the threshold for the linear torque versus angle curves to establish the flexion and extension angles to be used in the dynamic partial herniation protocol. Angular displacement (deg), axial compressive load (N), flexion/extension torques (Nm), and vertical position (mm) were A/D converted and sampled at a rate of 15 Hz through the preload procedure. The initial passive test [passive test [(1)]] procedure was used to establish a baseline average stiffness value using the methods of Drake et al. (2005) for each of the FSUs. The relationship that stiffness (Nm/deg) is equal to the applied moment or torque (Nm) divided by the angular rotation (deg) was used to calculate stiffness's. The target moment or torque and the corresponding angle (at the points of transition from the linear to exponential) were found at the point where the FSU moved out of the neutral zone in flexion and extension for the last three repeats of the passive test; as load-displacement curves have been shown to stabilize and be more consistent after two repeats (Dhillion et al. 2001). Each of the last three repeats of the passive test was split up into separate curves. A straight line was fit between the end points of each of these curves (the target torque and corresponding angle) and the slope of this line was taken to represent the average stiffness of the FSU for that repeat of the passive test. The averages of the three slopes (representing average stiffness values) were obtained and used to quantify the stiffness parameter (Figure 21).

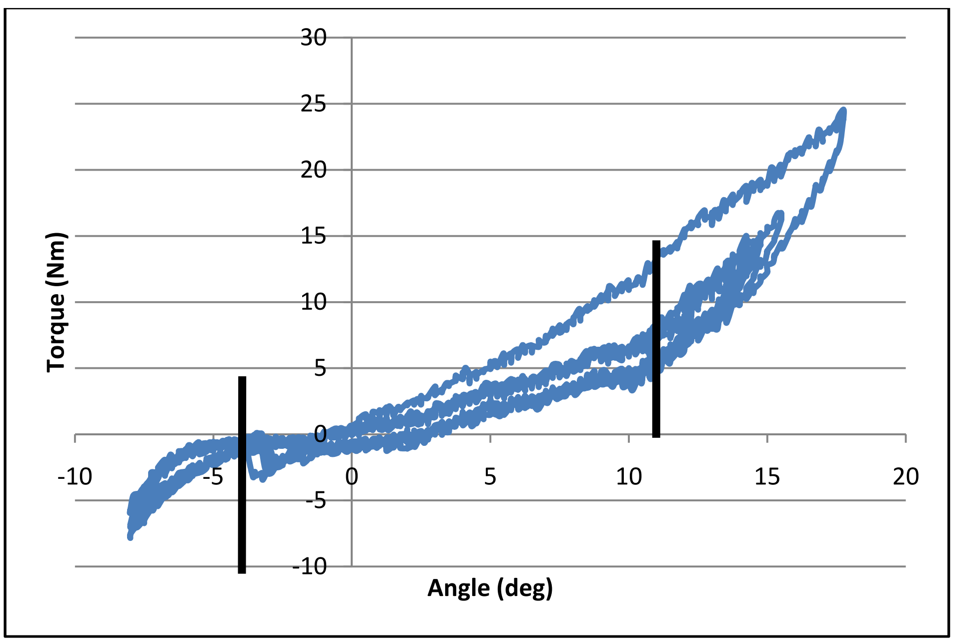

Figure 20: Plot of a typical angle (deg) versus torque (Nm) curve sampled during the passive test procedure. Angle 0 degrees was found during the preload procedure, while positive angles represent anatomical flexion of the FSU and negative angles represent anatomical extension. The elbow (point where relationship moves from linear to exponential) on the angle versus torque curve were chosen to define the boundaries of the neutral zone for each FSU. The approximate elbow of the curve is indicated by the black vertical lines.

The subsequent passive tests [passive test (2) – (4)] occurred throughout the procedure and employed the same methods used by Drake et al. (2005) to assess stiffness after various loading protocols. Briefly, under 1.5 KN of load this method drives the FSU to the target torques or moment as defined in the initial passive test [passive test (1)]; the point where the linear relationships becomes exponential. The angle at this target torque is used in conjunction with the relationship that stiffness equals the moment (or torque) in Nm/deg divided by the angular rotation in degrees to calculate average stiffness values. The target torques and corresponding angles in flexion and extension for the last three repeats of the passive test were plotted, their slopes found and the mean of these plots were used to represent average stiffness. Alternatively, the FSU could be driven to the target angle (the point where the linear relationships becomes exponential) and the torque recorded. However, since the FSUs are expected to become stiffer during prolonged loading (Callaghan and McGill 2001; Drake et al. 2005; Scannell and McGill 2009) driving to the target angle could produce torques that would damage the specimens.

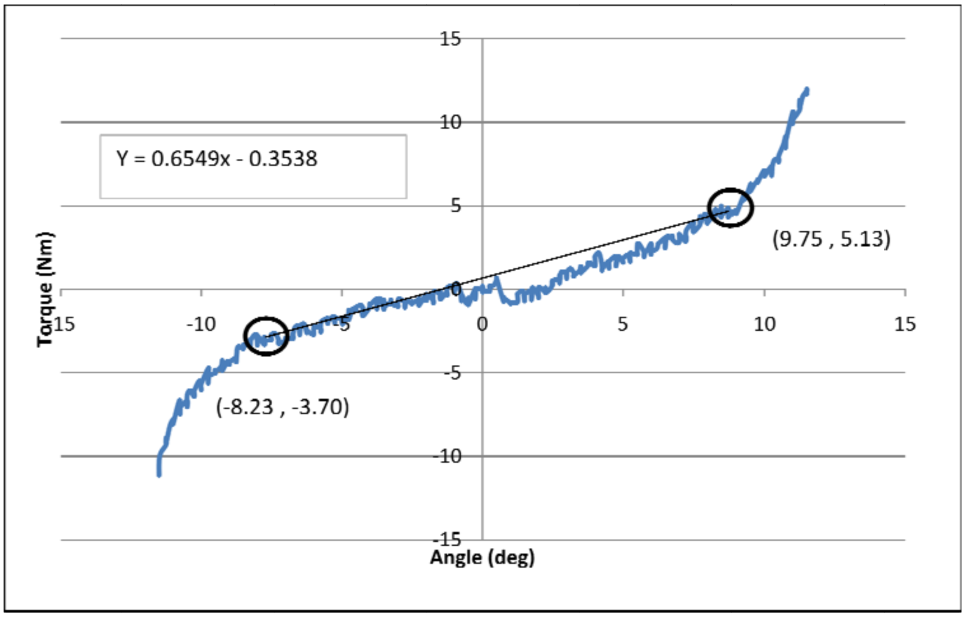

Figure 21: One repeat of a flexion/extension passive test using the defined torques and the angle endpoints to generate a straight line. Note the target torque and corresponding angle in both flexion and extension are used to plot a line to find the average slope (stiffness in Nm/deg) for the last three repeats of a passive test.

3.4. Partial Herniation Loading Protocol

The entire specimen population (N=64) was exposed to the partial herniation loading protocol. Axial compressive load on the FSU was keep at 1.5 KN while the servomotor system was programmed to flex and extend the FSU under position control to the angular displacements specified from the passive test procedure [passive test [(1)]] at a rate of 45°/s. The FSUs were subjected to 7000 cycles of flexion and extension at a rate of 1 Hz while under the axial compressive load. Angular displacement (deg), axial compressive load (N), flexion/extension torque (Nm), and vertical position (mm) were A/D converted and sampled at a rate of 15 Hz throughout the partial herniation protocol. The vertical position was found for each specimen in its neutral position (0 degrees angular displacement) after the herniation protocol and was compared to the baseline FSU height measurements taken after the preload [(1)] procedure to quantify specimen height changes as a result of the partial herniation loading protocol.

Pilot work using the porcine model and this loading protocol in addition to the medical imaging techniques (discograms and CT images) and FSU dissection procedures had indicated that this loading protocol would reliably produce partial herniations (Yates et al. 2008; 2009). Partial herniations will be defined by this investigation as done by Tampier et al. (2007); displacement of NP material into the AF fibres, but this displacement had not breached the outer layer of the AF fibres, resulting in a herniation that is contained in the disc space as defined by Fardon and Milette (2001). The pilot investigation produced 18 herniations out of the 22 specimens subjected to the loading protocol (81.81%). Of these 18 herniations 17 could be defined as partial herniation (94.44%) with 1 specimen illustrating a full herniation (5.56%); the NP was seen against the posterior longitudinal ligament, and had progressed through all the layers of the AF. Four specimens from the pilot study did not herniate during the loading protocol, representing 18.19% of the entire specimen pool (Yates et al. 2008; 2009). Therefore the post dynamic partial herniation procedure has the potential to produce three groups of FSUs (three categories of herniation), those without an IVD herniation (but with probable delamination of the annular fibres), those FSUs that have a partial herniation, and those FSU where a full herniation had occurred. All specimens, regardless of which of the three types of post partial herniation loading protocol damage categories they displayed, were put through all the procedures post partial herniation loading protocol.

3.4.1. Post Partial Herniation Loading Protocol Passive Test $^{(2)}$

All FSUs that have undergone the partial herniation loading protocol were subjected to a second passive test [passive test $^{(2)}$] to quantitatively assess how the stiffness of the FSUs had changed as a result of the partial herniation loading protocol. As in the initial passive test 5 repeats of the angle versus torque curve were produced in flexion and extension to a level just outside the neutral zone (where the angle versus torque curve begins to deviate from linear), and the same calculation described in the section 6.2.3. Passive Test (1) was preformed resulting in an average stiffness value. The difference between the post partial herniation loading protocol passive test (2) and the initial passive test (1) was used to quantify the average stiffness changes as a result of the partial herniation loading protocol.

3.4.2. Re-Injection of Radio-Opaque Contrast Solution and Post Herniation Medical Imaging

Pilot testing has indicated that a substantial proportion of the Omnipaque diffuses across the endplates of the IVD of each FSU, as was evident from a decreased contrast in the medical imaging procedures post-dynamic partial herniation protocol. However, the same pilot work has also indicated that the Omnipaque does not diffuse across the AF layers unless sufficient mechanical insult has occurred to lead to the process of NP tracking through the AF in a herniation. Proof of this statement comes from the findings that 4 of the 22 specimen's loaded in the pilot investigation illustrated no herniation after the partial herniation loading protocol was applied and the radio-opaque Omnipaque was re-injected (Yates et al. 2008; 2009). Additionally, a few specimens were repeatedly imaged using x-ray radiology (discograms) and CT images during the partial herniation procedure and Omnipaque absorption was confined to the endplate area of the IVD. In order to increase the contrast and quality of the medical imaging techniques to determine partial herniation, the FSU (still fixated in the cups) was removed from the Instron and 0.4ml of the Omnipaque was re-injected using a 21 gauge needle through the anterior wall of the AF into the IVD.

Medical imaging (sagittal plane film discograms and CT images) were taken of each FSU post dynamic partial herniation loading protocol with the same parameters as in the pre-test medical images stage. Image J in conjunction with the CT medical images was used to assess which categorical level of herniation the FSU had received; no detectable damage, partial herniation, or full herniation (Figure 22). The categorical damage level of each FSU was recorded for later use before the FSU was subjected to the next stage of the loading protocol.

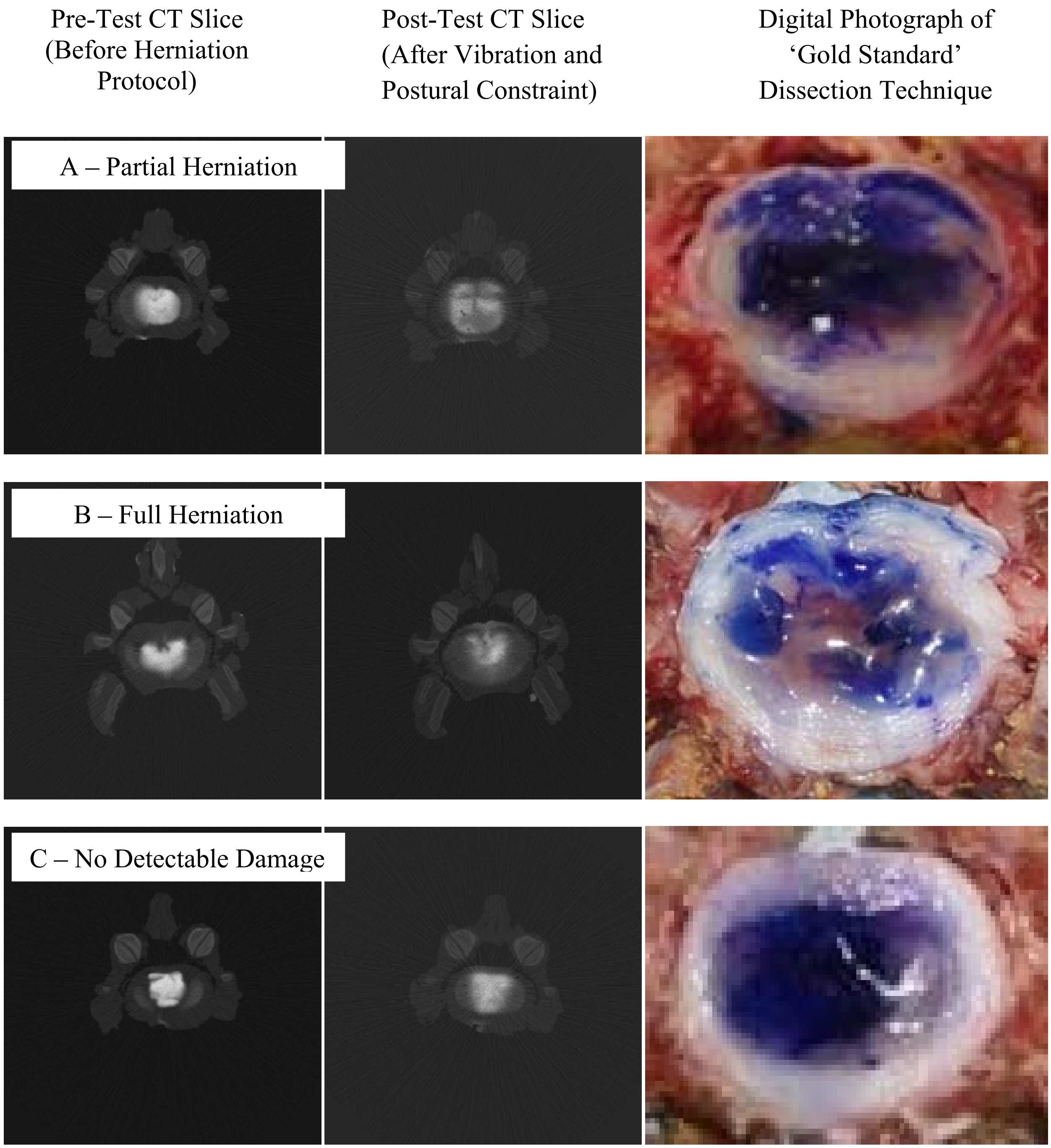

Figure 22: (A) Partial Herniation; note the progression of the nucleus pulposus has begun through the layers of the annulus fibrosus, but the farthest point of nuclear migration is contained in the outer to mid annular layers, and has not yet reached the vertebral foramen. (B) Full Herniation; the progression of the nucleus pulposus migration has breached the outer annulus fibrosus layers and nuclear material can be seen against the vertebral foramen. (C) No Detectable Damage; No migration of the nucleus pulposus can be seen.

A previous investigation allowed for the dissection of the specimens after the partial herniation loading protocol (herniations evident from blue dye tracking posterior / posterior lateral) to be compared to the medical images (CT scans and sagittal plane film discograms) where herniation can be seen through tracking of the radio-opaque dye. CT images were found to have high concordance (closely matched the geometric shape and categorical level of damage of the IVD herniation) to a dissection ‘gold standard’. Sagittal plane film discograms did not demonstrate concordance to a ‘gold standard’ dissection technique that was as high as the CT medical images technique. A trend was illustrated whereby and increase in the number of serial contrast enhanced CT scans in the CT procedure, lead to an increase in the concordance to a ‘gold standard’ dissection technique (Yates et al, 2009). The previous investigation (Yates et al. 2009) provided the required information to allowed the CT images to be considered the more effective imaging technique (had higher concordance to dissection) when compared to the discograms. Therefore, CT images were taken as the imaging ‘gold standard’ with which to determine IVD damage levels non-destructively in the current investigation.

3.4.3. Preload (2) followed by Passive Test (3)

The FSUs (still fixated in the cups) were re-mounted in the Instron for this stage of the procedure. A preload procedure [preload (2)] was repeated to load specimen using the same loading parameters as done in the initial preload before the partial herniation loading protocol. However, this new preload will not re-establish the neutral zone, rather it will consists of the preload force (0.3 KN compression) applied for 15 minutes in the neutral position as established via preload (1). All FSUs that have undergone the partial herniation loading protocol and subsequent re-injection of radio-opaque solution were subjected to a third passive test [passive test [(3)]] to quantitatively assess how the average stiffness of the motion segment had changed as a result of the herniation and re-injection protocol and to re-establish a baseline average stiffness value for vibration and postural constraint loading protocols. As in the initial passive test 5 repeats of the torque versus angular rotation curve were produced to the point of deviation from linear in the angle versus torque relationship, and the same calculation that were done in previous passive tests were performed resulting in an average stiffness values.

3.5. Vibration and Postural Constraint Loading

Once the partial IVD herniations had been produced and classified by herniation type (no detectable damage, partial herniation, or full herniation) with the aid of CT medical imaging techniques, the FSUs were subjected to complex loading parameters designed to assess the effects of WBV, shock loading, static load, and the combination of WBV and shock in two postural constraints (full flexion and neutral) on the progression on the IVD herniations at the three stages of IVD disc damage. The two postural controls implemented by this investigation were neutral lordosis as found by the initial pre-load procedure [preload [(1)]], or in full flexion as found by the maximal flexion angle in the initial passive test [passive test [(1)]] procedure representing the end of the linear angle versus torque relationship. Each of the postural considerations had four separate loading parameters associated with it consisting of WBV, shock, WBV with the addition of shock loading, and a static loading condition. Therefore, there were eight possible loading parameters (or groups) that the FSUs could be exposed to post partial herniation loading protocol. It is important to note that each FSU was only subjected to one of the below loading conditions.

1- Neutral posture and WBV

2- Neutral posture and shock

3- Neutral posture and WBV with the addition of shock loading

4- Neutral posture and static compressive force

5- Full flexion posture and WBV

6- Full flexion posture and shock

7- Full flexion posture and WBV with the addition of shock loading

8- Full flexion posture and static compressive force

WBV and shock loading data were obtained Milosavljevic et al, (2008a, 2008b, personnel communication) from a representative sample of sheep famers in New Zealand. Their research had indicated that the farmers spend a substantial proportion of their working day (approximately 90 minutes) operating All-Terrain Vehicles (ATVs). WBV data during ATV usage was collected from 12 farmers in accordance with the ISO 2631-1 standards for WBV data collection. A tri-axial accelerometer contained in a rubberized seat pad was placed on the seat of the ATV. Each farmer was instructed to ride their ATV for 20 minutes on a route that represented the typical terrain they would experience during a day's work operating the ATVs. The tri-axial accelerometer collected data in three directions Z (superior – inferior), X (anterior – posterior) and Y (lateral) at a rate of 200Hz while employing a 100 Hz anti-aliasing filter over the frequency range of 0 to 100 Hz. Shock loading was quantified using the ISO 2631-5 guidelines for the collection of mechanical shock loading parameters. Again, the X, Y and Z direction loading was collected at 200 Hz with the same anti-aliasing filter set with a cutoff of 100 Hz. This method was used to assess the exposure to mechanical shock loading on 30 farmers asked to ride there ATVs on ground that was representative of their daily route. Average riding time for the assessment of mechanical shock was 100.39 min with a minimum of 13.60 min collected for one farmer, and a maximum of 215.00 min collected for one farmer. A data base was complied containing the resulting acceleration (m/s^2) that was associated with each mechanical shock larger than 1g for each of the X, Y, Z directions (Milosavljevic 2008 personnel communication)

Analysis of the WBV data collected from the farmers indicated that a typical maximal acceleration of 2.37 m/s^2 occurred during WBV at a frequency of 4 Hz in the Z direction. Shock loading data over the 30 farmers was analyzed to assess the worst case scenario regarding exposure to mechanical shock loading in the Z direction. It was determined that the typical ATV operation of the farmers over one day would subject them to a maximum of 2000 shock loading events over 1g, with magnitudes reaching 18.38 m/s^2 in the Z direction, detailed force time histories were obtained from the data. From these histories it was determine that a typical time from min – max force in a shock loading event of magnitude 18.38 m/s^2 would take approximately 0.035 seconds. Farming experience, ATV operation times and anthropometry measurements, including average whole body mass (86 Kg), were also obtained from the sample of the farmers (Milosavljevic et al. 2008 a, 2008 b; Milosavljevic 2008 personnel communication).

The Instron was used to load the FSU in the vertical direction. Unfortunately, the Instron ram used to load the FSU in axial compression was not able to replicate the accelerations produced by the WBV or shock loaded experienced by the farmers. As a result, the relationship F = (m * a) was used to calculate the force (N) that would be produced by the acceleration present in the WBV and shock loading exposures. Work done by De Leva (1996) had indicated that 49.1 % the total body mass of collage age males is above the L4/L5 level of the lumbar spine. Therefore, since the average mass of the farmers was known (86 Kg), and the percentage of mass above the

L4/L5 lumbar joint can be found, estimations as to the load produced by the accelerations and mass of the farmers at the L4/L5 lumbar joint can be calculated for both the WBV and shock loading exposure. This force was then added to the estimated static force created by the average body mass above L4/L5 to estimate the total force at the L4/L5 lumbar spinal segment during vibration exposure. The force time histories of the forces experienced at the L4/L5 lumbar spinal level of the ATV operators were matched using the Instron, therefore applying the same forces to the FSUs. Below is an example of this calculation for the WBV loading parameter using the maximal acceleration of 2.37 m/s^2 in the positive and negative directions in the Z axis to calculate approximate forces on the L4/L5 joint. Shock loading of the FSUs occurred with forces that ranged from the approximate upper body mass of the ATV operators to the maximum compressive force due to the acceleration. Shock loading exposure magnitudes did not drop below the approximate upper body mass in an attempt to accurately reproduce the force-time histories regarding time from min-max force in shock loading exposures. By including a drop in the force below the approximate upper body mass in shock loading, the time from min-max force would have been increased while the overall range of the forces would also have increased. As a result of this time and force range increase the Instron's hydraulic system was not capable of providing forces with the ramp speeds required (output loading time) that were fast enough to accommodate such force changes over such a small time change. Therefore, in an effort to match the ramps seeds to the shock exposures, the shock waveform was designed to load the specimens to a maximum force from the approximate mass of the upper body. Table 2 illustrates the summary of the vibration to force calculation for WBV, shock loading, and in the static compressive force conditions.

Sample calculation for WBV force magnitude determination

Given
$a_{max\ (WBV)} = 2.37\ m/s^2$
$a_{min\ (WBV)} = -\ 2.37\ m/s^2$
$g = 9.81\ m/s^2$

Average mass of the farmers above L4/L5 joint = Total body mass (of 86 Kg) * 0.491
= 42.23 Kg

Average static force (N) produced by mass above L4/L5 = mass above L4/L5 * g
= 414.24 N

Therefore, using the relationship that average total force acting on the L4/L5 joint is proportional to...
$F_{total\ (L4/L5)}$ = [Mass (above L4/L5) * acceleration] + (static force from body above L4/L5), the maximal and minimal forces can be determined.

Therefore, Maximal force at L4/L5 during WBV would be
$F_{total\ (L4/L5)}$ max = 514.33 N
$F_{total\ (L4/L5)}$ min = 314.15 N

Table 2: Calculation of loading parameters consisting of WBV, mechanical shock loading, and static compressive force to be applied to FSU. These loading parameters were calculated using the relationship (F = m * a) from known mass and acceleration data and represent the conversion of acceleration (m/s^2) to force (N) to allow loading parameters to be applied via the Instron control panel.

Loading Parameter	Acceleration (m/s^2)		Whole Body Mass (Kg)	Mass above L4/L5 (Kg)	Force (N)	
	Max	Min			Max	Min
WBV	2.37	-2.37	86.00	42.23	514.33	314.15
Shock Load	18.38	1g *	86.00	42.23	1189.00	414.24*
Static Load	1g *	1g *	86.00	42.23	414.24*	414.24*

* Indicates force and acceleration values assumed to be due to body weight alone above L4/L5.

3.5.1. Simulating Whole Body Vibration loading

The WBV experienced by the farmers while operating their ATVs was simulated using a 4 Hz sine wave in the Z direction produced by the Instron for durations of 90 minutes (a full days riding). The set point of the load was of the magnitude 414.24 N (force from the upper body above L4/L5 alone), and the amplitude was 100.09N. This resulted in a sine wave with a max peak load of 514.33 N and a minimal peak load of 314.15 N. The PID (Proportion, Integrative, and Differential) parameters for the WBV 4 Hz sine wave were determined through manual loop shaping through the use of an oscilloscope and the Instron output channels. PID parameters were altered for the sine wave to account for the compliance of the FSU in the Instron mechanical system. Changes in the PID were made (P = 10, I = 1, D = 0.1) to maximize the response of the waveform in the Z direction. The result was the 4 Hz sine wave with a set point and amplitude described above that oscillated at a mean power frequency (MnPF) of 4.19 Hz. The WBV sine wave output closely matched the theoretical WBV sine wave input (Figure 23). Although data for the X and Y directions regarding acceleration were collected, and this information was converted into force (N) by the methods stated above, the Instron was not able to generate these forces in the X and Y directions during the WBV loading protocol. Therefore, the WBV occurred only in the vertical (Z) direction and can be equated to a cyclic compressive loading protocol. Angular displacement (deg), axial compressive load (N), flexion /extension torque (Nm), and vertical position (mm) were A/D converted and sampled at a rate of 15 Hz throughout the WBV loading parameters.

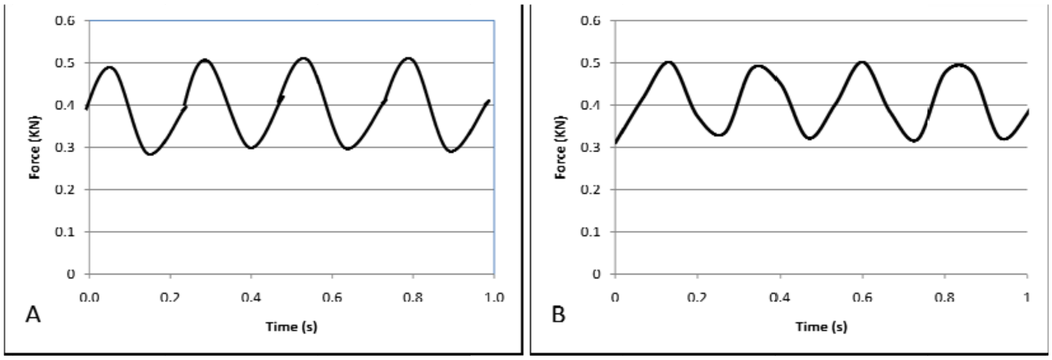

Figure 23: (A) Force-time history of the theoretical input WBV waveform where the sine waveform ranges from 314.15N – 514.33 N of compression with a set point of 414.24N and oscillates at 4 Hz. (B) Force-time history of the output WBV sine waveform implemented on the compliant FSUs. The sine waveform ranges from approximately 314.15 N – 514.33 N of compression with a set point of 414.24 N and has a MnPF of 4.19 Hz.

3.5.2. Simulating Shock Loading

The shock loading experienced by the farmers while operating their ATVs was simulated using a ramp waveform in the Z direction produced by the Instron. The specimens were exposed to a total of 2000 ramp waveforms to simulate 2000 mechanical shocks. The set point of the load for the ramp waveforms was 414.24 N (force from the upper body above L4/L4 alone). The ramp waveform was programmed to add 786 N of load (end point 1) to the set point load of 414.24 N resulting in approximately 1200 N of compression (to approximately the theoretical maximum of 1189 N from the acceleration to force calculation with respect to shock loading) at a rate of 240 KN/s (rate 1) and hold this new load for 0.05s (hold time 1). Following this, the ramp waveform was programmed to subtract the force added in end point 1 (786 N) from the new force on the FSU (1200 N) by specifying end point 2 at 1 N (represents the set point load of 414.24 N plus approximately 1 additional N of compression) at a rate of 240 KN/s (rate 2) and hold this force for 1 s (hold time 2). The ramp waveform was theoretically designed to mimic the force-time histories of the shock exposures. With this in mind, hold time 1 (representing the amount of time at the maximum load) should be almost zero, and both rate 1 and rate 2 should result in approximately 0.035s from the set point load (414.24 N) to maximum load (1200 N), and 0.035 s from maximal load (1200 N) back to set point (414.24 N) (Figure 24). Actual times from set point load to maximal load using the output ramp waveform with a compliant FSU in the system were found to be between (0.033 – 0.07)s, and therefore represent a close approximation of the force-time histories obtained from field data. To maximize the response of the ramp waveform, the PID parameters for the ramp waveform were determined through manual loop shaping through the use of an oscilloscope and the Instron output channels. PID parameters were altered for the ramp waveforms to account for the compliance of the FSU in the Instron mechanical system. Changes in the PID were made (P = 16, I = 1, D = 1.2) to maximize the response of the waveform in the Z direction. The shock waveform allowed for sufficient time between shock exposures so that the FSUs could re-establish most of the vertical displacement changes as a result of a single loading exposure, however cumulative height changes did occur due to multiple loading exposures (Figure 25). Although as with WBV data, X and Y accelerations that were collected and converted into force (N) by the methods stated above could not be implemented by the Instron as it was not able to generate these forces in the X and Y directions during the shock loading protocol. Therefore, the shock loading occurred only in the Vertical (Z) direction and can be equated to a high velocity cyclic compressive loading protocol. Angular displacement (deg), axial compressive load (N), flexion/extension torque (Nm), and vertical position (mm) were A/D converted and sampled at a rate of 30 Hz throughout the shock loading parameters.

A

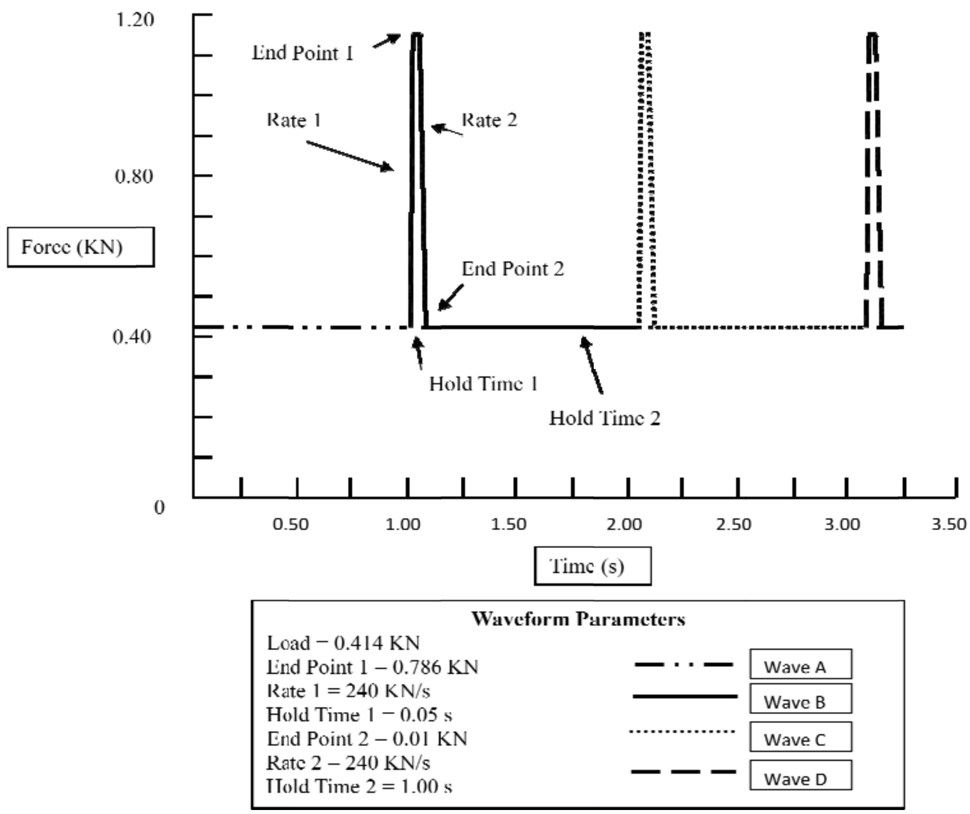

B

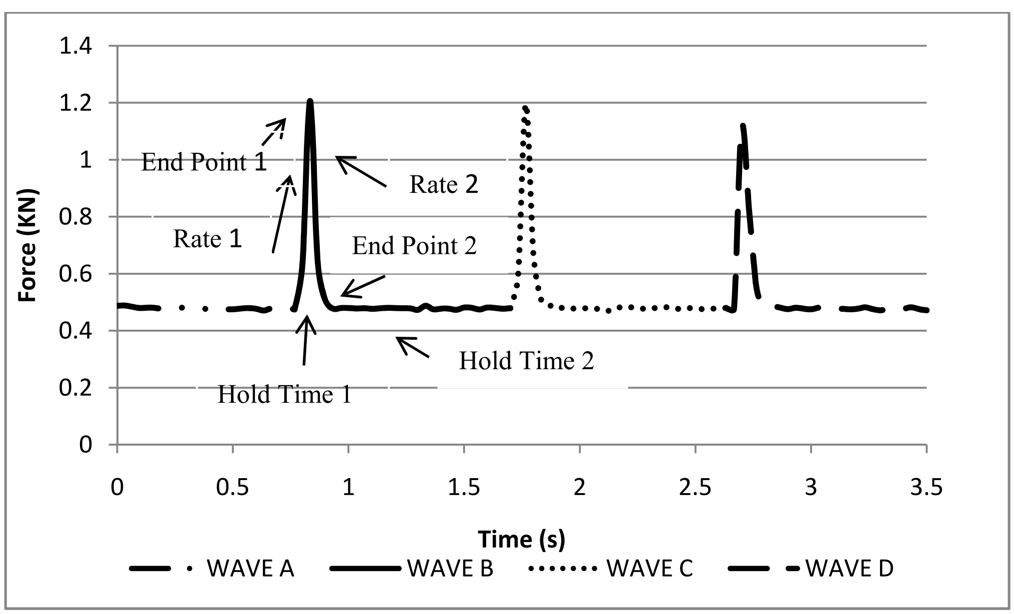

Figure 24: (A) Force-time history of the theoretical input ramp waveform to simulate shock. The ramp waveform ranges from 414.24N –1189N of compression with a set point of 414.24N. (B) Force-time history of the output ramp waveform implemented to simulate shock on the compliant FSUs. The ramp waveform ranges from approximately 414.24 N – 1189 N of compression with a set point of 414.24 N.

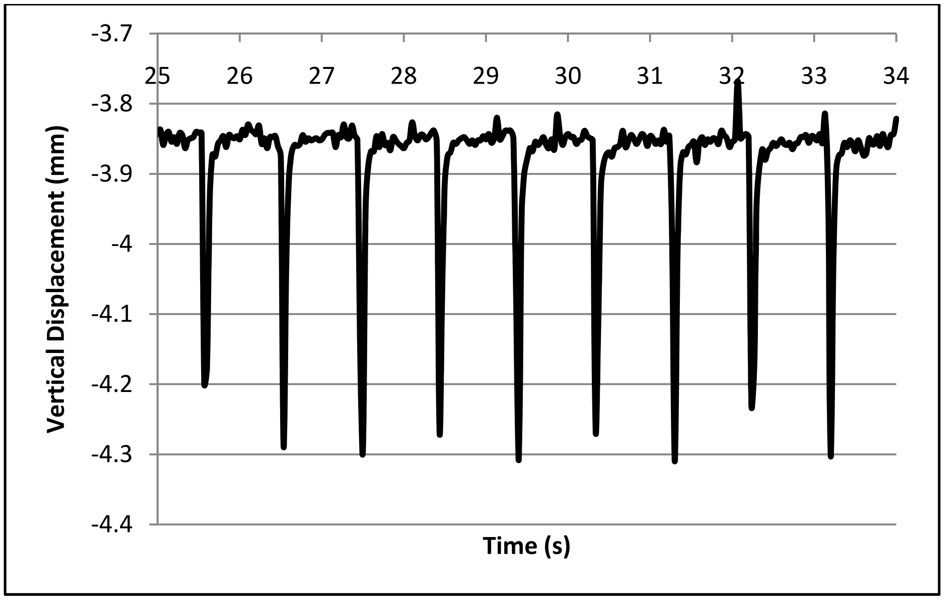

Figure 25: Displacement versus time graph of the shock waveform exposures. Note that the FSUs have sufficient time to allow re-establishment of most of the vertical displacements changes as a result of the loading exposures.

3.5.3. Simulating Whole Body Vibration Loading in Addition to Shock Loading

Shock load and WBV acceleration data (m/s^2) collected from ATV operation was converted to force measurement (N) parameters suitable for implementation by the Instron using the methods stated above. Shock loading was mimicked for this investigation by matching the force time histories from ATV riding and implementing a ramp waveform as previously described. WBV was simulated for this investigation by matching the force time histories from ATV riding and implementing a 4 Hz sine waveform. It was known that ATV operation for one day, resulting in a 90 minute riding time, was likely to expose the operator to 2000 mechanical shock loading events (over 1 G) while simultaneously exposing operators to WBV. This can be equated to 333.33 mechanical shock loading events per 15 minutes of WBV during ATV operation. However, the Instron can only display full cycles of the shock loading in real time so 5 blocks of 333.00 shocks over 15 min of WBV, and one block of 335 shocks over 15 min of

WBV were delivered to represent this exposure. WBV loading and Mechanical shock loading could not be delivered to the FSU simultaneously. Therefore to mimic exposure to WBV with the addition of shock loading, the FSUs were subjected to 15 min intervals of WBV and then subjected to 333 mechanical shock loading events or 335 mechanical shock loading events depending on the block number. This process was repeated 6 times until WBV exposure reached 90 minutes, and shock exposure reached 2000 cycles (Figure 26). Angular displacement (deg), axial compressive load (N), flexion/extension torque (Nm), and vertical position (mm) were A/D converted and sampled at a rate of 30 Hz throughout the shock loading parameters and at 15 Hz for the WBV parameters.

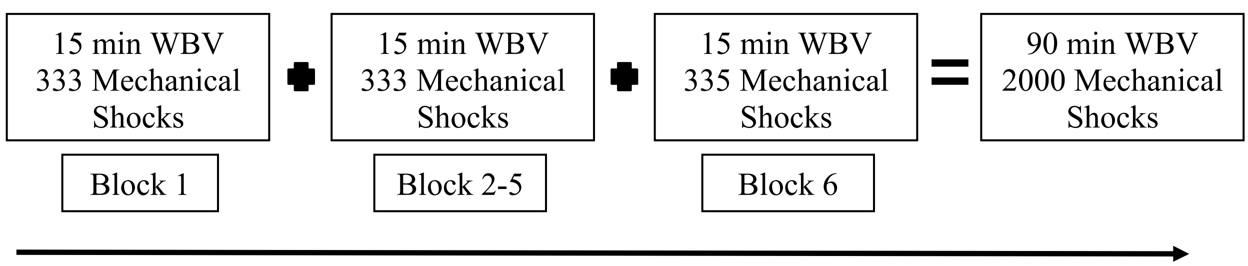

Figure 26: Illustration of the testing procedure employed to replicate WBV and mechanical shock loading. Note that this procedure resulted in 90 minutes of WBV exposures and approximately 2000 mechanical shocks, with blocks 1-5 being identical (15min WBV and 333 mechanical shocks) and block 6 loading specimens with 15 min WBV but 335 mechanical shocks.

3.5.4. Simulating Static Loading

Static loading parameters were designed to simulate sitting with the force of the upper body creating load on the L4/L5 joint of the spine. This loading parameter was designed to allow comparisons to be made between the vibration inclusive loading parameters (WBV and WBV with the addition of shock loading and shock loading alone) to a static non-vibration exposed sitting posture like that often adopted while performing deskwork. Muscular activation was ignored in the calculation of the static load force, in an attempt to mimic relaxed sitting. Static load was calculated as the force exerted by the average still upper body mass above the level of the L4/L5 spinal segment for the 30 farmers (42.23 Kg) and was converted into a force value by multiplying by gravity (9.81 m/s^2), resulting in a static compressive force of 414.24 N on the FSUs. Static load was applied through the Instron via an axial compressive force of 414.24 N in the Z direction for duration of 90 minutes (Figure 27). PID parameters were kept the same as in the WBV loading scenario (P = 10, I = 1, D = 0.1), as the compliance of the FSUs was not a large concern during this relatively low level prolonged static loading scenario.

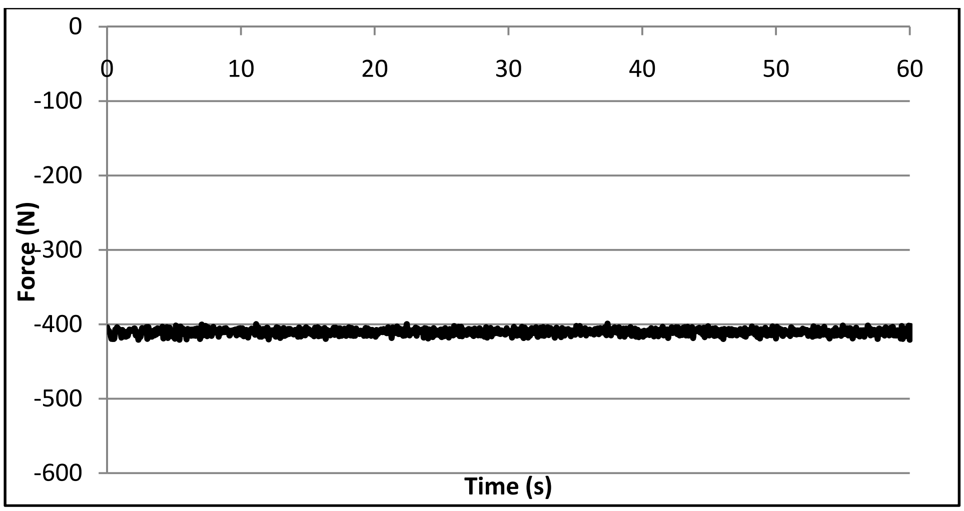

Figure 27: Force-time history of the static loading exposures. The compressive load level remained almost constant at 414.24 N. However, minor oscillations exist due to noise in the Instron mechanical control system.

3.5.5. Post Vibration and Postural Constraint Loading Passive Test [(4)]

Immediately following the exposure to one of the eight possible postural and vibration loading conditions that a FSU could be exposed to, another passive test [passive test [(4)]] was preformed. The post vibration exposure passive test used the same methods as previous passive tests to calculate the average stiffness of the porcine FSU post vibration and postural constraint loading exposure. Angular displacement (deg), axial compressive load (N), flexion/extension torque (Nm), and vertical position (mm) were A/D converted and sampled at a rate of 15 Hz throughout the procedure. Average stiffness changes due to the vibration and postural constraint loading protocols were quantified by finding the difference between passive test (4) and passive teat (3).The vertical specimen height changes just prior to passive test (4) were used on conjunction with the re-established baseline specimen height found in pre-load (2), to quantify the vertical specimen height changes as a results of the vibration and postural constraint loading protocols.

3.5.6. Re-Injection of Radio-Opaque Contrast Solution and Post Test Medical Imaging

In order to increase the contrast of the medical imaging techniques employed by this investigation, 0.4 ml of the radio-opaque contrast solution was re-injected through the anterior wall of the AF and into the IVD of each specimen still fixated in the custom plastic cups using a 21 gauge needle. Post vibration and postural constraint medical imaging (CT scans and sagittal plane film discograms) were performed to the same parameters as done for the baseline medical imaging assessment and for the post partial herniation loading protocol medical imaging assessment.

3.6. Dissection of FSU

The FSUs were removed from the custom cups and dissected with a single cut of a scalpel through the horizontal plane at the level of the intervening IVD. The dye that was present in the initial injection into the IVD had tracked along with the NP through the layers of the AF in the herniation process in those FSUs were disc damage was produced. Damage to the IVD was documented through digital photographs. Post dissection end plate area measurements were taken for use in calibrating distance measurements in Image J. A qualitative assessment was made regarding the concordance between the dissection photographs, sagittal plane film discograms, and the CT images in relation to their ability to detect partial IVD herniations.

3.7. Medical Imaging Data Reduction

3.7.1. Computed Tomography

CT images were required to be saved in the format produced by the CT scanner software (XCT, 2000 Research Plus) and viewed in Image J in order to effectively quantify the position of the NP within the IVD, and to categorically qualify the level of damage present. Once the CT images were opened in Image J they could be calibrated using a known distance (endplate area lateral distances as measured post dissection) to convert pixels into mm measurements. After calibration, the linear distance that the NP had progressed through the AF at each stage of the testing protocol (pre-test, post partial herniation loading protocol, post vibration and postural constraint loading protocol) were measured on a slice by slice basis using all 8 CT images obtained at each medical imaging stage in the investigation. Using all 8 of the CT images allowed for changes in the NP position to be quantified across the entire height of the IVD on a relative basis, although reductions in height after the loading protocols could result in fewer than 8 measurements being compared. Increased levels of disc damage were indicted by a shorter distance from the NP to the vertebral foramen; the point where the NP could penetrate the outer layers of the AF and bulge against the posterior longitudinal ligament resulting in a full herniation of the IVD. Figure 28 illustrates the distance measurements that were taken to quantify the extent of IVD damage as a result of this investigation's loading protocols. Measurements of the distance from the NP to the vertebral foramen (Δd) were taken using the linear measurement function in image J, and represent the shortest distance from the leading edge of the posteriorly migrating NP to the vertebral foramen.

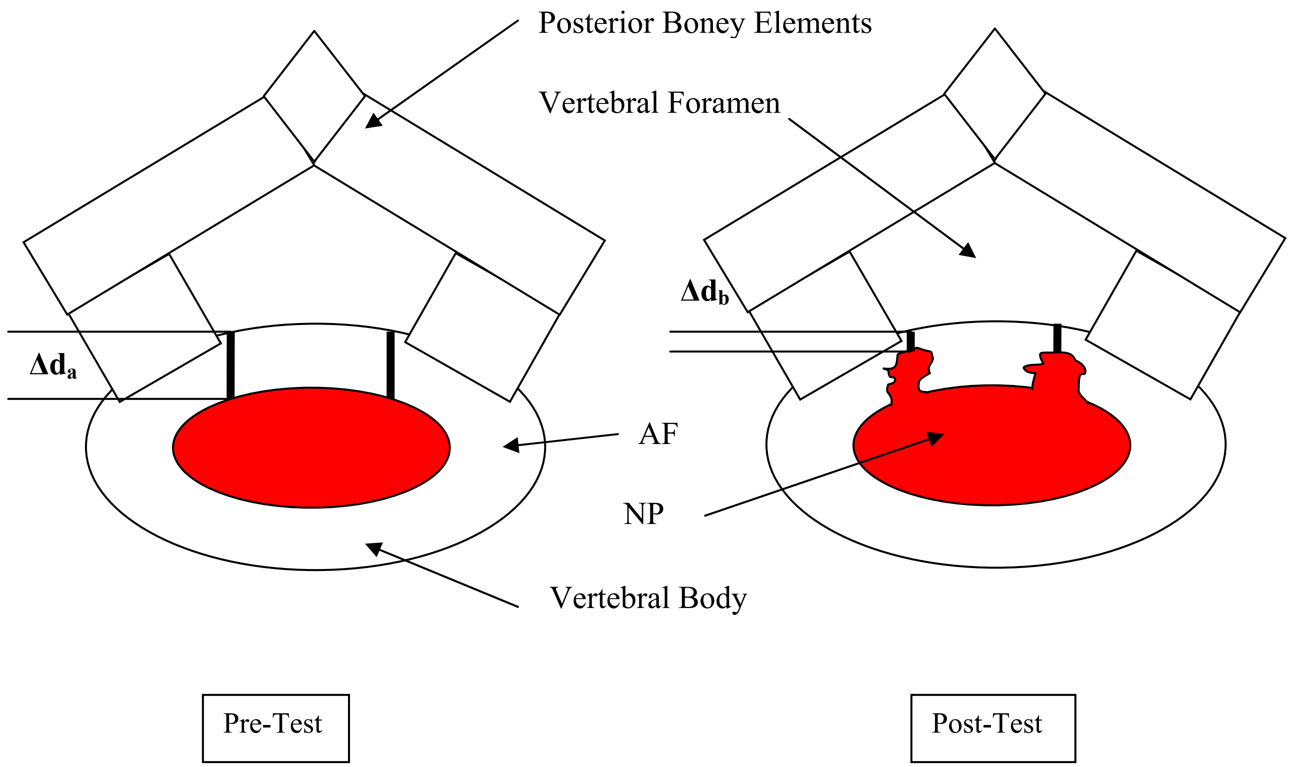

Figure 28: Illustration of a pre-test transverse CT image indicating the distance from the contained NP (by the inner walls of the AF) to the vertebral foramen. The measure (Δd_a) was used to establish the base line position of the NP within each FSU. In the pre-test image the shaded oval represents the area of the undamaged NP. The illustration of the post-test image indicates that the NP had begun to work its way through the AF (the IVD herniation process has begun) as can be seen by the decreased distance (Δd_b) between the NP that is between and within the layers of the AF and the vertebral foramen.

Measurements of the linear distance the NP had migrated through the AF and the calculation of the percentage of the total distance covered by the herniation (distance of tracking changes as a percent) were calculated as defined below. Quantitative comparisons were made between the baseline NP position and post partial herniation loading protocol position to assess the damage (NP migration) as a result of the mechanical insult to the FSUs produced by the herniation process. The most posterior position of the NP post vibration and postural constraint loading was compared to the most posterior baseline and most posterior post partial herniation loading protocols to quantify the increased level of damage (in relation to increased NP migration) as a result of the vibration and postural constraint loading protocols.

Linear Distance of Herniation

Where Δd is the distance from the NP to the vertebral foramen

$$\text{Linear distance of Herniation} = \Delta d_{(\text{post partial herniation loading protocol})} - \Delta d_{(\text{baseline measurement})}$$

Or alternatively (dependent upon the parameter of interest)

$$\text{Linear distance of Herniation} = \Delta d_{(\text{post vibration and postural constraint protocol})} - \Delta d_{(\text{post herniation loading protocol})}$$

Distance of Tracking (%) the NP has Progressed through the AF in Relation to Loading Protocol

$$\text{Distance of Tracking (\%) due to Herniation} = 1 - \left[\frac{\Delta d(\text{post partial herniation loading protocol})}{\Delta d(\text{base line measurement})}\right] * 100$$

Or alternatively (dependent upon the parameter of interest)

$$\text{Distance of Tracking (\%) due to Vibration} = 1 - \left[\frac{\Delta d(\text{post vibration and postural constraint loading protocol})}{\Delta d(\text{post partial herniation loading protocol})}\right] * 100$$

3.7.2. Categorical Damage Assessment

CT images were used to qualitatively assess how the categorical levels of IVD damage (no detectable damage, partial herniation, full herniation) progressed due to the vibration and postural constraint loading protocols. This assessment was done using the post partial herniation loading protocol CT images and the post vibration and postural constraint loading protocol CT images and the 3 categorical levels of IVD damage (progression). The following variables were assigned to each of the possible changes in the categorical damage assessment, and were used to implement statistical procedures described later in this investigation (Table 3).

Table 3: Variables qualitatively assigned to assess how the categorical level of damage to the IVD changed from the post partial herniation loading protocol CT images to the post vibration and postural constraint loading protocol CT images.

Variable	Categorical Damage Progression
W	No Detectable Damage – No Detectable Damage
X	No Detectable Damage – Partial Herniation
Y	Partial Herniation – Full Herniation
Z	No Detectable Damage – Full Herniation

3.7.3. Sagittal Plane Film Digital Discograms

Sagittal plane film discograms were not used to measure linear distances of herniation, or distance of tracking changes (%). Previous work had indicated that CT imaging was more accurate at detecting herniations and has higher concordance to a dissection “gold standard” than did sagittal plane film discograms (Yates et al. 2009). Therefore, CT imaging was used as the ‘gold standard’ with respect to non-invasive medical imaging techniques to quantify tracking changes in relation to the loading protocols implemented by this investigation However sagittal plane film discograms were used to further evaluate concordance between medical imaging type and a ‘gold standard’ dissection technique.

3.8. Calculation of Cumulative loading Exposures

Cumulative loading exposure magnitudes (MNs) were calculated for the partial herniation and vibration loading protocol using the force-time histories and discrete integration in Kin Analysis (University of Waterloo, Waterloo, Ont.) and peak loads (N) recorded. The estimated maximum compressive strength (N) for the FSUs in each of the 8 vibration and postural constraint loading groups and the partial herniation loading protocol were calculated using the estimated endplate area and the regression equation of Parkinson et al. (2005). The percentage of estimated maximum compressive strength (N) represented by each load used in this investigation was calculated to ensure the loads were below the 37.5 % maximum strength cutoff suggested by Parkinson and Callaghan (2007b) to be the point where weighting factors should be implemented in the calculation of cumulative loading exposures.

To calculate the cumulative loading experienced by each FSU during the partial herniation loading protocol, 3 blocks of 1000 cycles of flexion/extension were chosen at random from the entire data set. Using discrete integration in Kin Analysis the cumulative load for each of the 3 1000 cycle blocks was calculated and averaged together to represent the average cumulative loading exposure for 1000 cycles of the partial herniation loading protocol. The average cumulative load exposure for 1000 cycles was extrapolated to 7000 cycles.

Cumulative loading for the shock alone vibration and postural constraint loading group was calculated by randomly selecting 3 blocks of shock exposure (333 shocks each) from the entire data set. Discrete integration in Kin Analysis was used to calculate the cumulative load exposure for each of the 3 blocks, and the average of the 3 values was taken as the cumulative load due to shock exposure alone for 333 cycles. The average cumulative load exposure for 333 shocks was extrapolated to 2000 shocks.

Cumulative loading for the WBV vibration and postural constraint loading groups was calculated by randomly selecting 3 blocks of 15 min WBV exposures from the entire data set. Discrete integration in Kin Analysis was used to calculate the cumulative load exposure for each of the 3 blocks, and the average of these three blocks was used to represent the cumulative loading due to WBV for 15 min. The average cumulative load exposure for 15 min of WBV was extrapolated to the 90 min ATV riding time.

Cumulative loading for the vibration and postural constraint group of WBV with the addition of shock loading was calculated by summing the cumulative load exposures for 2000 mechanical shocks with the cumulative load exposures for 90 min of WBV.

3.9. Statistical Analysis

A one-way ANOVA (alpha level 0.05) was used to compare the 6 pre-herniation protocol measures [axial creep (mm), maximum torque (Nm), minimum torque (Nm), minimum angle (degrees), maximum angle (degrees), estimated end plate area (mm^2)] of all 8 vibration and postural constraint loading groups; full flexion and WBV, neutral and WBV, full flexion and static, neutral and static, full flexion and shock, neutral and shock, full flexion and WBV in addition to shock, neutral and WBV in addition to shock. Any significant differences were tested using a least significant difference (LSD) post-hoc testing (Alpha level 0.05).

A chi-squared analysis was used to compare the categorical level of damage progression using the definitions of no detectable damage, partial herniation, and full herniation between the 4 possible damage progression outcomes due to the vibration and postural constraint loading; no detectable damage – no detectable damage (W), no detectable damage – partial herniation (X), partial herniation – full herniation (Y), no detectable damage – full herniation (Z).

The concordance between sagittal plane film discograms, axial CT scans, and a 'gold standard' dissection technique was assessed for each specimen using the post vibration and postural constraint loading protocol medical imaging techniques (discograms and CT images) and the digital photographs post specimen dissection. The concordance criteria (level 0 – level 3) and a chi-squared analysis were implemented to test for level of concordance for the entire data set. The concordance between sagittal plane film discograms, axial CT scans, and the 'gold standard' dissection technique were also assessed for partial herniation only, using the same concordance criteria as defined above (level 0 – level 3) and the same chi-squared statistical procedure as used for the entire data set. By assessing only the partial herniation categorical damage level, a quantification of concordance to partial herniation could be made.

Multivariate analysis (MANCOVA) was used to compare tracking changes (distance of tracking %), average stiffness changes (Nm/deg), and specimen height changes (mm) in the presence of a covariate (cumulative loading) in the current investigation with an alpha level of 0.05. There were 3 main factors in the MANCOVA uni-variate procedure (posture, load, and time) and 1 covariate factor (cumulative load) used in conjunction with the 3 main factors in the multi-variate procedure. Levels for the main factors were as follows; 2 levels of posture (full flexion and neutral), 4 levels of load (WBV, Shock, Static, and the combination of WBV and Shock), 2 levels of time (pre - changes due to the partial herniation loading protocol, and post - changes due to the vibration and postural constrain loading protocol). The levels for the covariate were as follows; 4 levels of the cumulative loading covariate (1.05 MNs, 2.36 MNs, 2.55 MNs, and 3.41 MNs). The least significant difference (LSD) post –hoc test (alpha level 0.05) was used to determine statistical significance in the main effects while the Wilks' Lambda statistic was used to determine statistical significance in the multivariate analysis.

Unfortunately, during the procedures of the current investigation several parameters of interest were lost due to equipment malfunction. Of the sagittal plane film discograms, 5 out of 64 specimens were missing. For the parameter of average stiffness changes, a total of 3 comparisons were not possible due to corrupted data files (1 for FF and shock in the post test measures, 1 for FF and WBV in the post test measures, and 1 for FF and static in the post test measures). For specimen height changes, 5 potential comparisons were missing including 2 for the FF and WBV post test measures, 1 for the FF and Static pre test measures, 1 for the FF and Static post test measures, and 1 for the N and WBV in addition to shock post test measures. No distance of tracking changes, pre-herniation specimen similarity measures, or CT medical images were missing in the current investigation.

3.10. Investigation Methodology Overview:

To summarize the current investigations design; the specific hypothesis of this investigation, the variable of interest for each hypothesis, the type of variable, and the statistical procedure used to test the hypothesis are listed in a table format (Table 4).

Table 4: Summary of the current investigations design; the specific hypothesis of this investigation, the variable of interest for each hypothesis, the type of variable, and the statistical procedure used to test the hypothesis are listed.

Hypotheses	Variable of Interest	Variable Type	Statistical Procedure
1. Vibration exposures will exacerbate existing IVD tracking changes produced by a partial herniation protocol; the combination of WBV and shock will lead to the largest IVD tracking changes, followed by less IVD tracking changes due to WBV and then minimal IVD tracking changes due to shock alone. Static loading is not expected to change the level IVD tracking changes.	Distance of Tracking Changes - CT imaging – Percentage of distance tracked (%)	Numerical	MANCOVA Main Factors - Posture: two levels (Full Flexion and Neutral) - Loading exposures: four levels (Static/WBV/shock/WBV + shock) - Time (two levels (Pre – changes due to herniation and Post – changes due to vibration Covariate - Cumulative Load (1.05, 2.36, 2.55. 3.41) MNs
2. Vibration exposures will influence average stiffness changes during loading. Increases in average stiffness will rank as follows in descending order; WBV and shock, WBV, shock, static loading.	Average stiffness changes (Nm/deg)	Numerical	MANCOVA Main Factors - Posture: two levels (Full Flexion and Neutral) - Loading exposures: four levels (Static/WBV/shock/WBV + shock) - Time (two levels (Pre – changes due to herniation and Post – changes due to vibration Covariate - Cumulative Load (1.05, 2.36, 2.55. 3.41) MNs
3. Vibration exposures will influence specimen height changes during loading. Specimen height decreases will rank as follows in descending order; WBV and shock, WBV, shock, static loading.	height changes (mm)	Numerical	MANCOVA Main Factors - Posture: two levels (Full Flexion and Neutral) - Loading exposures: four levels (Static/WBV/shock/WBV + shock) - Time (two levels (Pre – changes due to herniation and Post – changes due to vibration Covariate - Cumulative Load (1.05, 2.36, 2.55. 3.41) MNs

Hypotheses	Variable of Interest	Variable Type	Statistical Procedure
4. Posture will influence the parameters of IVD tracking changes (increase), average stiffness changes (increase) and specimen height changes (increase) within the vibration exposures; fully flexed postures are hypothesized to lead to larger changes in these parameters than neutral postures.	Distance of Tracking Changes - CT imaging – Percentage of distance tracked (%) - Average stiffness changes (Nm/deg) - height changes (mm)	Numerical	MANCOVA Main Factors - Posture: two levels (Full Flexion and Neutral) - Loading exposures: four levels (Static/WBV/shock/WBV + shock) - Time (two levels (Pre – changes due to herniation and Post – changes due to vibration Covariate - Cumulative Load (1.05, 2.36, 2.55. 3.41) MNs
5. The partial herniation loading protocol will be more damaging to the IVD than then vibration and postural constraint loading protocols and will lead to larger relative increases in average stiffness, IVD tracking changes, and specimen height lost from established baselines.	Distance of Tracking Changes 4. CT imaging – Percentage of distance tracked (%) Average stiffness changes (Nm/deg) height changes (mm)	Numerical	MANCOVA Main Factors - Posture: two levels (Full Flexion and Neutral) - Loading exposures: four levels (Static/WBV/shock/WBV + shock) - Time (two levels (Pre – changes due to herniation and Post – changes due to vibration Covariate - Cumulative Load (1.05, 2.36, 2.55. 3.41) MNs
6. Concordance will be high between medical imaging and a 'gold standard' dissection techniques. However, Computed Tomography image concordance will be higher than discogram image concordance.	Match classification 5. No Match 6. Partial Match 7. Full Match	Categorical	Chi Square (χ^2)
7. IVD damage level classification will increase due to the vibration and postural constraint loading protocols.	Damage Classification ▪ No Damage ▪ Partial Herniation ▪ Full Herniation	Categorical	Chi Square (χ^2)

Chapter 4: Results

4.1. Cumulative Loading Exposure Calculations

The estimated maximum compressive strength (N) for the specimens in the 8 vibration and postural constraint loading groups ranged from 10429.81 N – 11547.06 N. Considering the partial herniation loading protocol the peak load each specimen was exposed to was 1500 N. This peak load represented between 12.99 % and 14.38 % of the estimated maximum compressive strength of the spines. This range of peak load exposures (12.99 % - 14.38 %) is well below the 37.5 % of maximum predicted strength cutoff where loading exposures with peak loads should be weighted differently (Parkinson and Callaghan 2007b). The cumulative load for the partial herniation loading protocol (7000 cycles of the flexion and extension under 1.5 KN of axial compression) that was common to all specimens in this investigation was calculated to be 10.71 MNs (Table 5).

The peak loads for each of the 8 vibration and postural constraint loading protocols were as follows; full flexion and WBV (513.89 N), full flexion and shock (1189.00 N), full flexion and static (414.24 N), full flexion and WBV with the addition of shock (1189.00 N), neutral and WBV (513.89 N), neutral and shock (1189.00 N), neutral and static (414.24 N), neutral and WBV with the addition of shock (1189.00 N). These peak loads represented between 3.85 % and 10.73 % of the estimated maximum compressive strength of the spines. This range of peak load exposures (3.85 % - 10.73 %) is well below the 37.5 % of maximum predicted strength cutoff where loading exposures with peak loads should be weighted differently (Parkinson and Callaghan 2007b). The cumulative loads for the 8 vibration and postural constraint loading groups were found to be 3.41 MNs (WBV with shock), 1.05 MNs (shock), 2.55 MNs (static), and 2.36 MNs (WBV) (Table 5).

Table 5: A Table representing the cumulative loading exposures calculated for this investigation. Estimated (Est) endplate area (EPA) values were used in conjunction with the regression equation for Parkinson et al. (2005) to calculate the estimated maximum compressive strength (N) of the specimens. Peak load (N), percent of estimated compressive strength (%), and the cumulative loading exposure (MNs) are shown for each of the 8 vibration and postural constraint loading protocols and for the partial herniation loading protocol. Standard errors of the estimated EPA values are indicated in parenthesis.

Vibration and Postural Constraint Group	Est EPA (mm^2)	Est Maximum Compressive Strength (N)	Herniation Protocol			Vibration Protocol		
			Peak Load (N)	Percent Est Compressive Strength (%)	Cumulative Load (MNs)	Peak Load (N)	Percent Est Compressive Strength (%)	Cumulative Load (MNs)
FF + WBV	800.32 (82.61)	11547.06	1500.00	12.99	10.71	513.89	4.45%	2.36
FF + Shock	766.11 (84.69)	11081.46	1500.00	13.54	10.71	1189.00	10.73%	1.05
FF + Static	743.39 (54.96)	10772.24	1500.00	13.92	10.71	414.24	3.85%	2.55
FF + WBV + Shock	766.09 (68.58	11081.18	1500.00	13.54	10.71	1189.00	10.73%	3.41
N + WBV	775.33 (58.15)	11206.94	1500.00	13.38	10.71	513.89	4.45%	2.36
N + Shock	718.23 (61.39)	10429.81	1500.00	14.38	10.71	1189.00	10.73%	1.05
N + Static	746.91 (37.59)	10820.15	1500.00	13.86	10.71	414.24	3.85%	2.55
N + WBV + Shock	749.70 (67.99)	10858.12	1500.00	13.81	10.71	1189.00	10.73%	3.41

4.2. Specimen Similarity between the Eight Vibration and Postural Constraint Groups

In the current investigation there were 2 postural constraints (full flexion and neutral) and 4 vibration loading conditions (static, WBV, shock, WBV in combination with shock). This resulted in 8 vibration and postural constraint groups; full flexion and static, full flexion and WBV, full flexion and shock, full flexion and WBV in combination with shock, neutral and static, neutral and WBV, neutral and shock, neutral and WBV in combination with shock. Six separate one-way ANOVAs were used to compare the 6 pre-herniation protocol parameters [axial creep (mm) due to the initial pre-load, max torque (Nm), min torque (Nm), max angle (deg), min angle (deg) as found in passive test 1, and estimated endplate area (mm^2)] between the 8 vibration and postural constraint groups. No significant differences were found in any of the six pre-herniation protocol parameters (Table 6); axial creep ($p = 0.7711$), max torque ($p = 0.5259$), min torque ($p = 0.6647$), max angle ($p = 0.1117$) min angle ($p = 0.3691$), estimated endplate area ($p = 0.3742$). Therefore, the random assignment of specimens to each of the 8 vibration and postural constraint loading groups was effective based on the 6 pre-herniation protocol parameters.

Table 6: Specimen similarity between 8 vibration and postural constraint loading groups based on 6 pre-herniation parameters; axial creep (mm), max torque (Nm), min torque (Nm), max angle (deg), min angle (deg), and estimated endplate area (mm^2) denoted as Est EPA.

Group	Axial Creep (mm)	SD	Max Torque (Nm)	SD	Min Torque (Nm)	SD	Max Angle (deg)	SD	Min Angle (deg)	SD	Est EPA (mm^2)	SD
FF+WBV	-0.54	0.13	10.02	1.97	-1.18	0.38	13.44	2.06	-6.38	1.46	800.32	82.61
FF+Shock	-0.52	0.13	11.51	2.51	-1.24	1.53	15.80	3.08	-5.40	2.68	766.11	84.69
FF+Static	-0.66	0.34	9.38	4.21	-2.43	1.53	13.57	3.71	-6.86	1.90	743.39	54.96
FF+Shock+WBV	-0.50	0.20	9.33	2.99	-1.83	1.84	12.00	2.12	-7.00	1.17	766.09	68.58
N+WBV	-0.51	0.27	9.32	4.17	-2.78	3.95	13.60	3.20	-5.53	3.74	775.33	58.15
N+Shock	-0.64	0.23	9.76	2.92	-1.61	0.67	12.64	2.63	-5.66	2.73	718.23	61.39
N+Static	-0.54	0.15	8.15	3.64	-1.18	0.99	12.88	1.66	-5.85	2.60	746.91	37.59
N+WBV+Shock	-0.57	0.21	8.25	2.25	-2.13	1.81	11.93	1.62	-7.88	1.18	749.70	67.99
P Value	0.7711		0.5259		0.6647		0.1117		0.3691		0.3742	

4.3. Specimen Herniation and Damage Progression

The partial herniation loading protocol employed by this investigation (7000 cycles of flexion and extension under 1.5 KN of axial compressive load) was very successful in producing partial IVD herniations. Using the pre-testing to post partial herniation CT medical images for comparison and the 3 categorical variables for herniation (partial, full, no damage); 58 out of 64 specimens (90.63%) were found to have herniated partially, 4 out of 64 specimens (6.25 %) were found to have fully herniated, while no damage was detected in 2 out of 64 specimens (3.13%). The vibration and postural constraint loading did not lead to sufficient mechanical insult to the specimens to alter the categorical determination of the degree of herniation (partial, full, no damage). The categorical level of damage that was sustained in each specimen as a result of the partial herniation loading protocol was unchanged after the vibration and postural constraint loading. Also note that all specimens in this investigation had no detectable damage to the IVD or endplates prior to the partial herniation loading protocol (Table 7). No categorical damage progression due to vibration and postural constraint loading does not imply these loads were not damaging to the specimens. The results reported for specimen height lost, tracking changes, and stiffness changes indicated that vibration and postural constraint loading protocols lead to sufficient mechanical insult to create damage exacerbation in the FSUs.

Table 7: Categorical assessment of damage progression at the 3 imaging stages in the study; pre-testing, post herniation loading, post vibration and postural constraint loading. Full flexion postures are indicated by FF, and neutral postures are indicated by N.

Date	Vibration and Postural Load	Damage Progression (Herniation Classification)			Date	Vibration and Postural Load	Damage Progression (Herniation Classification)		
		Pre Test	Post Herniation	Post Vibration			Pre Test	Post Herniation	Post Vibration
Oct 27/08	FF + WBV	No Damage	Partial	Partial	Nov 27/08	N + WBV	No Damage	Partial	Partial
Nov 19/08	FF + WBV	No Damage	Partial	Partial	Dec 08/08	N + WBV	No Damage	Partial	Partial
Dec 09/08	FF + WBV	No Damage	Partial	Partial	Jan 07/09 B	N + WBV	No Damage	Partial	Partial
Jan 13/09 B	FF + WBV	No Damage	Partial	Partial	Jan 13/09	N + WBV	No Damage	Partial	Partial
Jan 21/09 A	FF + WBV	No Damage	No Damage	No Damage	Jan 21/09 B	N + WBV	No Damage	Partial	Partial
Jan 26/09A	FF + WBV	No Damage	Full	Full	Jan 26/09B	N + WBV	No Damage	Full	Full
Feb 19/09 A	FF + WBV	No Damage	Partial	Partial	Feb 17/09 B	N + WBV	No Damage	Partial	Partial
Feb 19/09 B	FF + WBV	No Damage	Partial	Partial	Feb 24/09	N + WBV	No Damage	Partial	Partial
Oct 28/08	FF + Shock	No Damage	Partial	Partial	Oct 30/08	N + Shock	No Damage	Partial	Partial
Nov 5/08	FF + Shock	No Damage	Full	Full	Dec 01/08	N + Shock	No Damage	Partial	Partial
Dec 08/08	FF + Shock	No Damage	Partial	Partial	Dec 15/08 A	N + Shock	No Damage	Partial	Partial
Jan 12/09	FF + Shock	No Damage	Partial	Partial	Jan 15/09 B	N + Shock	No Damage	Partial	Partial
Jan 19/09 B	FF + Shock	No Damage	Partial	Partial	Feb 02/09 A	N + Shock	No Damage	Partial	Partial
Feb 02/09 B	FF + Shock	No Damage	Partial	Partial	Feb 06/09	N + Shock	No Damage	Partial	Partial
Feb 05/09 B	FF + Shock	No Damage	Partial	Partial	Feb 09/09 B	N + Shock	No Damage	Partial	Partial
Feb 13/09	FF + Shock	No Damage	Partial	Partial	Feb 12/09 B	N + Shock	No Damage	Partial	Partial
Nov 11/08	FF + WBV + Shock	No Damage	Partial	Partial	Nov 20/08	N + WBV + Shock	No Damage	Partial	Partial
Nov 26/08	FF + WBV + Shock	No Damage	Partial	Partial	Dec 17/08	N + WBV + Shock	No Damage	Partial	Partial
Dec 11/08	FF + WBV + Shock	No Damage	Partial	Partial	Jan 15/09 A	N + WBV + Shock	No Damage	Partial	Partial
Jan 08/09	FF + WBV + Shock	No Damage	Partial	Partial	Jan 23/09	N + WBV + Shock	No Damage	Partial	Partial
Jan 27/09B	FF + WBV + Shock	No Damage	Partial	Partial	Jan 30/09	N + WBV + Shock	No Damage	Partial	Partial
Feb 05/09 A	FF + WBV + Shock	No Damage	Partial	Partial	Feb 09/09 A	N + WBV + Shock	No Damage	Partial	Partial
Feb 23/09 A	FF + WBV + Shock	No Damage	Partial	Partial	Feb 17/09 A	N + WBV + Shock	No Damage	Full	Full
Mar 02/09 B	FF + WBV + Shock	No Damage	Partial	Partial	Feb 20/09	N + WBV + Shock	No Damage	Partial	Partial
Nov 24/08	FF + Static	No Damage	Partial	Partial	Nov 3/08	N + Static	No Damage	Partial	Partial
Dec 02/08	FF + Static	No Damage	Partial	Partial	Nov 12/08	N + Static	No Damage	Partial	Partial
Dec 15/08 B	FF + Static	No Damage	Partial	Partial	Jan 07/09 A	N + Static	No Damage	Partial	Partial
Jan 09/09	FF + Static	No Damage	Partial	Partial	Jan 19/09 A	N + Static	No Damage	Partial	Partial
Feb 12/09 A	FF + Static	No Damage	Partial	Partial	Feb 23/09 B	N + Static	No Damage	Partial	Partial
Mar 02/09 A	FF + Static	No Damage	Partial	Partial	Feb 27/09	N + Static	No Damage	Partial	Partial
Mar 04/09	FF + Static	No Damage	Partial	Partial	Mar 05/09 B	N + Static	No Damage	Partial	Partial
Mar 05/09 A	FF + Static	No Damage	Partial	Partial	Mar 06/09	N + Static	No Damage	No Damage	No Damage

4.4. Concordance between Sagittal Plane Film Discogram, Axial Computed Tomography, and a 'Gold Standard' Dissection Technique.

4.4.1. Concordance for Partial Herniation, Full Herniation, and No Detectable Damage.

A chi-squared (χ^2) analysis was used to assess the concordance between sagittal plane film discograms, axial CT and a 'gold standard' dissection technique. Three categorical levels of concordance were constructed to qualitatively determine how closely the medical imaging techniques (discograms and CT scans) matched the dissection results regarding herniation progression. Concordance level 0 indicated that the medical imaging technique did not match the dissection. A concordance level 0 was assigned when the images failed to detect a herniation confirmed through dissection, or if the images falsely predicted a herniation not illustrated in the dissection technique (Figure 29). Concordance level 1 indicated that the medical imaging technique partially matched the dissection results. A concordance level 1 was assigned when the images detected a herniation confirmed through dissection, but the degree of herniation damage (progression of the NP through and between the layers of the AF) did not match the dissection technique (Figure 30). Concordance level 2 indicated that the medical imaging technique was a full match to the dissection. A concordance level of 2 was assigned when the images detected a herniation that was confirmed through dissection, and the degree of herniation damage (progression of the NP through and between the layers of the AF) was a match to the dissection technique (Figure 31).

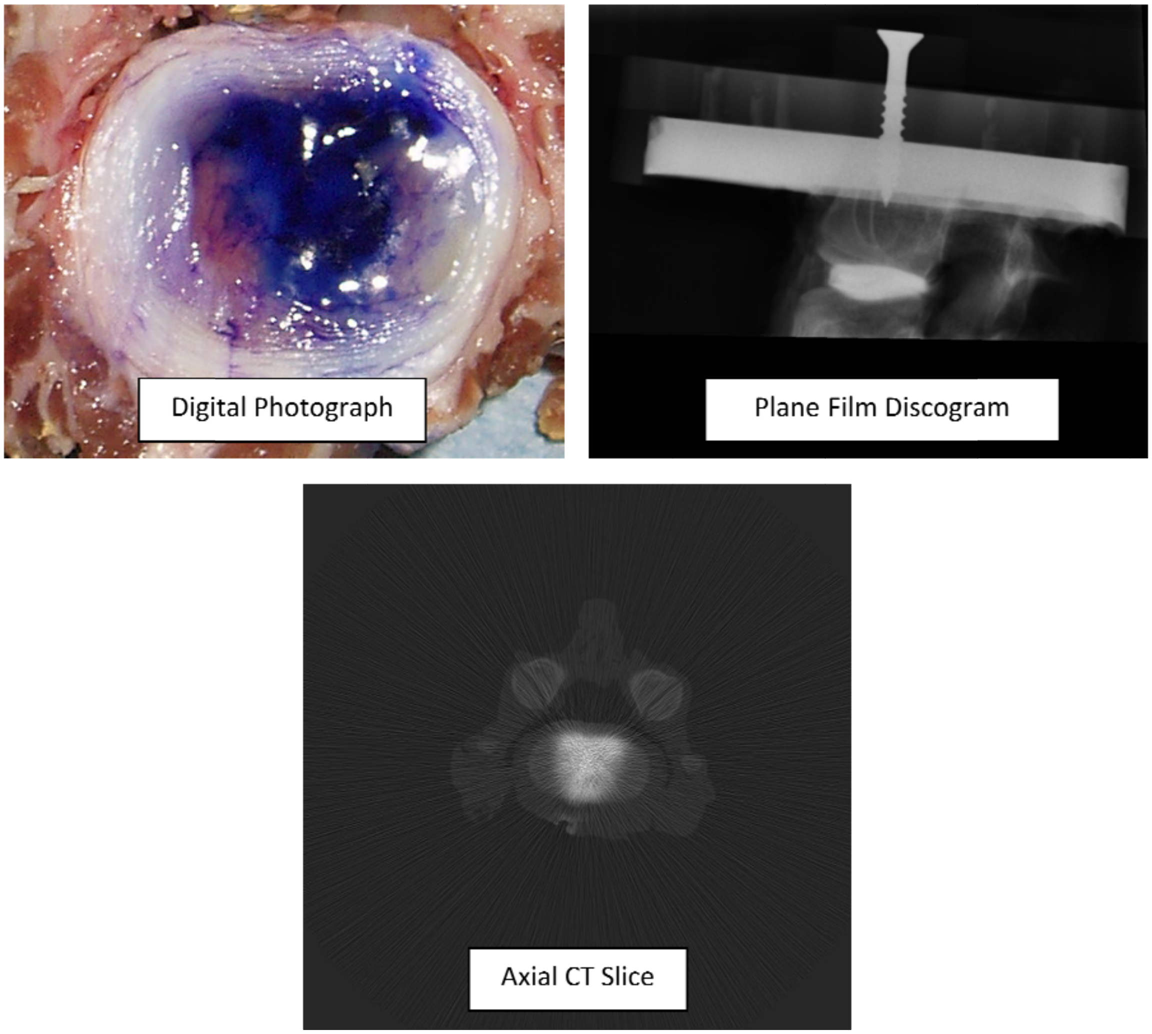

Figure 29: Illustration of a No Match (0) to dissection technique in contrast enhanced discogram and a Partial Match (1) to dissection technique in contrast enhanced Computed Tomography (CT) slice. Note only a single CT slice is shown, however 8 slices were taken to assess concordance. For both the CT image and digital photograph the posterior aspect of the spine is orientated up. For the plane film discogram, the posterior aspect is orientated to the right.

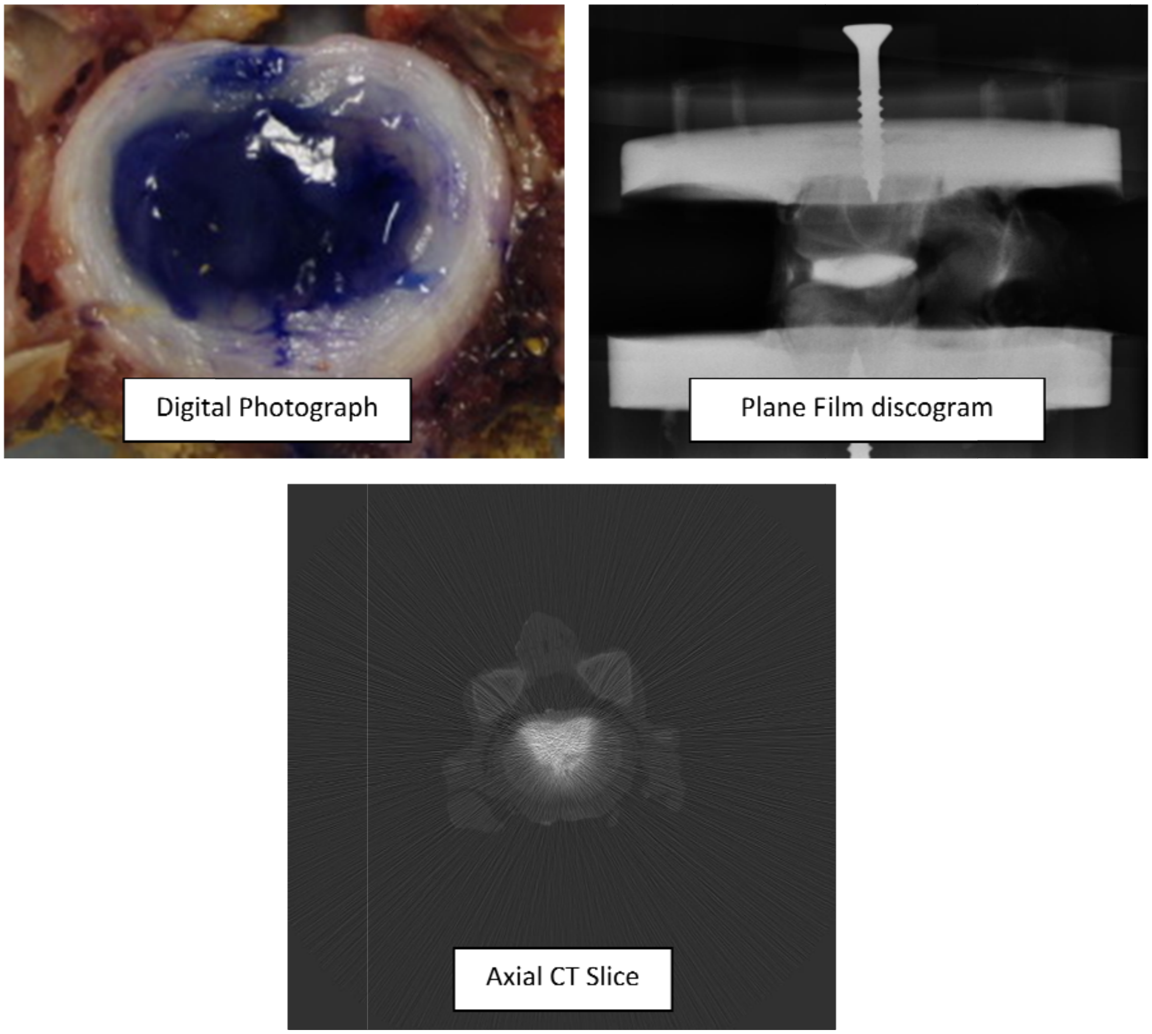

Figure 30: Illustration of a Partial Match (1) to dissection technique in both the contrast enhanced discogram and Computed Tomography (CT) slice. Note only a single CT slice is shown, however 8 slices were taken to assess concordance. For both the CT image and digital photograph the posterior aspect of the spine is orientated up. For the plane film discogram, the posterior aspect is orientated to the right.

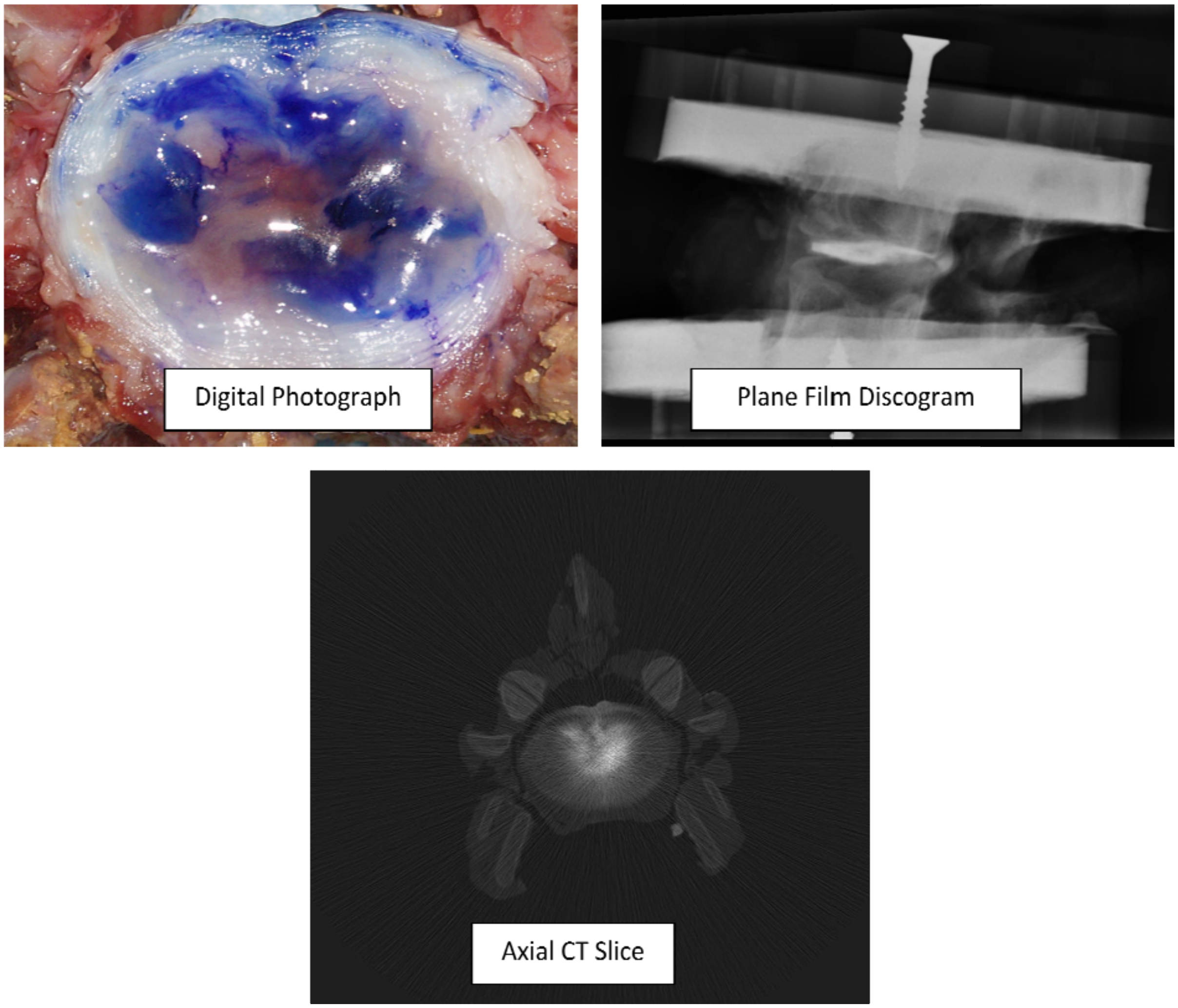

Figure 31: Illustration of a Full Match (2) to dissection technique in both the contrast enhanced discogram and Computed Tomography (CT) slice. Note only a single CT slice is shown, however 8 slices were taken to assess concordance. For both the CT image and digital photograph the posterior aspect of the spine is orientated up. For the plane film discogram, the posterior aspect is orientated to the right.

Implementing the above categorical concordance criteria (level 0-2) the following frequency counts occurred when considering the entire data set (full herniation, partial herniation, no detectable damage) the CT medical imaging; level 0 (0 observations), level 1 (19 observations), level 2 (45 observations). Considering the discogram medical imaging the following frequency counts occurred; level 0 (2 observations), level 1 (36 observations), level 2 (21 observations), and specimens where discograms were missing due to equipment malfunction

(5 observations). To effectively implement the chi-squared analysis none of the frequency counts can be zero, as occurred in the CT medical imaging level 0 (no match) concordance criteria. Therefore the concordance levels of 0 (no match) and 1 (partial match) were collapsed together for both the discogram and CT medical imaging technique to allow the chi-squared analysis to remain a valid test.

The distribution in the Chi-Squared analysis was likely not due to chance alone ($P < 0.0001$) (Table 8). There appeared to be a medical imaging technique bias in the concordance assessment between CT imaging and the dissection technique. There was a tendency for the contrast enhanced CT medical images to produce more level 2 (full match) concordance criteria than the contrast enhanced discograms. Theoretically, if the level of concordance was due to chance alone there would be a 50% probability that either medical imaging type (CT or discogram) would produce a full match (level 2) or a no – partial match (levels 0 and 1 combined). However, since 5 observations for the discogram medical imaging technique were missing, the theoretical probability of either medical imaging type producing a given level of concordance is altered slightly. The missing observations are reflected in Table 8 by noting the 52.03 column percent for CT and the 47.97 column percent for discogram, these numbers represent the theoretical distribution of the chi-square if due to chance alone corrected for the missing discograms.

The CT imaging technique resulted in 68.18 % for the full match concordance criteria and only 33.33 % for the no-partial match concordance criteria. This indicated that the CT images produced more full matches with the dissection technique than predicted (52.03% from the column percent for CT). In total (considering both image types concordance to dissection) 53.66 % of all the images assessed were classified as full match for concordance criteria, indicated by the full match row total percent. However, note that 70.31% of the CT images were classified as full matches, while only 35.59% of the discogram images were classified as full matches.

There was also a tendency for the discogram images to produce more no-partial matches than the CT images. The discogram imaging technique resulted in 66.67% for the no-partial match concordance criteria and only 31.82 % for the full match concordance criteria. This indicated that the discogram images produced more no-partial matches with the dissection technique than predicted (47.97 % from the column percent for discogram). In total (considering both image types concordance to dissection) 46.34 % of all the images assessed were classified as no-partial match for the concordance criteria, indicated by the no-partial match row percent. However, note that 64.41 % of the discogram images were classified at no-partial matches, while only 29.69 % of the CT images were classified as no-partial matches.

Table 8: Chi-squared table for concordance assessment between Computed Tomography (CT), sagittal plan film discogram, and 'gold standard' dissection technique for the entire data set. Numbers contained in the ovals and rectangles represent valid comparison discussed in the results.

Group Frequency Percent Row Percent Column Percent	Outcome Computed Tomography	 X-rays (Discogram)	 Total
Full Match	45 36.59 68.18 $\boxed{70.31}$	21 17.07 31.82 $\boxed{35.59}$	66 $\boxed{53.66}$
No Match And Partial Match	19 15.45 33.33 $\boxed{29.69}$	38 30.89 66.67 $\boxed{64.41}$	57 $\boxed{46.34}$
Total	64 52.03	59 47.97	123 100

4.4.2. Concordance for Partial Herniation Alone

A chi-squared analysis was used to assess the concordance between sagittal plane film discogram, axial CT slices and the “gold standard” dissection technique for only the partial herniations. The same three levels of categorical concordance described in the previous section (Concordance for Partial Herniation, Full Herniation, and No Detectable Damage) were implemented to assess how closely the medical imaging technique (discograms or CT scans) matched the ‘gold standard’ dissection technique. By considering only the partial herniations, the full herniation and partial herniation specimens were removed from the analysis. This resulted in 6 specimens being removed from the chi-squared analysis; the 4 specimens with full herniations and the 2 specimens with no detectable damage. Due to the removal of the full herniation and no detectable damage specimens the following concordance criteria were removed from the chi-squared analysis; 5 concordance level 2 (full match) for CT image type, 3 concordance level 2 (full match) for the discogram image type, 1 concordance level 1 (partial – no match) for the CT image type, and 3 concordance level 1 (partial – no match) for the discogram image type.

The distribution in the Chi-Squared analysis for partial herniations alone was likely not due to chance alone ($p < 0.0002$) (Table 9). As with the concordance for the entire data set, there appeared to be a medical imaging type bias in the concordance assessment between CT imaging and the ‘gold standard’ dissection technique. There was a tendency for the contrast enhanced CT medical images to produce more level 2 (full match) concordance criteria than the contrast enhanced discograms. Theoretically, if the level of concordance was due to chance alone there would be a 50% probability that either medical imaging type (CT or discogram) would produce a full match (level 2) or a no – partial match (levels 0 and 1 combined). However, since 5 observations for the discogram medical imaging technique were missing, the theoretical probability of either medical imaging type producing a given level of concordance is altered slightly. The missing observations are reflected in Table 8 by noting the 52.25 column percent for CT and the 47.75 column percent for discogram, these numbers represent the theoretical distribution of the chi-square if due to chance alone corrected for the missing discograms and for the removed full herniation specimens and the removed specimen with no detectable damage.

The CT imaging technique resulted in 68.97 % for the full match concordance criteria and only 33.96 % for the no-partial match concordance criteria. This indicated that the CT images produced more full matches with the dissection technique than predicted (52.25 % from the column percent for CT). In total (considering both image types concordance to dissection) 52.25 % of all the images assessed were classified as full match for concordance criteria, indicated by the full match row total percent. However, note that 68.97 % of the CT images were classified as full matches, while only 31.03 % of the discogram images were classified as full matches.

There was also a tendency for the discogram images to produce more no-partial matches than the CT images. The discogram imaging technique resulted in 66.04 % for the no-partial match concordance criteria and only 31.03 % for the full match concordance criteria. This indicated that the discogram images produced more no-partial matches with the dissection technique than predicted (47.75 % from the column percent for discogram). In total (considering both image types concordance to dissection) 47.75 % of all the images assessed were classified as no-partial match for the concordance criteria, indicated by the no-partial match row percent. However, note that 66.04 % of the discogram images were classified at no-partial matches, while only 31.03 % of the CT images were classified as no-partial matches.

Table 9: Chi-squared table for concordance assessment between Computed Tomography (CT), sagittal plan film discogram, and 'gold standard' dissection technique for the partial herniations alone. Numbers contained in the ovals and rectangles represent valid comparison discussed in the results.

Group Frequency Percent Row Percent Column Percent	Outcome Computed Tomography	X-rays (Discogram)	Total
Full Match	40 36.04 68.97 $\boxed{68.97}$	18 16.22 31.03 $\boxed{33.96}$	58 $\boxed{52.25}$
No Match And Partial Match	18 16.22 33.96 $\boxed{31.03}$	35 31.53 66.04 $\boxed{66.04}$	53 $\boxed{47.75}$
Total	58 52.25	53 47.75	111 100

4.5. Herniation Damage Progression Illustrated through Tracking Changes

Tracking changes were assessed by measuring the most posterior linear distance of the NP in the IVD using Image J and the eight CT slices obtained at each of the medical imaging stages of the investigation (pre-test, post- partial herniation, and post vibration and postural constraint loading). These linear distances of NP motion were converted to tracking changes representing the percent of posterior tacking, or how far the NP had moved in the posterior direction in relation to baseline (pre-test image) towards the intervertebral foramen. The intervertebral foramen was used as the most posterior aspect in the tacking changes variable due to the fact that a herniation that had breached the outer most layers of the AF and protruded into this structure was considered a full herniation, and further quantification of a herniations posterior motion would have been unreliable beyond this structure.

A MANCOVA with main factors of posture (full flexion or neutral) load (WBV, shock, static, WBV with the addition of shock) and time (pre and post test comparisons) and a covariate of cumulative load (1.05, 2.36. 2.55, 3.41) MNs was used to compare tracking changes due to the partial herniation protocol (pre-test values) and due to the vibration and postural constraint loading (post-test values) as well as interaction effect between the factors of load, posture and time and to illuminate any interaction effects of posture load and time. Multi-variate analysis indicated a significant vector for the Wilks' Lambda test for overall effects of load ($p = 0.0144$) and time ($p < 0.0001$) between the three outcome variable of distance of tracking changes, specimen height changes, and average stiffness changes in the presence of the cumulative loading covariate. The multivariate analysis indicate no other significant overall effects with Wilks' Lambda values as follows; posture ($p = 0.6437$), posture*load ($p = 0.0736$), load*time ($p = 0.4197$), posture*time (0.48826), posture*load*time ($p = 0.3049$).

The uni-variate analysis indicated that main effect of time ($p < 0.0001$) was significant, and the LSD post-hoc testing indicated that changes due to the partial herniation loading protocol (mean 41.77, SD 24.04) were significantly larger than changes due to the vibration and postural constraint loading protocol (mean 4.42, SD 5.81) as shown in Figure 32. The Main effect of load ($p = 0.0144$) was also significant, and the LSD post-hoc testing indicated that the combination of WBV and shock (mean 31.00, SD 26.39) produced significantly larger distance of tracking changes than the static loading (mean 16.65, SD 21.52), shock alone (mean 22.99, SD 25.87) or WBV alone (mean 24.93, SD 28.39) as shown in Figure 33. The main effect of posture was not significant ($p = 0.5408$) indicating that full flexion posture (mean 25.58 SD 26.15) did not lead to larger distance of tracking changes that neutral postures (mean 22.29 SD 25.58) as indicated by Figure 34. There were no significant interaction effects for the distance of tracking changes variable; posture*load (p = 0.8413), load*time (p = 0.8065), posture*time (0.8713), posture*load* time (0.7959). If we consider the posture*load*time interaction an important piece of information can be determined; after the partial herniation loading protocol, there was no statistical difference in the tracking changes indicating that the random assignment of the specimens to the 8 vibration and postural constraint loading groups was effective based on the distance of tracking parameter (Figure 35). The posture*load*time interaction was not significant for the distance of tracking changes due to the vibration and postural constraint loading protocols, although WBV + shock lead to larger changes over both postures, followed by WBV alone, shock alone, and static produced no distance of tracking changes (Figure 36). The group means and standard deviations (SD) for each of the 8 vibration and postural constraint loading groups for the posture*load*time interaction can be found in Table 9.

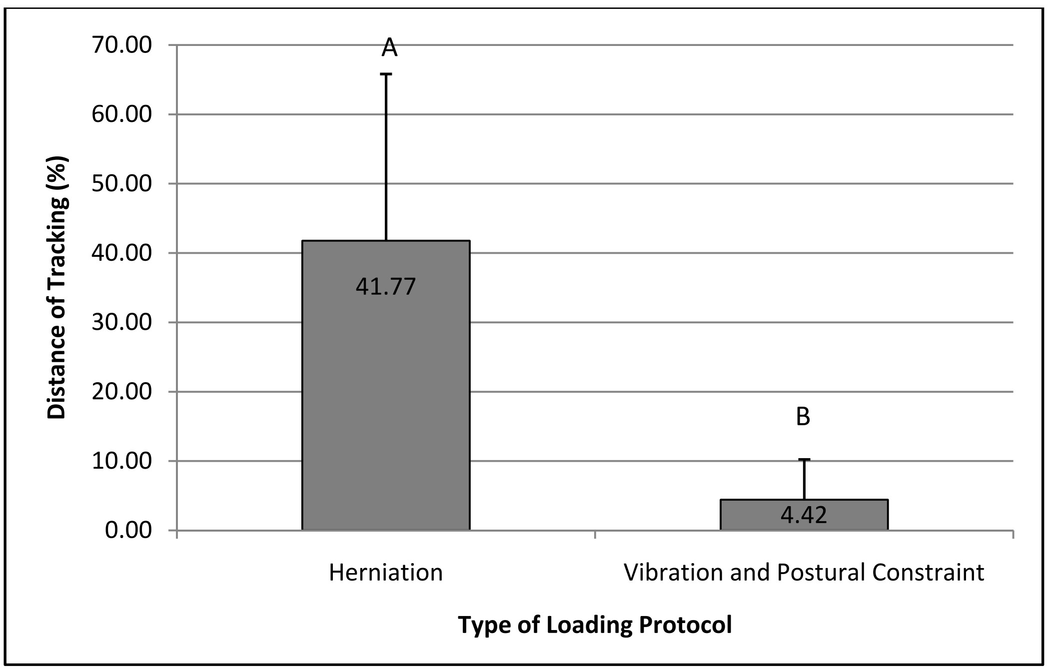

Figure 32: A graph of the distance of tracking changes due to the partial herniation loading protocol (pre-test time measures) and the vibration and postural constraint loading protocol (post-test time measures) . Statistical differences were indicated (P < 0.0001) and least significant different (LSD) post – hoc testing indicated differences between the loading protocols as indicated by different letters.

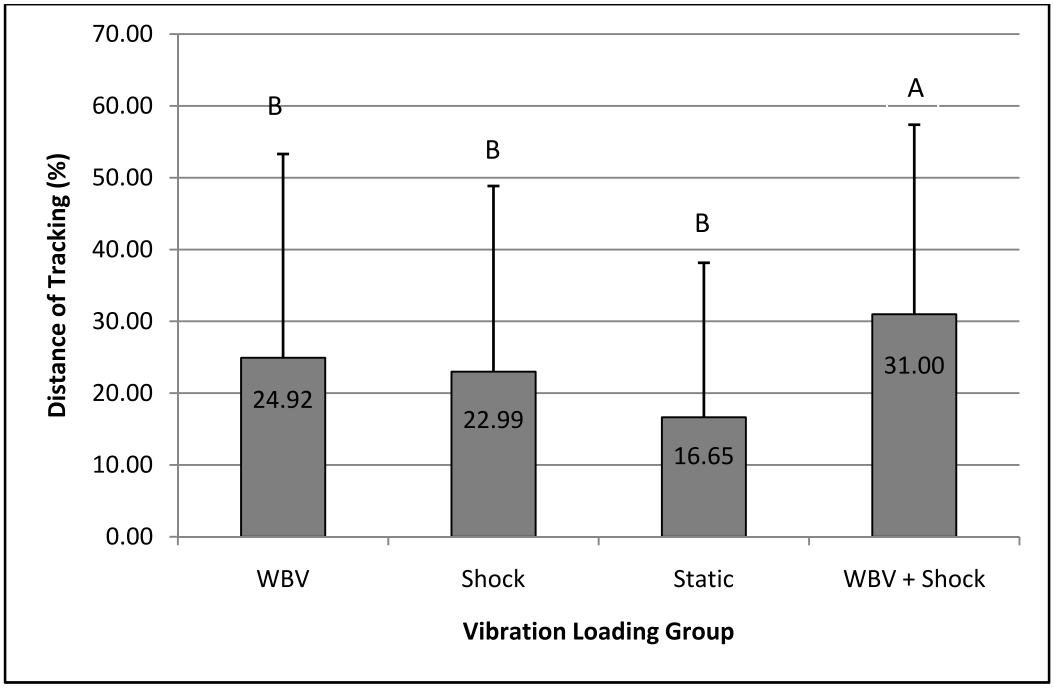

Figure 33: A graph of the distance of tracking changes due to the partial herniation and vibration and postural constraint loading protocols collapsed together and collapsed by posture. Statistical differences were indicated ($p = 0.0144$) and least significant difference (LSD) post-hoc testing was used to indicate loading group mean differences (indicated by different letters).

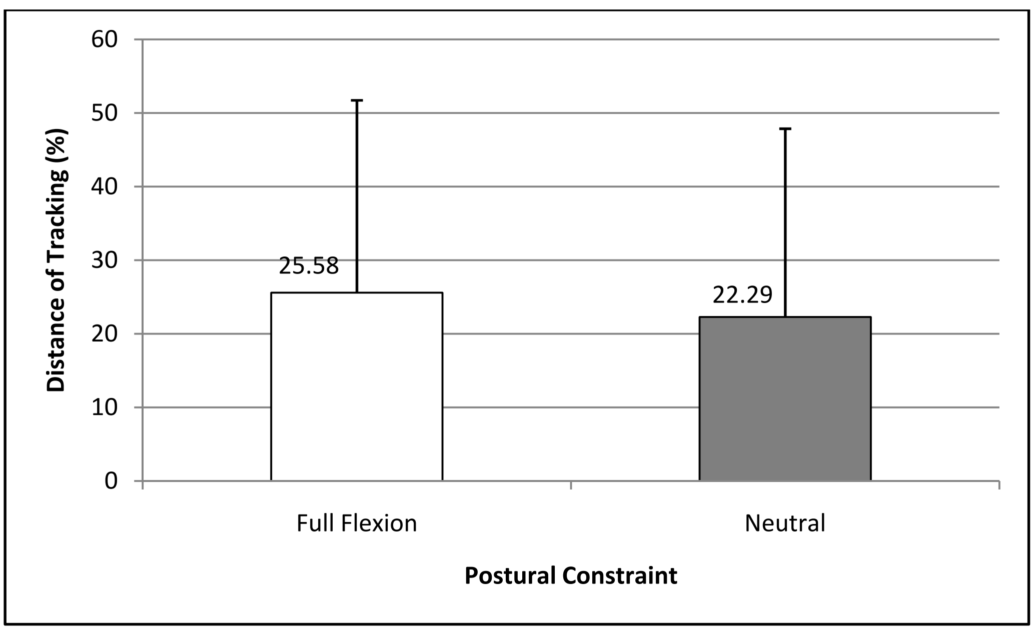

Figure 34: A graph of the partial herniation and vibration and postural constraint distance of tracking changes collapsed together for the factor of posture (full flexion or neutral). No statistical differences were found ($p = 0.6437$) indicating that posture did not significantly affect the herniation progression (as indicated by distance tracking changes).

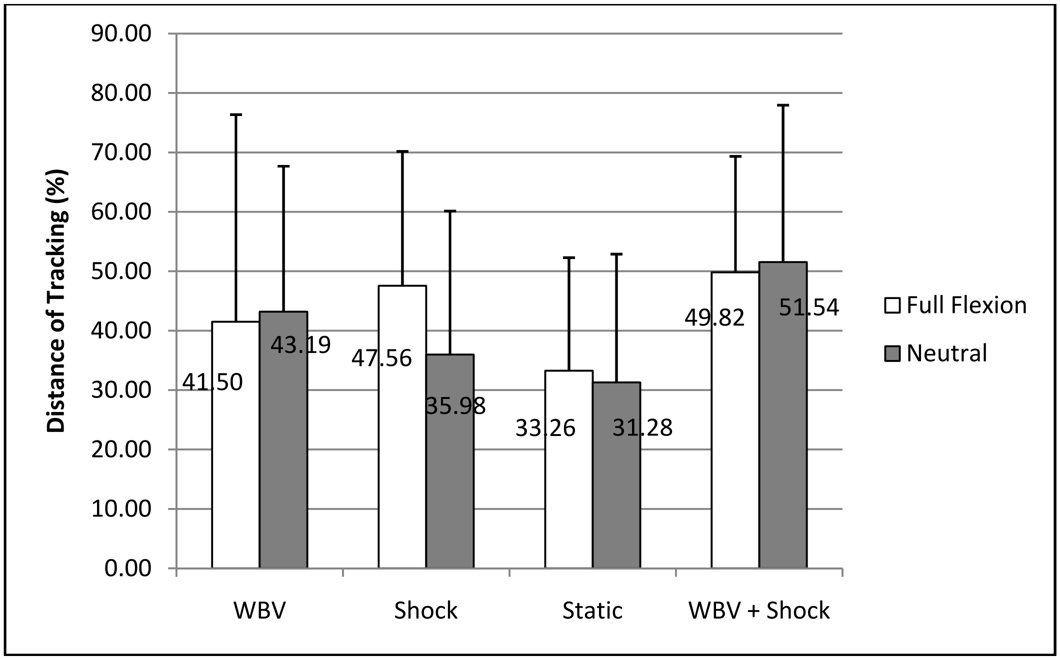

Figure 35: A graph of the posture by load by time interaction for distance of tracking changes (illustrating the 8 vibration and postural constraint loading groups) for pre-test (partial herniation) loading protocol. None of the 8 vibration and postural constraint loading groups were statistically different from each other (p = 0.7959).

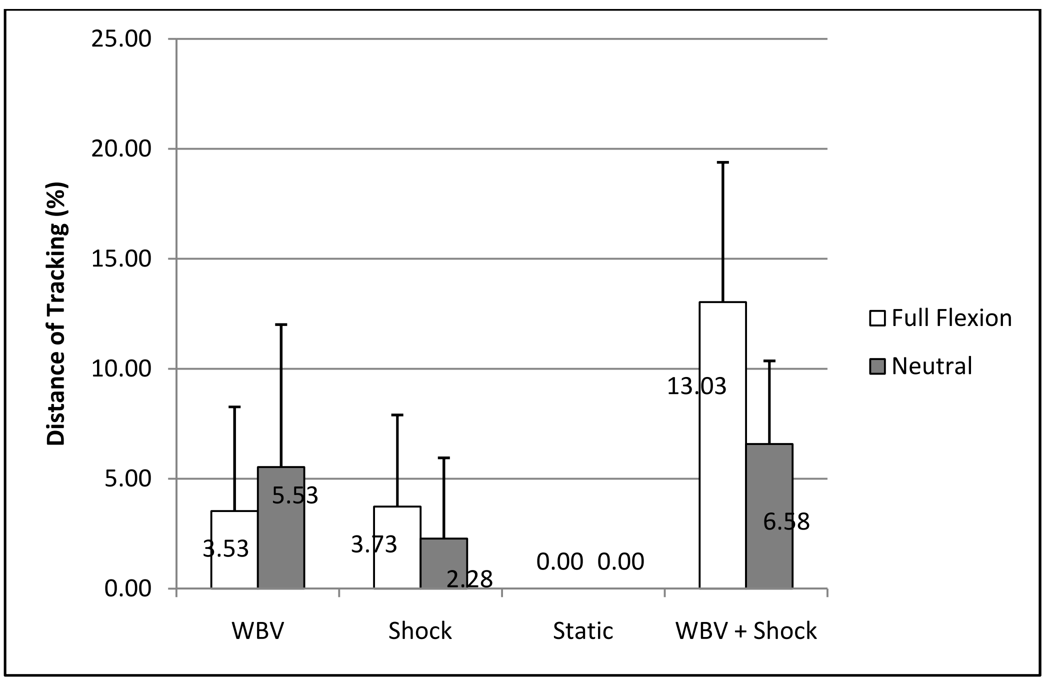

Figure 36: A graph of the posture by load by time interaction for distance of tracking changes (illustrating the 8 vibration and postural constraint loading groups) for the post-test (vibration and postural constraint) loading protocol. None of the 8 vibration and postural constraint loading groups were statistically different from each other (p = 0.7950).

Table 10: Group means and standard deviations (SD) for each of the 8 vibration and postural constraint loading groups for the posture*load*time interaction for the distance of tracking (%) variable. The pre time value represents the partial herniation loading protocol, and the post time value represents the vibration and postural constraint loading protocol.

Posture	Load	Time (pre-post)	Distance of Tracking (%)	
			Mean	SD
Full Flexion	WBV	Herniation	41.50	34.87
Full Flexion	WBV	Vibration	3.53	4.74
Full Flexion	Shock	Herniation	47.56	22.62
Full Flexion	Shock	Vibration	3.73	4.17
Full Flexion	Static	Herniation	33.26	19.05
Full Flexion	Static	Vibration	0.00	0.00
Full Flexion	WBV + Shock	Herniation	49.82	19.52
Full Flexion	WBV + Shock	Vibration	13.03	6.36
Neutral	WBV	Herniation	43.19	24.50
Neutral	WBV	Vibration	5.53	6.48
Neutral	Shock	Herniation	35.98	24.17
Neutral	Shock	Vibration	2.28	3.67
Neutral	Static	Herniation	31.28	21.62
Neutral	Static	Vibration	0.00	0.00
Neutral	WBV + Shock	Herniation	51.54	26.43
Neutral	WBV + Shock	Vibration	6.58	3.78

It should also be noted that there were large variation between specimens regarding the amount of tracking changes due to the partial herniation loading protocol (Figure 37). The range of the distance of tracking changes due to the partial herniation loading protocol (pre-test measures only) grouped by a factor of load were as follows; WBV 0.00 % - 100.00 %, shock 12.52 % - 100.00 %, static 0.00 % - 58.33 %, and WBV + Shock 4.19 % - 100.00%.

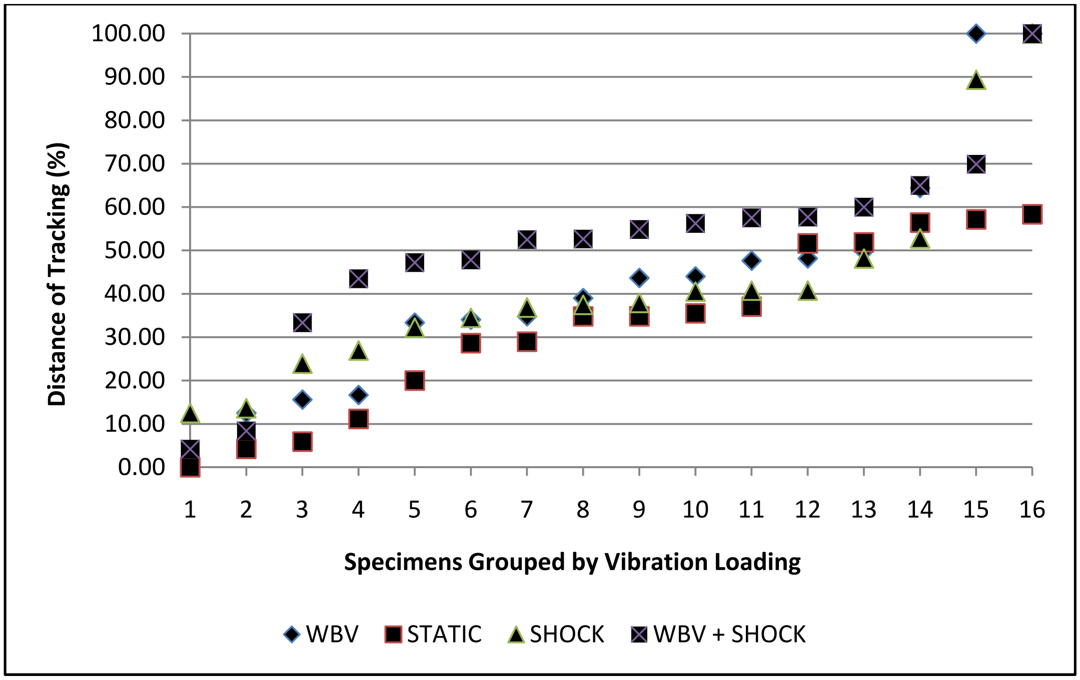

Figure 37: A graph of distance of tracking changes due to the partial herniation loading protocols (pre-test time measures) collapsed by posture. Tracking changes within each of the vibration loading groups were ranked in order to illustrate the large range of tracking changes due to the partial herniation loading protocol.

It should also be reported that there were large variations in the tracking changes in the specimens in response to the vibration loading protocols (Figure 38). Specimens exposed to the combination of WBV and shock illustrated distance of tracking changes ranging from 4.18% to 21.05 %, exposure to WBV loading caused tracking changes in the specimens that ranged from 0.00 % -15.37 %, shock loading alone lead to tracking changes in the specimens that ranged from 0.00 % - 10.35 %, while static loading did not cause any tracking changes in the specimens (range from 0.00 % to 0.00 %).

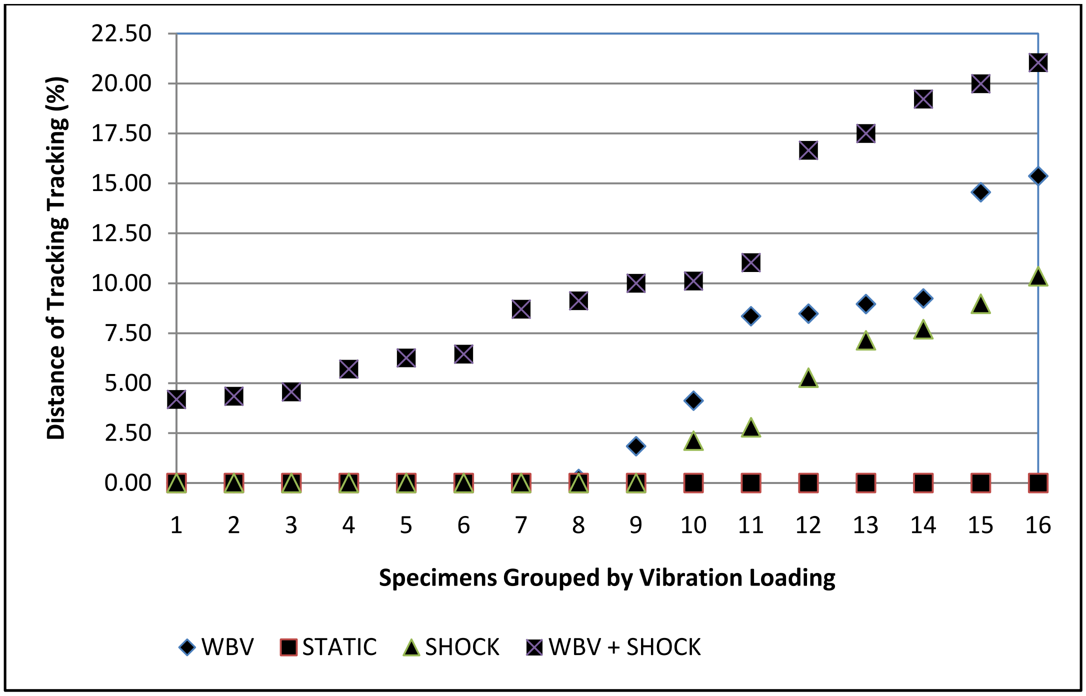

Figure 38: A graph of the distance of tracking changes due to the vibration and postural constraint loading protocols (post-test time measures) collapsed by posture. Tracking changes within each of the vibration loading groups are ranked in order to illustrate the large range of tracking changes due to vibration loading.

4.6. Specimen Height Changes

Specimen height changes were assessed by measuring the vertical height displacements of each specimen via the position output channel from the Instron control tower. Two specimen height changes were assessed for each specimen; height displacements due to the partial herniation loading protocol (post-partial herniation height – pre-test baseline height), and height displacements due to the vibration and postural constraint loading protocol (post vibration and postural constraint loading height – re-established baseline height). A MANCOVA with main factors of posture (full flexion or neutral) load (WBV, shock, static, WBV with the addition of shock) and time (pre and post test comparisons) and a covariate of cumulative load (1.05, 2.36. 2.55, 3.41) MNs was used to compare specimen height changes due to the partial herniation protocol (pre-test values) and due to the vibration and postural constraint loading (post-test values) as well as interaction between the factors of load, posture and time and to illuminate any interaction effects of posture load and time. Multi-variate analysis indicated a significant vector for the Wilks' Lambda test for overall effects of load ($p = 0.0144$) and time ($p < 0.0001$) between the three outcome variable of distance of tracking changes, specimen height changes, and average stiffness changes in the presence of the cumulative loading covariate. The multivariate analysis indicate no other significant overall effects with Wilks' Lambda values as follows; posture ($p = 0.6437$), posture*load ($p = 0.0736$), load*time ($p = 0.4197$), posture*time (0.48826), posture*load*time ($p = 0.3049$).

Uni-variate analysis indicated a significant time effect ($p < 0.0001$), and least significant difference (LSD) post-hoc testing indicating that the partial herniation loading protocol (mean -2.97 SD 1.05) produced larger height changes than the vibration and postural constraint loading protocol (mean -0.24 SD 0.19) as illustrated in Figure 39. The main effects of load ($p = 0.8980$) was not significant with WBV (mean-1.70 SD 1.66), Shock (mean -1.70 SD 1.70), Static (mean -1.69 SD 1.75) and WBV in combination with shock (mean -1.55 SD 1.16). The main effect of posture ($p = 0.3441$) was not significant with full flexion postures (mean -1.77 SD 1.67) not indicating larger height changes than neutral postures (mean-1.55 SD 1.46) as seen in Figure 40.

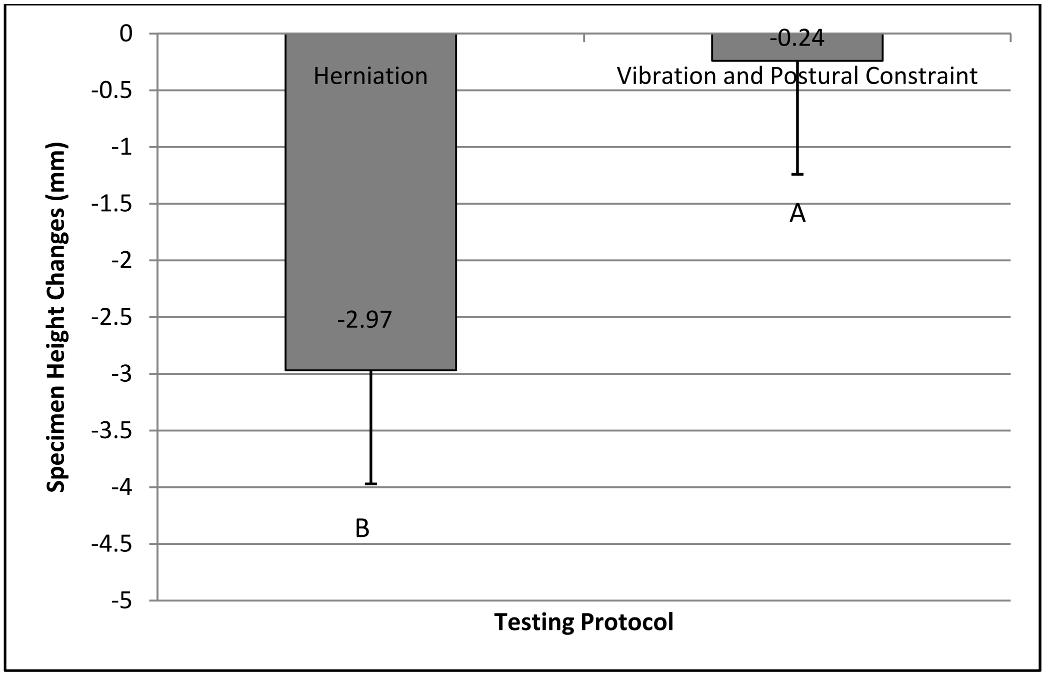

Figure 39: A graph of the specimen height changes due to the partial herniation loading protocol (pre-test measures) and the vibration and postural constraint loading protocol (post-test measures). Statistically significant differences were found ($P < 0.0001$) and are indicted by a least significant difference (LSD) post hoc-test illustrated with different letters.

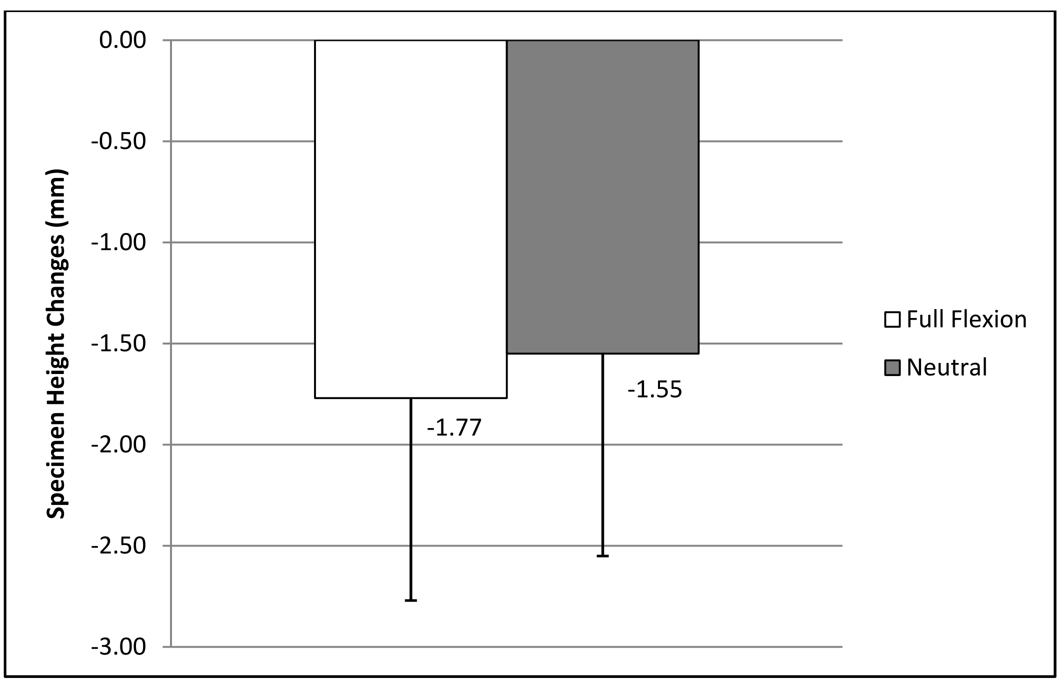

Figure 40: A graph of the specimen height changes grouped by posture ($P = 0.3441$). There is no significant difference in height changes between the postures (full flexion and neutral).

There were no significant interaction effects for the specimen height change variable; posture*load (p = 0.4862), load*time (0.1377), posture*time (0.3238), and posture*load* time (0.7317). If the posture*time interaction is further considered we can illustrate that the static postures (full flexion and neutral) adopted in the vibration and postural constraint loading protocols had no statistically significant effects on the specimen height changes; full flexion (mean -0.24 SD 0.15) and neutral (mean -0.24 SD 0.22). Furthermore, posture had no significant influence during the partial herniation loading protocol with full flexion specimen height changes (mean -3.10 SD 1.18) and neutral height changes (mean -2.83 SD 0.91) illustrating no statistical differences (Figure 41).

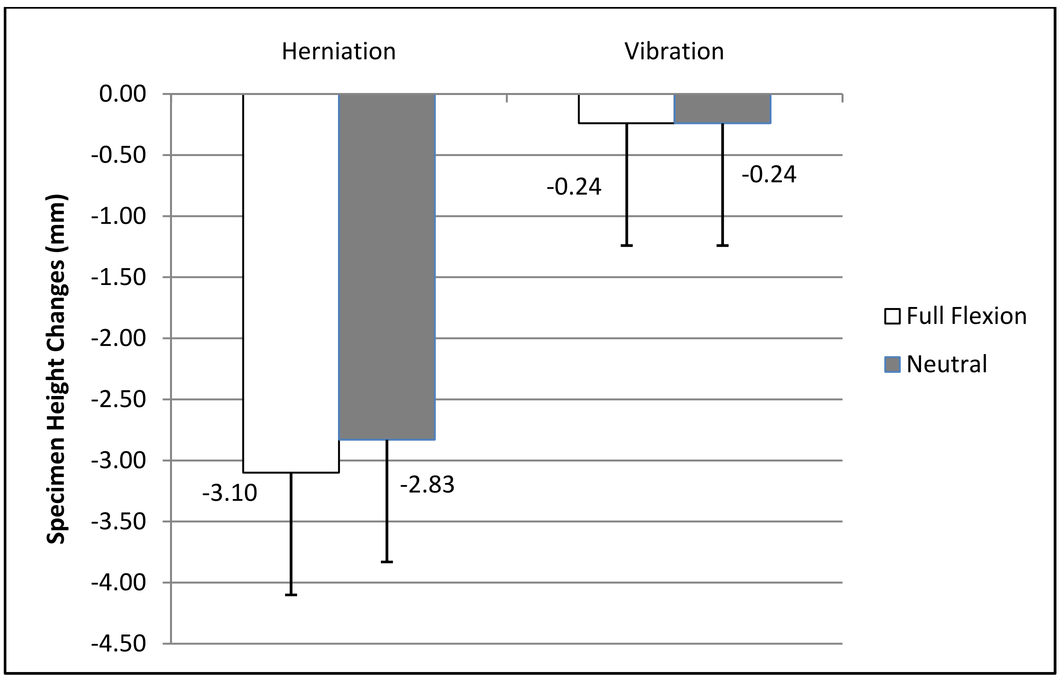

Figure 41: A graph of the posture*time interaction (p = 0.3238) for both the partial herniation loading protocol, and the vibration and postural constraint loading protocols.

If we consider the posture*load*time interaction (p = 0.7317) an important piece of information can be determined; after the partial herniation loading protocol, there was no statistical difference in the specimen height changes indicating that the random assignment of the specimens to the 8 vibration and postural constraint loading groups was effective based on the specimen height changes parameter (Figure 42). The posture*load*time interaction was not significant for the specimen height changes due to the vibration and postural constraint loading protocols, although WBV + shock lead to larger changes over both postures, than the WBV alone, shock alone, and static loading protocols. (Figure 43). The group means and standard deviations (SD) for each of the 8 vibration and postural constraint loading groups for the posture*load*time interaction can be found in Table 10.

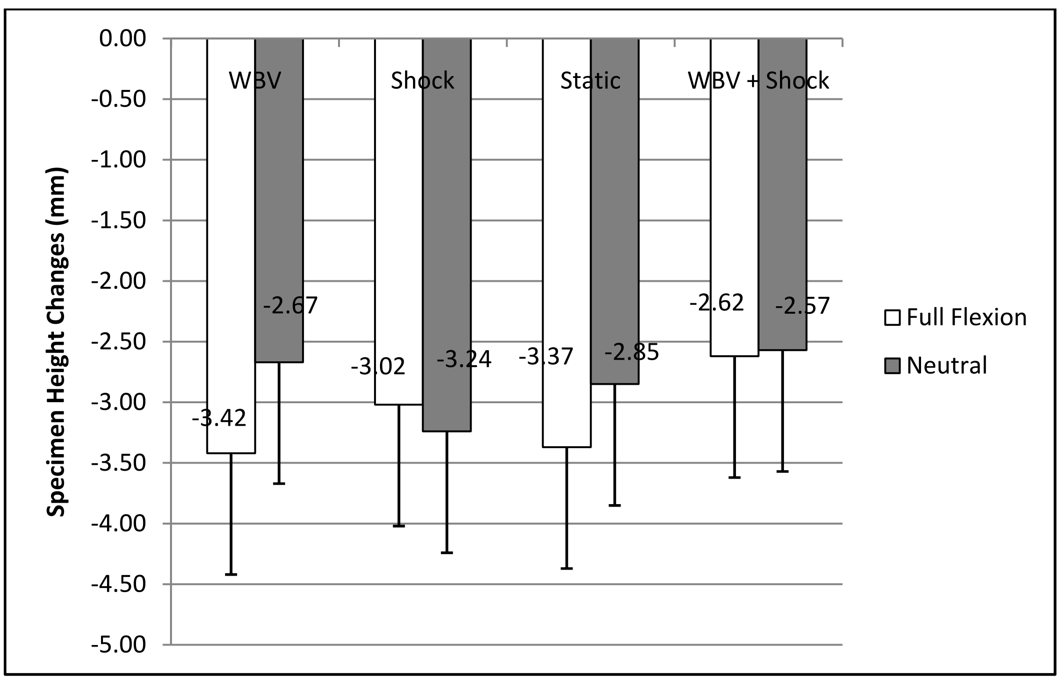

Figure 42: A graph of the posture by load by time interaction for specimen height changes (illustrating the 8 vibration and postural constraint loading groups) for pre-test (partial herniation) loading protocol. None of the 8 vibration and postural constraint loading groups were statistically different from each other (p = 0.7317).

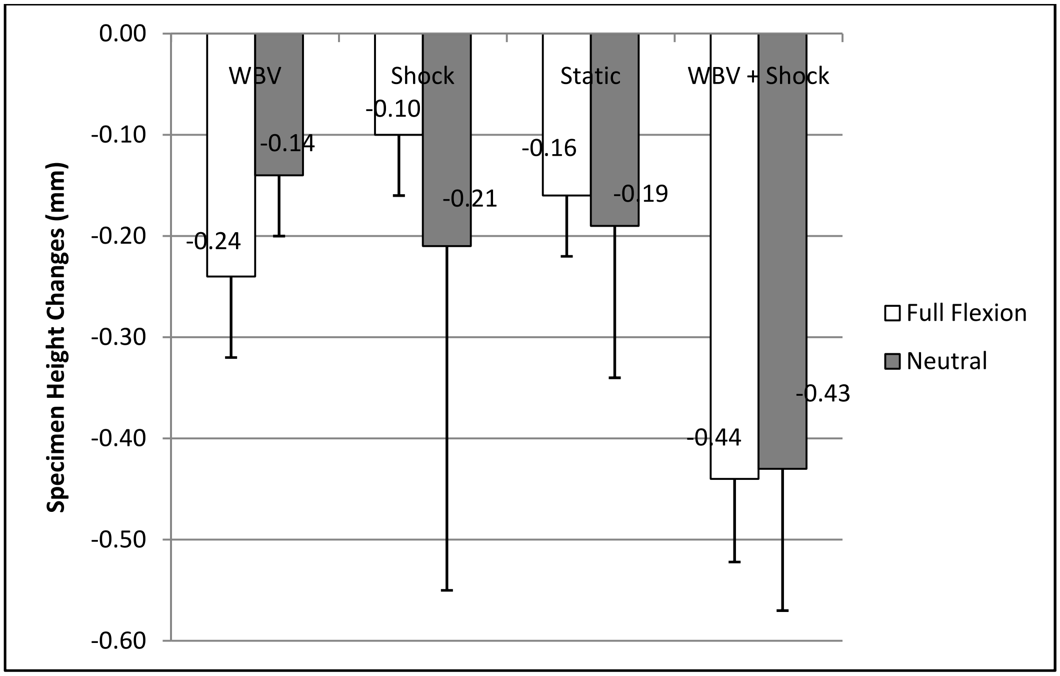

Figure 43: A graph of the posture by load by time interaction for specimen height changes (illustrating the 8 vibration and postural constraint loading groups) for the post-test (vibration and postural constraint) loading protocol. None of the 8 vibration and postural constraint loading groups were statistically different from each other (p = 0.7317).

Table 11: Group means and standard deviations (SD) for each of the 8 vibration and postural constraint loading groups for the posture*load*time interaction for the specimen height changes variable. The pre time value represents the partial herniation loading protocol, and the post time value represents the vibration and postural constraint loading protocol.

Posture	Load	Time	Specimen Height Changes (mm)	
			Mean	SD
Full Flexion	WBV	Herniation	-3.42	1.55
Full Flexion	WBV	Vibration	-0.24	0.08
Full Flexion	Shock	Herniation	-3.02	0.74
Full Flexion	Shock	Vibration	-0.10	0.06
Full Flexion	Static	Herniation	-3.37	1.63
Full Flexion	Static	Vibration	-0.16	0.06
Full Flexion	WBV + Shock	Herniation	-2.62	0.50
Full Flexion	WBV + Shock	Vibration	-0.44	0.08
Neutral	WBV	Herniation	-2.67	0.51
Neutral	WBV	Vibration	-0.14	0.06
Neutral	Shock	Herniation	-3.24	1.41
Neutral	Shock	Vibration	-0.21	0.34
Neutral	Static	Herniation	-2.85	0.89
Neutral	Static	Vibration	-0.19	0.15
Neutral	WBV + Shock	Herniation	-2.57	0.54
Neutral	WBV + Shock	Vibration	-0.43	0.14

4.7. Average Stiffness Changes

Average stiffness changes were assessed using the repeated passive test procedures and the methods employed by Drake et al. (2005) and described in detail in the methods section of this investigation. Briefly, the average stiffness (slope of the line) between the target torques in both flexion and extension as determined from the initial passive test were calculated for the last three repeats of each of the passive test procedures. The average of the slope of these 3 repeats was used to represent the average stiffness of each specimen for that particular passive test. Average stiffness changes due to the partial herniation loading protocol were assessed by finding the change in stiffness after the partial herniation loading protocol (passive test ^{2}) from the baseline stiffness measure (passive test [1]). Average stiffness changes due to the vibration and postural constraint loading protocol were assessed by finding the changes in stiffness after the vibration and postural constraint loading protocol (passive test [4]) from the re-established baseline stiffness just prior to the vibration and postural constraint loading protocol (passive test [3]).

A MANCOVA with main factors of posture (full flexion or neutral) load (WBV, shock, static, WBV with the addition of shock) and time (pre and post test comparisons) and a covariate of cumulative load (1.05, 2.36. 2.55, 3.41) MNs was used to compare specimen height changes due to the partial herniation protocol (pre-test values) and due to the vibration and postural constraint loading (post-test values) as well as interaction between the factors of load, posture and time and to illuminate any interaction effects of posture load and time. Multi-variate analysis indicated a significant vector for the Wilks' Lambda test for overall effects of load ($p = 0.0144$) and time ($p < 0.0001$) between the three outcome variable of distance of tracking changes, specimen height changes, and average stiffness changes in the presence of the cumulative loading covariate. The multivariate analysis indicate no other significant overall effects with Wilks' Lambda values as follows; posture ($p = 0.6437$), posture*load ($p = 0.0736$), load*time ($p = 0.4197$), posture*time (0.48826), posture*load*time ($p = 0.3049$).

Uni-variate analysis indicated that time was a significant main effect ($p < 0.0001$) and a least significant difference (LSD) post-hoc test indicated that the stiffness due to the partial herniation loading protocol (mean 0.47 SD 0.45) was significantly larger than the stiffness due to the vibration and postural constraint loading protocols (mean 0.10 SD 0.12) as indicated in Figure 44. Posture did not significantly affect average stiffness changes ($p = 0.2417$); full flexion (mean 0.33 SD 0.47) and neutral (mean 0.25 SD 0.28) an indicated by Figure 45. The main effect of load ($p = 0.0710$) was not statistically significant with WBV (mean 0.40 SD 0.53), Shock (mean 0.30 SD 0.36), Static (mean 0.29 SD 0.39), and WBV in combination with Shock (mean 0.18 SD 0.15) have no significant differences from each other.

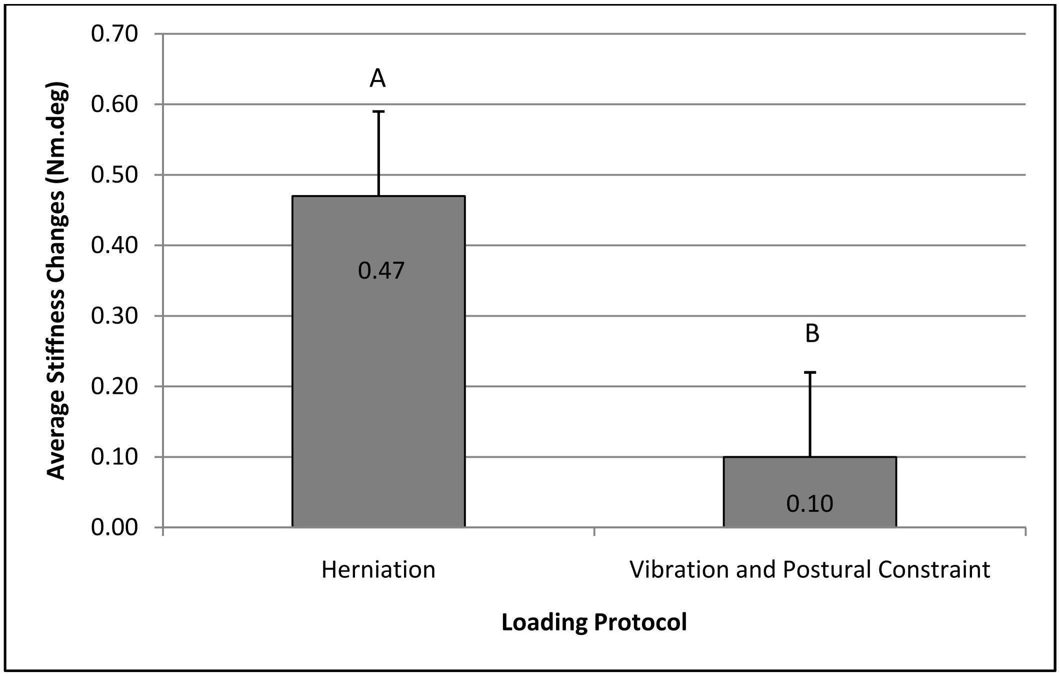

Figure 44: A graph of the average stiffness changes due to the partial herniation loading protocol and the vibration and postural constraint loading protocol. Statistically significant differences were found ($P < 0.0001$) and are indicted by least significant difference (LSD) post hoc-testing illustrated with different letters.

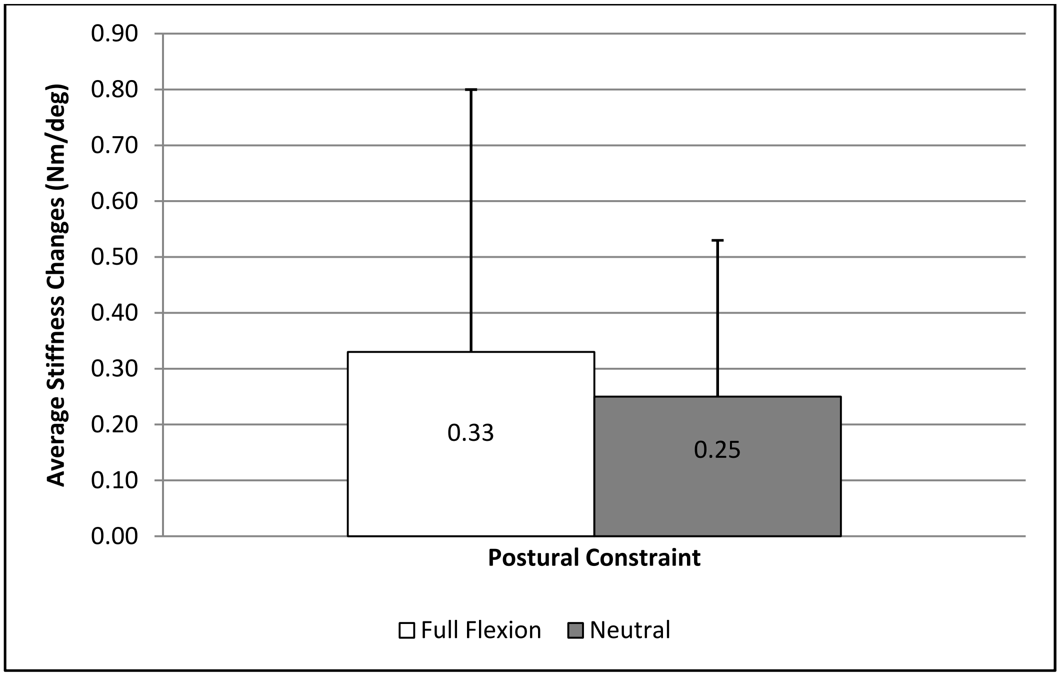

Figure 45: A graph of the average stiffness changes grouped by posture ($p = 0.2417$).There is no significant difference in average stiffness changes between the postures (full flexion and neutral).

There was a significant interaction effects for the average stiffness change variable. The interaction of posture*load was significant ($p = 0.0053$) and a least significant difference (LSD) post-hoc test indicated that full flexion and WBV (mean 0.62 SD 0.74) was significantly different from neutral and WBV (mean 0.24 SD 0.23), full flexion and shock (mean 0.19 SD 0.20) was significantly difference from neutral and shock (mean 0.41 SD 0.44), full flexion and static (mean 0.41 SD 0.53) and significantly difference from neutral and static (mean 0.18 SD 0.16), and the full flexion and WBV + shock (mean 0.16 SD 0.15) was statistically different from neutral and WBV + shock (mean 0.19 SD 0.15) with a P value of $p < 0.001$ for all comparisons stated above. Other interaction effects for the average stiffness changes parameter were not statistically significant; load*time ($p = 0.1840$), posture*time ($p = 0.1253$), and posture*load*time ($p = 0.1649$). The average stiffness changes after the partial herniation loading protocol for each of the 8 vibration and postural constraint loading groups can be considered not statistically significantly different as the posture*load*time interactions (p = 0.1649) was found to be not significant.

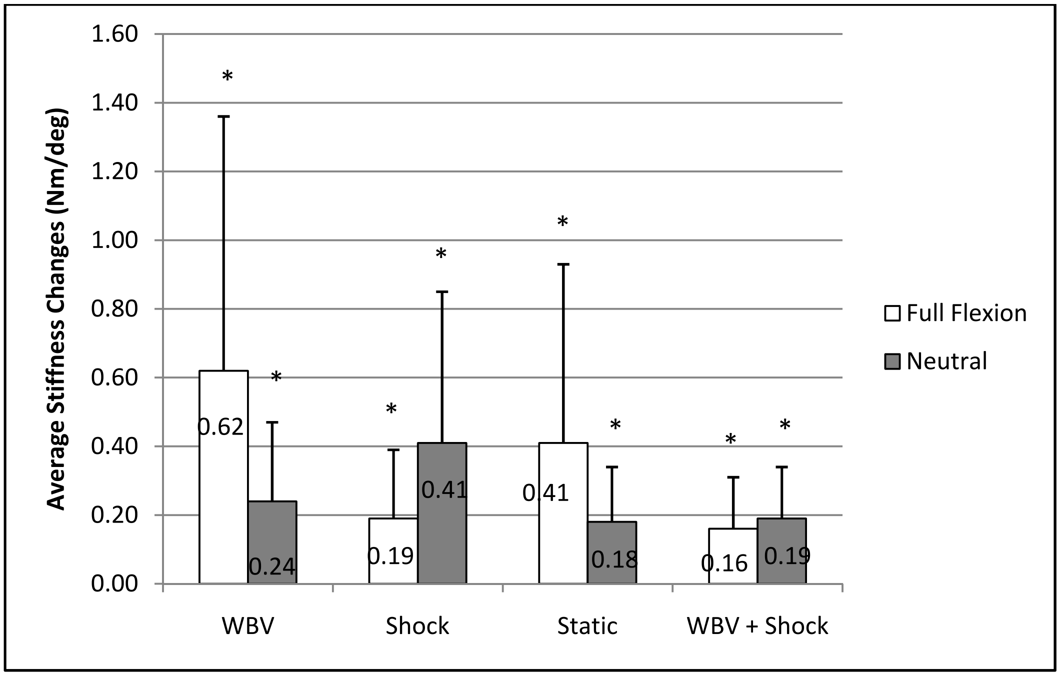

Figure 46: A graph of the interaction of posture by load (p = 0.0053) for average stiffness changes. Least significant difference (LSD) post-hoc testing indicated statistical difference (p < 0.001) between similar load by different postures as illustrated by asterisks on the graph.

4.8. Summary of Significant Findings

1. Specimens were similar between the 8 vibration and postural constraint loading groups based on the six pre-herniation loading parameters; axial creep, max torque, min torque, max angle, min angle, estimated end plate area.

2. After the partial herniation loading protocol the 8 vibration and postural constraint loading groups were not significantly different based on the parameters of specimen height changes or the distance of tracking changes. However, the average stiffness between the neutral and WBV - full flexion and WBV, neutral and shock - full flexion and shock, neutral and static - full flexion and static, and the neutral and WBV + shock - full flexion and WBV + shock groups were significantly different.

3. The partial herniation loading protocol was successful in creating partial IVD herniations in the majority of specimens in the current investigation.

4. The variables of categorical damage progression were successful in detecting large herniation type damage resulting from the partial herniation loading protocol, but were insufficiently sensitive to detect smaller increases in herniation type damage resulting from the vibration and postural constraint loading protocols.

5. Overall, the partial herniation loading protocols lead to increased relative distance of tracking changes, specimen height changes, and average stiffness changes compared to the vibration and postural constraint loading groups.

6. The combination of vibration (load) and posture (postural constraint) loading groups lead to sufficient mechanical insult to the specimens to cause increased distance of tracking changes, specimen height changes, and average stiffness changes.

7. The concordance to the 'gold standard' dissection technique was higher for the contrast enhanced CT images that for the discograms.

8. Vibration loading parameters significantly influenced distance of tracking changes, and specimen height changes, while average stiffness changes illustrated no significant trends within the context of the current investigation.
    a. The distance of tracking changes were largest for the WBV and shock in combination group, followed by the WBV, shock, and static groups respectively. However, only the WBV in combination with shock group collapsed over time and posture was significantly different.
    b. Specimen height changes were largest for the WBV and shock in combination group, but not significantly. Overall there were no significant differences between WBV, shock, static, or WBV + shock loading groups.

9. Posture constraints did not significantly influence the distance of tracking changes, specimen height changes, or average stiffness changes in the vibration and postural constraint loading groups.

Chapter 5: Discussion

5.1. Addressing the Hypothesises

Hypothesis 1

It was hypothesised that vibration exposures would exacerbate IVD damage (as illustrated through distance of tracking (%) changes). As expected a trend was indicated whereby the vibration loading protocol of WBV in addition to shock produced the largest distance of tracking changes (%) in this investigation, followed in order by largest distance of tracking (%) in the WBV alone, and shock alone vibration loading groups. Static loading provided insufficient mechanical insult to the specimens to cause any distance of tracking (%) changes. However, the only significant difference was between the WBV in combination with shock group and the other three loading groups. The results of this investigation support hypothesis 1.

Hypothesis 2

Vibration exposures were hypothesised to influence average stiffness changes, it was thought that average stiffness changes (increases) would rank in the following descending order; WBV with the addition of shock, WBV, shock, static loading. Although Vibration loading exposures increased the average stiffness of the specimens, there were no meaningful significant differences between the 4 vibration loading exposures (WBV with the addition of shock, WBV, shock, static). Hypothesis 2 was not supported by the results of the current investigation.

Hypothesis 3

Vibration exposures were hypothesised to influence specimen height changes. Specimen height lost changes were hypothesised to decrease in the following descending order: WBV with the addition of shock, WBV, shock, static loading. The WBV with addition of shock loading group produced larger height changes (losses) than occurred in any of the other three vibration loading groups (WBV, shock, static) although not statistically significantly. There were no statistical differences in height changes between the WBV, shock, and static vibration loading groups. The results of this investigation partially support hypothesis 3.

Hypothesis 4

Posture was hypothesised to influence the parameters of IVD distance of tracking changes (increase), average stiffness changes (increase), and specimen height changes (increase in specimen height lost) during the vibration and postural constraint loading protocols. It was hypothesised that fully flexed postures would lead to larger changes in these parameters than neutral postures. Posture had no significant effects on distance of tracking changes, average stiffness changes, or specimen height changes during the vibration and postural constraint loading protocol. Hypothesis 4 was not supported by the results of this investigation.

Hypothesis 5

The partial herniation loading protocol was hypothesised to lead to more relative damage to the IVD than the vibration and postural constraint loading. The increased damage was hypothesised to be shown through increased relative distance of tracking changes, larger stiffness changes (increases), and larger specimen height changes (increase in specimen height lost) as a result of the partial herniation loading protocol. The partial herniation loading protocol lead to significantly larger relative distance of tracking changes, significantly larger relative stiffness increases, and significantly larger relative specimen height decreases than the vibration and postural constraint loading protocol. The results of this investigation support hypothesis 5.

Hypothesis 6

The concordance was hypothesised to be higher between Computed Tomography and a ‘gold standard’ dissection technique, than between discograms and the ‘gold standard’ dissection technique. Computed Tomography resulted in more level 2 (full match) concordance criteria than discograms, while discograms resulted in more level 0-1 (no match and partial match) concordance criteria than Computed Tomography when considering both the entire data set (full herniations, partial herniations, and no detectable damage) and only the partial herniaitons. The results of this investigation support hypothesis 6.

Hypothesis 7

IVD damage level classification was hypothesised to increase due to the vibration and postural constraint loading protocols. Although other indicators of damage (distance of tracking changes, average stiffness changes, and specimen height changes) were altered by the vibration and postural constraint loading protocol, insufficient mechanical insult was provided to change the categorical damage classification level. Hypothesis 7 was not supported by this investigation.

5.2. Specimen Similarity

Six pre-herniation protocol parameters [axial creep (mm), max torque (Nm), min torque (Nm), max angle (deg), min angle (deg), estimated endplate area (mm^2)] were used to establish similarity between the 8 vibration and postural constraint loading groups (full flexion and WBV with the addition of shock, full flexion and WBV, full flexion and shock, full flexion and static, neutral and WBV with the addition of shock, neutral and WBV, neutral and shock, neutral and static). There were no statistical differences in any of the 6 pre-herniation protocol parameters between any of the 8 vibration and postural constraint loading groups. Therefore, the random assignment of specimens into each of the 8 vibration and postural constraint loading groups was effective.

The same 6 parameters (pre-herniation protocol) were effectively used by Drake et al. (2005) to illustrate similarity between 2 groups (axial torque and no axial torque) of C3/C4 porcine FSUs in their investigation. They reported axial creeps of -0.96mm (0.29) and -0.71mm (0.29), max torques of 26.8 Nm (4.9) and 26.8 Nm (4.7), min torques of -8.9 Nm (4.0) and -11.6 Nm (4.7), max angles of 20.97 deg (2.26) and 21.59 deg (3.12), min angles of -3.33 deg (1.68) and -3.33 deg (1.68), estimated end plate area of 7.8 mm^2 (0.7) and 7.6 mm^2 (0.9) for FSUs exposed to the axial torque and no axial torque respectively (Drake et al 2005). The estimated endplate area, and axial creep values reported by Drake et al. (2005) compared well with those found in the FSUs used for the current investigation. However, the pre-herniation protocol measures of max/min torque and max/min angle were less in the current investigation than those reported by Drake et al. (2005). A possible explanation for the lower max/min torques and angles in the current investigation would be that the current investigation used both C3-C4 and C5-C6 FSUs, while Drake et al. (2005) used only C3-C4 FSUs. It is conceivable that the C3-C4 FSUs are more mobile (have larger ranges of motion at higher torque values) during the initial passive test than the C5-C6 FSUs. It follows than that the inclusion of C5-C6 FSUs into the groups of this current investigation could have lowered the max/min torques and angles illustrated in pre-herniation protocol measures within the 8 vibration and postural constraint loading groups.

Estimated endplate area, and max/min angles were reported by Parkinson and Callaghan (2009) for 4 groups of C3-C4 and C5-C6 FSUs (grouped by loading magnitude). Estimated endplate areas, max angle in deg (flexion angle), and min angle in deg (extension angle) were reported to range from 653.1mm^2 (39.2) – 692.7mm^2 (35.4), 14.3 deg (3.0) – 16.0 deg (2.1), and 2.9 deg (3.0) – 4.4 deg (2.4) respectively within the 4 loading groups. The max/min angles (termed flexion and extension angles) found in the investigation by Parkinson and Callaghan (2009) were very similar to those reported in the current investigation, however the estimated endplate area was slightly less than the current investigation illustrated.

End plate area measurements alone have been used to establish similarity between groups of porcine FSUs under compressive testing by several investigators (Parkinson et al. 2005; Parkinson and Callaghan 2007b; Drake and Callaghan 2009). Parkinson et al. (2005) reported estimated endplate areas of 718 mm^2 (63) and 724 mm^2 (60) for two groups of FSUs (C3-C4s and C5-C6s respectively) with no statistical differences between the two groups. Similarly, Drake and Callaghan (2009) reported and average estimated endplate area of 7.8 cm^2 (0.4) for a group of 16 C5-C6 FSUs and illustrated no differences between the 8 FSUs in 2 separate loading groups. No differences between loading groups of FSUs based on estimated endplate areas were also found by Parkinson and Callaghan (2007b). Estimated end plate areas in different groups in the above mentioned investigations are very similar to those reported by the current investigation.

Results from the analysis indicated minimal differences between the 8 vibration and postural constraint loading groups after the partial herniation loading protocol. Distance of tracking changes and specimen height changes were not significantly different between the 8 vibration and postural constraint loading groups after the partial herniation loading protocol. However, average stiffness values were different between the 8 vibration and postural constraint loading groups after the herniation protocol. Overall, the 8 vibration and postural constraint loading groups were similar, based on the 6 pre-herniation protocol measures, and the distance of tracking changes and specimen height changes due to the partial herniation loading protocol meaning that the random assignment of specimens to the 8 vibration and postural constraint loading groups was effective overall. However, average stiffness was not similar between the 8 vibration and postural constraint groups after the partial herniation loading protocol meaning the random assignment of specimen to the 8 vibration and postural constraint loading groups was ineffective based on average stiffness.

5.3. Specimen Herniation and Damage Progression

In the current investigation the categorical levels of damage progression (no detectable damage, partial herniation and full herniation) were unable to classify changes in NP posterior migration seen in the distance of tracking changes variable due to the vibration and postural constraint loading protocols. It is likely that the categorical damage level classifications were not sensitive enough to detect the NP posterior migration changes resulting from the vibration and postural constraint loading protocols. To the authors knowledge, this investigation represents the first attempt to use a categorical damage level classification system to attempt to identify NP posterior migration resulting from vibratory loading in postural constraints after herniation initiation via a partial herniation loading protocol. However, the categorical damage classification system was effective at detecting larger changes in NP posterior migration seen in the partial herniation loading protocol.

Several other investigators have used similar categorical damage level classifications to assess NP migration in response to a herniation protocol similar to the one used in the current investigation (Tampier et al. 2007; Scannell and McGill 2009). Using a similar herniation protocol to the current investigation (1.5 KN axial load and 4400 – 14000 flexion/extension cycles) Tampier et al. (2007) were able to classify 8 out of 16 FSUs as illustrating full herniation, 4 out of 16 FSU as partially herniated, and 4 out of 16 FSU as having no detectable damage. Employing 5400 – 10800 cycles of flexion/extension and 1.5 KN of axial load Scannell and McGill (2009) were able to reliably produce partial IVD herniations. Aultman et al. (2005) have indicated that herniations have been detected in a few as 6000 cycles under 1.5 KN of axial compression, while Drake and Callaghan (2009) indicated that specimens had herniated after an average of 5750 (1065) cycles of flexion/extension under 1.5 KN load. Herniation initiation was detected in as few as 3000 cycles of flexion/extension by Drake et al. (2005) again under 1.5 KN of axial compressive load.

Using the identical loading protocol (1.5 KN axial compressive load and 7000 cycles of flexion/extension) in conjunction with the same porcine model and the same categorical damage classification system, a previous investigation created 17 partial herniations out of 22 specimens (77.27%), 1 out of 22 (4.55%) specimens illustrated a full herniation, and 4 out of 22 (18.18 %) specimens illustrated no detectable damage (Yates et al. 2008; 2009). The current investigation was more effective at producing partial IVD herniations with 58 out of 64 (90.63 %) specimen's illustration partial herniation, 4 out of 64 (6.25 %) specimens illustrated full herniation, and no detectable damage found in 2 out of 64 (3.13%) specimens.

5.4. Concordance between Computed Tomography, Sagittal Plane Film Discogram, and a 'Gold Standard' Dissection Technique

The use of x-rays (discograms) alone has been indicated to fail to detect IVD herniations (in 7 out of 14 cadaver motion segments) or indicate damage severity less than that found in a 'gold standard' dissection techniques in 7 out of 14 cadaver motion segments (Gordon et al. 1991). While Tampier et al. (2007) indicated the discograms were not particularly effective in IVD herniation detection with only 4 out of 8 full herniations and 1 out of 4 partial herniations correctly diagnosed when compared to a dissection 'gold standard'. CT has been illustrated to have greater success in identify IVD herniations (Deyo et al. 1990), and has been shown to correctly predict the type of disc damage (Bernard 1990). The current investigation has shown that CT medical imaging techniques produced higher concordance to a 'gold standard' dissection technique than did sagittal plane film discograms both when the entire data set are considered (the inclusion of full herniation and no detectable damage in addition to partial herniation) and when only considering the partial herniations. When the chi-squared run for the entire data set is compared to the chi-squared run only for the partial herniations, minimal differences are found. In both chi-squared analyses the CT medical imaging techniques produced more full matches to a 'gold standard' dissection technique that did the sagittal plane film discogram, while the sagittal plane film discograms produced more no match - partial matches. The CT medical imaging technique and the discogram medical imaging technique had the same approximate concordance for the full data set (including full herniations, partial herniations, and no detectable damage) as found in Table 8 as for the partial herniations alone (Table 9). The CT medical imaging technique had high concordance to the 'gold standard' dissection technique for the full data set, as well as for the partial herniations alone.

A previous investigation that also examined concordance, but between varying numbers of CT slices, sagittal plane film discograms, and a 'gold standard' dissection technique also indicated that CT medical images had greater concordance than did sagittal plane film radiographs to a 'gold standard' dissection (Yates et al. 2009). The previous investigation indicated that overall 45.45 % of the CT medical images were classified as full match concordance criteria, while only 13.64 % of sagittal plane film discograms were full matches. Conversely, 54.55 % of the CT images were classified as no match – partial match, while 86.36 % of the sagittal plane film discograms were classified as no match – partial match. However, it is important to note that concordance results represent overall concordance with collapsed groups of CT slice numbers, ranging from 3 – 8 slices. (Yates et al. 2009). Marshall (2008) used similar concordance classifications and found that CT scans and x-ray images (discograms) were equally good at identifying IVD damage in the form of herniations. However, only one axial slice was taken using the CT medical imaging technique, and a heavy metal barium solution was used to track herniations radiologically. The heavy metal may have lead to increased beam hardening artifacts in the CT images, thus reducing concordance to dissection. The current investigation produced superior concordance to Yates et al. (2009) and Marshall (2008) with 70.31 % of the CT images classified as full match, 35.59% of the sagittal plane film discograms classified as full match, 29.69 % of CT images were classified as no match – partial match, and 64.41 % of the sagittal plane film discograms were classified as no match – partial match.

It appears that increasing the number of axial CT slices increased the concordance between CT medical imaging and the 'gold standard' dissection technique. However CT medical imaging employing axial slices numbering 3 or more will produce superior concordance to a 'gold standard' dissection than will sagittal plane film radiographs. The best concordance illustrated to date occurring between the 8 axial CT slices and a dissection 'gold standard' as indicated by the current investigation. This being said, only 68.18 % of the CT images were a full match to a 'gold standard' dissection technique when considering the full data set (full herniations, partial herniations, and no detectable damage) and only 68.97 % of the CT images were a full match to a 'gold standard' dissection technique when considering only the partial herniations. If the CT medical imaging technique is to become a non-invasive 'gold standard' for in-vitro investigations into the IVD herniation process in the porcine model the concordance for full matches to dissection techniques should be higher than (68.18 - 68.97) %. To increase the number of full matches between CT medical images and dissection we could increase the number of slices obtained of the herniation process, of we could decrease the slice thickness of each CT slice. By increases the number of slices and or decreasing the slice thickness a more accurate picture regarding the herniation process would be obtained.

5.5. Distance of Tracking Changes

The partial herniation loading protocol produced significantly larger relative distance of tracking changes than did the vibration and postural constraint loading protocols, and there was a large variability in the distance of tracking due to the partial herniation loading protocol. To the authors knowledge the current investigation represents the first time that the distance of tracking (position of the NP within the IVD) has been measured using CT medical imaging in an in-vitro investigation implementing a porcine spine model with the intent to create IVD herniations. Several other investigations have tracked the IVD herniation process in a porcine model in response to a herniation loading protocol (axial load with repeated flexion/extension motions). Radiological evidence (sagittal plane film discograms) of the progressive nature of IVD herniation was indicated by Callaghan and McGill (2001), and we know from several other investigations that the herniation protocol will lead to significant posterior and or posterior lateral tracking of the NP through the layers of the AF resulting in IVD herniations under modest loads and repetitive flexion/extension (Callaghan and McGill 2001; Aultman et al. 2005, Tampier et al. 2007; Yates et al. 2008, 2009, Drake et al. 2005; Drake and Callaghan 2009). Scannell and McGill (2009) were able to use plane film discograms to evaluate clinically significant NP movement due to a herniation loading protocol that produced posterior and or posterior-lateral movement of the NP, and indicated that extension motions can reverse NP posterior migration back towards a more neutral location.

Fully flexed postures did not lead to increased distance of tracking changes during the vibration and postural constraint loading protocols when compared to neutral postures. However, many investigations have indicated that non-neutral spinal postures under loading can lead to IVD damage and herniation in-vitro; cyclic loading in flexed postures (Adams and Hutton 1985); cyclic compression in 7 degrees flexion and less than 3 degrees axial rotation (Gordon et al. 1991), and complex non-neutral postures and varied loading (Adams et al. 2000) have all been illustrated to lead to IVD herniation. Repeated motion (flexion/extension) and modest axial compressive loading have also been shown to reliably produce IVD herniations in an in-vitro spine model (Callaghan and McGill 2001). Furthermore, the ultimate compressive strength of porcine FSUs has been illustrated to be reduced by as much as 23-47% when loaded to failure in fully flexed postures versus neutral postures (Gunning et al. 2001). Additionally, there is an epidemiological link between vibration exposures in non-neutral postures and IVD herniations. Sitting postures (with flexion of the lumbar spine) have been indicated to increase the risk of lumbar IVD herniations under WBV (motor vehicle operation) exposures (Kelsey and Hardy 1975). Vibration exposures in a seated posture were also found to be associated with lumbar disc herniations (Bovenzi and Hulshof 1999), while early degeneration of the lumbar spine has been linked to WBV exposures in non-neutral spinal postures (Kittusamy and Buchholz 2004).

It would appear the flexed postures would have exacerbating effects on the distance of tracking changes (leading to larger NP migrations) when compared to neutral postures as indicated by both epidemiological evidence (in-vivo) and in-vitro models. However, in the current investigation posture did not lead to larger distance of tracking changes. Perhaps sufficient mechanical insult was created to the tissue of the IVD in the FSUs during the partial herniation loading protocol that postural factors that theoretically would have mitigated distance of tracking changes were negligible. Another possibility to explain the lack of influence that posture appeared to have on the outcome variables (distance of tracking changes, average stiffness changes, and specimen height changes) in the current investigation could be that perhaps specimens were not placed into a flexed posture for a sufficient length of time for posture to significantly influence the outcome variables.

Another potential explanation for why posture was not found to be an IVD herniation damage exacerbator in the current investigation may come when the mechanical properties of the posterior AF are considered. The posterior fibres of the AF resist tension in the IVD during bending (flexion) style movements. Our full flexion parameter was at the end range of motion of the porcine motion segment within a defined neutral zone. Perhaps at the end of the neutral zone, the fibres in the posterior of the AF have become taught (to resist tension of the spine during bending) and would not allow cleft formation to occur, thus limiting the potential progression of the NP through and between the layers of the AF in the disc herniation process. Perhaps if flexion postures in a range between the neutral zone position and the end of the neutral zone were employed the posterior fibres of the AF would not be as taught, and could allow for cleft formation leading to herniation exacerbation. It appears that vibratory loading alone, without the influence of posture produced sufficient mechanical stress in the IVD of the FSUs to lead to increased distance of tracking changes after partial herniations were initiated.

Vibration loading exposures (WBV with the addition of shock, WBV, shock) lead to sufficient mechanical insult to the IVD of the FSUs to increase the distance of tracking changes after the partial herniation loading protocol. Static loading exposures lead to no changes in the distance of tracking changes after the partial herniation loading protocol. Several investigations have noted that cyclic loading exposures (when combined with postural deviations) can create

IVD damage and Herniation (Adams and Hutton 1985; Gordon et al. 1991; Parkinson and Callaghan 2009). However, to the authors knowledge the current investigation represents the first time that CT medical imaging techniques have been used to measure the distance of tracking (NP migration) in response to vibration and postural constraint loading protocols in an in-vitro porcine spine model.

Although there is limited experimental evidence linking vibration exposures and postural deviations to IVD herniations, a strong epidemiological link exists. Vibration exposures have been indicated to pose a significant risk of injury to the lumbar spine, specifically IVD herniations (ISO 2631-5). Kelsey and Hardy (1975) added evidence to the epidemiological link between vibration exposure and IVD herniation by concluding that person exposed to WBV had an increased relative risk of 2.75 for IVD herniation in the lumbar spine if they spent a substantial portion of their working shift exposed to seated vibration. Additionally, increased cumulative vibration exposures in an occupational setting have been indicated to increase the risk of IVD herniation (Bovenzi et al. 2002). The current investigation adds some basic scientific evidence that vibration exposures can lead to IVD herniations, at least in the porcine model.

5.6. Specimen Height Changes

The partial herniation loading protocol produced significantly larger relative specimen height decreases than the vibration and postural constraint loading protocols. Several other investigations have indicated that porcine FSUs will sustain specimen height losses as a result of a herniation loading protocol (Callaghan and McGill 2001; Drake and Callaghan 2009). Under position control loading Callaghan and McGill (2001) have shown that axial loads of 260 N with 83700 (3818) flexion/extension cycles, axial loads of 867 N with 70550 (29477) flexion/extension cycles, and axial loads of 1472 N with 34974 (9549) flexion/extension cycles produced average specimen height changes of -5.21mm (2.12), -8.88mm (2.48), and -11.18mm (2.17) respectively. Under 1.5 KN axial loads and up to 10000 flexion/extension cycles specimen height losses of 3.50 mm (0.88) were indicated by Drake and Callaghan (2009). Specimen height losses in the current investigation were less than those reported by Callaghan and McGill (2001), probably due to the large differences in cycles of flexion/extension and axial compressive loads. However, the specimen height losses from the current investigations partial herniation loading protocol compare well with the specimen height losses reported by Drake and Callaghan (2009) while employing a similar herniation loading protocol.

Specimen height changes were not significantly affected by posture (full flexion or neutral). However, specimen height changes were affected by vibration loading group (WBV with the addition of shock, WBV, shock, static). The combination of WBV and shock produced more specimen height changes (losses) than the other vibration loading groups, with no pattern of differences found between shock, WBV, or static vibration loading groups. Vibration loading group did not have a significant effect of the specimen height changes variable. Although no investigations were found that directly examined FSU specimen height changes in response to vibration and postural constraint loading, several investigations have employed low rate cyclic compressive loading (which can be equated to low rate vibration loading) and examined specimen height changes (Parkinson and Callaghan 2009, 2007a, 2007b). Using cyclic compressive waveforms at 0.5 Hz with peak forces of varying percentages of maximum predicted loads (10%, 30%, 50%, 70% and 90%) it has been illustrated that specimen height losses during the 10 % maximum predicted strength waveform were 3.3mm (0.4) with an average of 14400 (6858) cycles of loading (Parkinson and Callaghan 2009). Employing a similar waveform to Parkinson and Callaghan (2009) and peak loads of 40%, 50%, 70%, and 90 % maximum predicted strength, porcine FSU were loaded to a maximum of 21600 cycles or until failure. Results indicated that specimens loaded at 40 % maximum predicted strength sustained height losses averaging 6.44 mm (0.09) at failure (Parkinson and Callaghan 2007b). At 50% maximum predicted strength with varying static loading insertions into a 2 second duty cycle and a similar cyclic waveform to Parkinson and Callaghan (2009), average specimen height losses were of a magnitude of approximately 3.00 mm with porcine FSUs loaded until failure or for 12 hours whichever came first (Parkinson and Callaghan 2007a). The vibration loads in the current investigation ranged from 3.85 % - 10.73 % of the predicted maximum compressive strength of the specimens and occurred over a shorter time period than the investigations conducted by Parkinson and Callaghan (2007a, 2007b, 2009). Lower predicted maximum compressive loads and shorter loading times are a probable explanation for the small specimen height decreases seen in the current investigation in response to vibration and postural constraint loading, than those reported by Parkinson and Callaghan (2207a, 2007b, 2009). Disc height lost in-vivo due to vibration exposures over a working shift has been indicated to be highly dependent on the magnitude of vibration exposures, with increasing vibration exposures leading to larger disc height loss (Brinckmann et al. 1998). It is likely that the relationship described by Brinckmann et al. (1998) between increased vibration exposures and increased height lost could explain why the WBV with the addition of shock loading group (larger exposures) illustrated larger height losses than the static, WBV, of shock loading groups.

Sullivan and McGill (1990) vibrated in-vivo participants using a 2 mm/s^2 waveform at 5 Hz in a sitting position. By measuring the entire height of the spine in a sitting posture they indicated that the entire spine lost more height (9.0 mm) over a 30 min vibration exposure than in

30 min of relaxed sitting (1 mm). However several hours after vibration exposure, spine height losses compared to a baseline (after rising from bed) were 3.6 mm compared to spine height loss of 10.6 mm in those participant not exposed to vibration. The authors termed this increased height several hours after vibration exposure the rebound effect of vibration, and hypothesised that an inflammatory response to the mechanical insult provided by the vibration exposure may be the cause of this effect (Sullivan and McGill 1990). A similar increase in height after vibration exposure was indicated by Hirano et al. (1987) several hours after in-vivo rabbits were vibrated via a 2.5 cm stroke with 45 repeats/min for a 30 minute exposure time. The authors measured water content in the IVDs of the rabbits and indicated a decreased water content and height immediately after vibration exposure, and an increased water content and height several hours after the vibration exposure when compared to rabbits that were statically loaded (Hirano et al. 1987). The current investigation did not illustrate a rebound effect of vibration, the WBV or shock vibration inclusive loading group did not have significantly difference specimen height changes than the static vibration loading group. A likely explanation for the lack of a rebound effect of vibration in the current investigation would be that spines were loaded in an in-vitro setting and not in-vivo as in the two investigations that have indicated the rebound effects (Sullivan and McGill 1990; Hirano et al. 1987). Spines loaded in an in-vitro setting will not elicit the inflammatory response (Sullivan and McGill 1990) or water content diffusion mechanisms into the IVD (Hirano et al. 1987) that were hypothesised to be responsible for the rebound effect of vibration.

5.7. Average Stiffness Changes

The partial herniation loading protocol produced significantly larger relative increases in specimen average stiffness than did the vibration and postural constraint loading protocols. Stiffness values have been illustrated to increase in response to a herniation protocol of repeated flexion/extension motions under axial compressive loads (Callaghan and McGill 2001, Drake et al. 2005, Scannell and McGill 2009). Increases in the axial compressive load applied during a herniation protocol, or increases in the number of repetitive flexion/extension cycles have been shown to lead to larger stiffness increases (Callaghan and McGill 2001). Direct comparison of the average stiffness values obtained during the partial herniation loading protocol by the current investigation to the stiffness values from the investigation by Callaghan and McGill (2001) would be difficult. The current investigation employed axial loads of 1.5 KN and a fixed number of flexion/extension cycles (7000), while Callaghan and McGill (2001) employed similar axial compressive load (1.472 KN) but had substantially higher cycles of flexion/extension (ranging from 34974 (9549) to 84220 (4875). Callaghan and McGill (2001) illustrated that stiffness increased (approximately 2 Nm/deg for similar axial loads and control mechanisms to the current investigation), while the current investigation illustrated average stiffness increases of 0.47 (0.45) Nm/deg. The differences in stiffness between the current investigation and the data of Callaghan and McGill (2001) are likely due to the different flexion/extension cycle numbers between the two investigations.

Average stiffness changes in response to a similar herniation protocol as used in the current investigation were reported by several investigators (Scannell and McGill 2009; Drake et al 2005). Porcine FSU average stiffness was illustrated to increase from a baseline value after a preload procedure to 6000 cycles of flexion/extension under 1.472 KN of axial load (Drake et al.

2005). Considering the data of Drake et al. (2005) average stiffness increases of 1.0 Nm/deg were common. Scannell and McGill (2009) illustrated similar average stiffness changes to those found by Drake et al. (2005). Under 1.472 KN of axial compressive load and 5400 – 10800 cycles of flexion/extension average stiffness values increased from baseline values of 1.31 (0.42) Nm/deg to 2.44 (0.63) Nm/deg representing a change in mean stiffness values of 1.13 Nm/deg (Scannell and McGill 2009). Average stiffness values reported in the current investigation were less than those found by Drake et al. (2005) and Scannell and McGill (2009) under a similar herniation protocol. A possible explanation for the different average stiffness values between the current investigation and previous literature may be found if the potting procedures are considered. Previous investigations implemented 18 gauge galvanized steel wire to secure porcine FSUs to the cups, while the current investigation implemented high strength plastic zip ties. Perhaps the zip ties allowed for some movement of the FSUs in the cups during the repeated passive test procedures used to establish stiffness changes, which would have reduced the average stiffness measures. However, no movement between the specimen and cup was qualitatively seen during the current investigation.

No previous studies were found that examined the flexion/extension stiffness of motion segments (cadaver or animal model) in response to vibration loading. However, as noted by Callaghan and McGill (2001) porcine FSU average stiffness will increase with an increase in axial load, and increasing flexion/extension cycles. The average stiffness of FSUs increased as a result of the vibration and postural constraint loading procedures, but this average stiffness increase was relatively small compared to the average stiffness changes due to a herniation loading protocol. Vibration loading applied lower loads for a shorter period of time (example shock loading peak loads of 1189 N for a short period of time at the maximum force of the shock waveform) when compared to herniation loading (approximately 1.5 KN throughout the entire loading time). Therefore, the lower magnitude of loading in the vibration and postural constraint loading protocols may be responsible for the relatively small average stiffness increases illustrated in the current investigation due to these loading exposures.

Posture (full flexion or neutral) and vibration load (WBV with the addition of shock, shock, WBV, static) did not significantly influence average stiffness changes in the 8 vibration and postural constraint loading groups. There were significant posture by load interactions between all vibration loading groups (WBV, shock, static, and WBV in addition to shock) and the two postural constraints (full flexion and neutral). These significant posture by load interactions are likely due to the large variability in the measurement of average stiffness (as the associated outliers present in the data). Justification for the variability of average stiffness measures affecting the posture by load interaction is evident from the fact that there is no pattern of stiffness change within the vibration loading groups between full flexion and neutral posture in Figure 46; differences in the posture by load interaction appear to be randomly dispersed between the 4 possible loading groups (WBV, shock, static, and WBV in combination with shock). Perhaps the small magnitudes of loading present in the combination of vibration and postural constraints loading were responsible for producing insufficient average stiffness changes to lead to more significant differences between the 8 vibration and postural constraint loading groups.

5.8. Cumulative Loading

The relative distance of tracking changes were larger for the partial herniation loading protocol than for the vibration and postural constraint loading protocols. A possible explanation for this finding may be the different cumulative loading exposures between the partial herniation loading protocol (10.71 MNs) and the vibration and postural constraint loading protocol (ranging from 1.05 MNs – 3.41 MNs). It appears that larger cumulative loading exposures lead to larger distance of tracking changes. However the previous statement must be tempered somewhat as the herniation loading implement dynamic flexion/extension motions while the vibration loading implemented static postures. Callaghan (2005) noted that cumulative compression to injury was effected by the magnitude of load applied, while Parkinson and Callaghan (2009) also indicated that load magnitude would affect the number of cycles (cyclic loading) to failure, with increased compressive loads resulting in decreased cycles to failure. It appears from the work of Callaghan (2005) that provided the load magnitude is sufficient (axial compressive load) in a herniation protocol to produce damage, increasing the cumulative load (through more cycles of flexion/extension) would increase the damage severity of an IVD herniation. Therefore, it appears likely that the larger cumulative loading exposures in the partial herniation loading protocol may partially explain the larger distance of tracking changes illustrated when compared to the vibration and postural constraint loading protocols. However, the results from the multi-variate MANCOVA analysis indicated that time (changes from the partial herniation loading protocol to the vibration and postural constraint loading protocol was significant even when the variance from the different cumulative loads used in the current investigation were considered.

In general the same relationship between increased cumulative load and increased distance of tracking changes hold when the vibration and postural constraint loading protocols are considered. Larger cumulative loading exposures lead to larger distance of tracking changes; WBV with the addition of shock resulted in a average of 13.03 % tracking change for full flexion and 6.58 % tracking changes for neutral (cumulative load 3.41 MNs), WBV resulted in an average of 3.53 % tracking changes in full flexion and 5.53 % tracking changes in neutral (cumulative load 2.36 MNs), shock alone resulted in an average of 3.73 % tracking changes in full flexion and 2.28 % tracking changes in neutral (cumulative load 1.05 MNs), and static resulted in no tracking changes (0.00%) in either full flexion or neutral with a cumulative load of 2.55 MNs. The multi-variate analysis in the MANCOVA statistical procedure indicated that in the presence of the different cumulative loading exposure for vibration and postural constraint loading the main effect of load (vibration exposure) was still significant.

The exception to the cumulative load – distance of tracking changes relationship is the static loading exposure group (2.55 MNs) with a cumulative load greater than the WBV (2.36 MNs) or shock (1.05 MNs) loading exposures but no distance of tacking changes, while both WBV and shock loading groups illustrated distance of tacking changes. It appears that the shape of the waveform (simulating WBV, shock, or static load) may affect the distance of tracking changes despite the general cumulative load – distance of tracking changes relationship.

Specimen height changes were also affected by the magnitude of cumulative load exposure. The partial herniation loading protocol (cumulative load of 10.71 MNs) produce significantly more specimen height loss than then vibration and postural constraint loading protocols (Cumulative load ranging from 1.05 MNs – 3.41 MNs). Within the vibration and postural constraint loading groups the WBV with the addition of shock had the largest cumulative load exposure (3.41 MNs) and the largest height loss changes. However, the cumulative load – height loss relationship did not hold for the WBV, shock of static loading groups with no significant height losses between these groups and cumulative loads of 2.36 MNs, 1.05 MNs, and 2.55 MNs respectively. The multi-variate analysis in the MANCOVA statistical procedure indicated that in the presence of the different cumulative loading exposure for vibration and postural constraint loading the main effect of load (vibration exposure) was still significant.

Average stiffness changes also appear to be effected by the cumulative loading exposures. The partial herniation loading protocol (cumulative load 10.71 MNs) resulted in significantly larger average stiffness increases than the vibration and postural constraint loading protocols (cumulative loads ranges from 1.05 MNs – 3.41 MNs). However, there was no relationship in the average stiffness changes due to the vibration and postural constraint loading protocols based on the different cumulative loads caused by those exposures. Perhaps the average stiffness changes due to the vibration and postural constraint loading groups were too small to illustrate a link between average stiffness and cumulative load exposure as illustrated when comparing the partial herniation loading protocol to the overall average of the vibration and postural constraint loading protocols.

5.9. Limitations

There are several limitations that should be reviewed when considering the findings and conclusions of the current investigation. The current investigation employed a porcine model to create IVD herniations. Although porcine cadaver material cannot be directly equated to human tissues, porcine FSUs have been illustrated to be a close approximation of the human lumbar spine in functional, anatomical and geometrical characteristics (Yingling et al. 1999; Oxland et al. 1991). Also the use of a porcine model provided a homogeneous specimen pool that had similar physical activity level, weight, diet, age, and size characteristics, and represented a population of FSUs that were likely to herniate under proper loading conditions. The porcine model used in the current investigation was an in-vitro model. As such, the FSUs did not have the capability to regenerate or repair tissue in the current investigation; however loading times were keep sufficiently short enough that even in-vivo regeneration or tissue repair would have been unlikely.

The reinjection of the radio-opaque contrast solution during the testing procedure of the current investigation may have had several effects on the FSUs that should be noted. The re-injection of just the radio-opaque contrast solution (in the absents of the blue dye mixture) occurred to increase the contrast of the medical imaging techniques employed by this investigation. Subsequent re-injections lead to more artifacts in the medical imaging techniques (especially beam hardening in the CT images) that somewhat decreased resolution and quality of these images. However, the overall concordance was still high for discograms and CT images compared to a ‘gold standard’ dissection technique, with CT images representing the highest concordance in the current investigation. Re-injection of the contrast solution could have altered the hydration level of the IVD, and the specimen height and average stiffness parameters. The second pre-load procedures after the post partial herniation loading protocol medical imaging techniques was designed to minimize the effects on hydration level, specimen height and average stiffness changes due to contrast solution reinjection in the FSUs. In-vivo, the spine can become rehydrated and have increased height after a nights rest. It is not unreasonable to conclude that the current investigations specimens could have represented IVDs that had sustained herniation damage, were marginally rehydrated due to a nights rest (due to the reinjection) and then subjected to vibration exposures. The herniation – rest – vibration scenario is quiet common in the occupational ATV riding population (and likely so in many other occupational settings) who spend substantial portions of their working days doing manual materials handing task, rest for a period of time, and then ride their ATVs (or other equipment) exposing them to vibration and postural constraints.

The vibration exposures in the current investigation did not have equivalent cumulative loading exposures. To a certain extent the outcome variables in the current investigation (particularly the distance of tracking changes) illustrated a general trend whereby higher cumulative loading exposures lead to larger changes. However the cumulative load to larger outcome variable changes relationship did not hold unanimously. The WBV, and shock alone vibration exposures had lower cumulative loads then the static exposures, yet the WBV and shock alone loading lead to larger distance of tracking changes. Perhaps the shape of the waveform influenced the distance of tracking changes in the vibration exposures, and changes were not due solely to cumulative loading exposures.

In an occupational setting, shock loading exposures would be unlikely to occur in a set cycle time as occurred in the current investigation; it is more likely that shock exposures would have occurred sporadically throughout the vibration exposure times. Equipment limitations prevented the current investigation from introducing sporadic shock exposure, and results in blocks of WBV followed by blocks of shock in the WBV in combination with shock loading groups, or simply subsequent shocks alone in the shock loading groups. However cumulative loading exposures were considered in the current investigation, and recent work using a similar porcine model has indicated that insertions of static rest periods into a loading protocol would not reduce the risk of injury (compression induced) to the tissue of the FSUs (Parkinson and Callaghan 2007a).

Another limitation found in the current investigation was the lack of muscular effort consideration in the calculation of the compressive forces due to the vibration exposures.

Although our vibration compressive forces were similar to those reported in the literature, we were arguably on the low end of the scale considering the magnitude of the compressive force applied to our sample of porcine spines. Perhaps including larger compressive forces in the vibration exposures could have lead to larger damage exacerbations in the IVD herniation process. However, we did vibrate the porcine spines at the resonate frequency of human lumbar spine, and given the porcine spines similarity to the human spine, it is likely the vibration of the porcine spines at a resonate frequency resulted in the output force (experience by the spine) exceeding the input force (vibration waveform) as commonly occurs with vibration at the resonate frequency.

5.10. Suggestions for Future Investigations

Future investigations could replicate the waveforms used by the current investigation to deliver vibration loads, but hold the cumulative loading exposures constant by adjusting the vibration loading exposure times for each waveform. Such an investigation could add valuable insight into the hypothesis that waveform shape could influence IVD herniation exacerbation in addition to cumulative loading exposures. Perhaps further investigations could also implement an intermittent shock exposure to assess what affect it would have on IVD herniation exacerbation or they could vibrate spines at higher compressive magnitudes to investigate what effects larger vibration loads would have on IVD herniation exacerbation. Another option for future work could be to investigate more prolonged vibration exposure (perhaps a few days worth of exposure time condensed to a few hours) to determine what effects prolonged vibration and postural constraint exposures would have on the FSUs. Perhaps more prolonged vibration loading in combination with postural constraints may illustrate postural effects that were lacking in the current investigation. A wider range of flexed postures should also be tested in conjunction with vibration exposure to determine if posterior AF fibres that are under less tension (caused by smaller flexed angles) could allow increased cleft formation (while under vibration type loading) and the associated IVD herniation damage progression. The damage detection techniques ('gold standard' dissection technique and the imaging techniques) implemented by the current investigation were of a macroscopic nature. Perhaps exposures to vibration and postural constraint loading produced microscopic damage to the IVD of the specimen that was not detected by the methods employed in the current investigation. Future work could expose FSUs to vibration and postural constraints and investigate whether these exposure variables create sufficient mechanical insult to the IVD to produce microscopic damage.

Investigations regarding increasing the concordance between CT medical imaging techniques and the dissection 'gold standard' should occur to increase the diagnostic effectiveness of the CT medical images in determining herniation style damage in the porcine model. Work has already begun in our laboratory to create a model from the serial axial CT slices obtained from the current investigation with the intent of recreating the herniation process in three-dimensional space within the model. A reconstruction of a herniated IVD can be compared to the same specimen at baseline (without herniation damage) to further assess the extent and shape of the IVD herniation. Future work on the IVD herniation model based on high concordance CT medical images hold the potential to allow for more accurate identification of disc damage and herniation pathway development in the porcine model, and will allow us to better understand the loading parameters responsible for IVD herniation creation, and how these herniations progress.

5.11. Conclusions

The intent of this investigation was to assess if vibration and postural constraint loading would exacerbate IVD damage (illustrated though specimen height changes, average stiffness changes, and distance of tracking changes) after the initiation of a partial IVD herniation. Although the partial herniation loading protocol produced significantly larger relative distance of tracking changes, larger relative height loss changes, and larger relative stiffness increase changes compared to the vibration and postural constraint loading protocols, the vibration loading lead to sufficient mechanical insult to cause further relative distance of tracking changes, height losses, and stiffness increases. The vibration and postural constraint loading protocols were successful in leading to sufficient mechanical insult to increase the damage to the IVD via herniation mechanism.

Within the vibration and postural constraint loading groups posture did not significantly influence distance of tacking changes, specimen height changes, or average stiffness changes. However, the type of vibration exposure (load) was illustrated to significantly influence tracking changes, and influence specimen height changes, but had no significant trends in average stiffness changes. Larger cumulative loads as a result of the vibration waveforms (load) on the FSU lead to larger distance of tracking changes. WBV in combination with shock produced the largest increase in distance of tracking changes, followed by WBV and shock alone respectively. Static loading exposures although representing higher cumulative loads that WBV alone or shock alone did not lead to distance of tracking changes. Specimen height loss was not significantly affected by posture, but was affected by vibration loads. The WBV in addition to shock loading produced the largest specimen height changes, with no statistically differences between shock, WBV, or static. Average stiffness was not significantly affected by posture, nor was a significant trend illustrated based on load (vibration loading). Overall, the WBV in combination with shock vibration loading exposure was most damaging to the FSU, followed by the WBV and shock alone vibration exposures respectively. Static loading did not produce significant increases in the damage to the FSUs.

Specimens were effectively randomly assigned between the 8 vibration and postural constraint loading groups, thus maximizing the potential that changes seen in the FSUs were due solely to the vibration loads and postural constraints. The current investigation was very successful at producing partial IVD herniations. Unfortunately, the categorical variables used in the assessment of damage progressive were not sensitive enough to classify IVD damage progression from the partial herniation loading protocol to the vibration and postural constraint loading protocols. Concordance was greater between CT medical images and a ‘gold standard’ dissection technique than between discograms and a ‘gold standard’ dissection technique, indicating that CT medical imaging provided a more accurate representation of the degree and shape of an IVD herniation then discograms.

Appendix A: Example of VDV Calculations used by the ISO 2631 -1 (1997) Standards

Calculate Vibration Dose Value (VDV)

The frequency weighted VDV was calculated from the X,Y,Z directions using the fourth power of acceleration. Where a is the acceleration, w_i is the vibration direction weighting (w_x = 1.4, w_y = 1.4, w_z = 1.0)

$$VDV_i = \left[w_i \int_0^T a^4(t)dt \right]^{\frac{1}{4}}$$

Total VDV (VDV_t)

The total VDV over the period of collection, represented by the vector sum of the VDV in each direction

$$VDV_t = \left(VDV_x^4 + VDV_y^4 + VDV_z^4 \right)^{\frac{1}{4}}$$

Daily VDV

Once the VDV_t is calculated, it can be extrapolated to the total vibration exposure time. In the example below the vibration exposure was for 20 minutes.

$$VDV = VDV_t \left[\frac{T_{total}}{T_{20}} \right]^{\frac{1}{4}}$$

(Milosavljevic et al. 2008 a)

Appendix B: Example of Calculations used by the ISO 2631 - 5 (2004) Standards

Acceleration Dose (D_k)

The D_k parameter was calculated as the sixth power of the acceleration (units are in m/s^2). Where A_{ik} represents the i^{th} peak in the lumbar spine acceleration response a_{lk} (t) and 'k' corresponds to the X,Y,Z axis.

$$D_k = \left[\sum_i A_{ik}^6 \right]^{1/6}$$

Average Daily Dose (D_{kd})

The (D_{kd}) was calculated to scale the vibration exposure to the average workday (units are still m/s^2). Where t_d represents the duration of daily exposure, and t_m represents the period of time over which D_k was being measured.

$$D_{kd} = D_k \left[\frac{t_d}{t_m} \right]^{1/6}$$

Equivalent Static Compressive Stress (S_{ed})

The (S_{ed}) is calculated in order to begin to assess the health effects of the vibration exposure. S_{ed} is the weighted sum of the X, Y, Z direction daily acceleration dose values (D_{kd}). The ISO 2631-5 (2004) recommends values of $M_x = 0.015$ Mpa / (m/s^2), $M_y = 0.035$ Mpa / (m/s^2), and $M_z = 0.032$ Mpa / (m/s^2). Where k is the X, Y, Z direction.

$$S_{ed} = \left[\sum_{k=x,y,z} \left(m_k D_{kd} \right)^6 \right]^{1/6}$$

Factor R (R)

Factor R is used to assess the adverse health effects related to the exposure to vibration. R takes into account the age of the individual (and decreased strength). Where

N = the number of exposure days / year

i = the year counter

n = the number of years of exposure

c = a constant that represents the static stress due to gravity alone (c = 0.25 Mpa is usually used for the driving posture)

S_{ui} = the ultimate strength of the lumbar spine for a person of age (b + i) taken from the equation $S_{ui} = 6.75 - 0.066\,(b + i)$

b = the age at which vibration exposure began

S_{ed} = the daily equivalent static compression dose calculated by a weighted sum of the 3 orthogonal daily acceleration values.

$$R = \left[\sum_{i=1}^{n} \left(\frac{S_{ed} \cdot N^{1/6}}{S_{ui} - c} \right)^{6} \right]^{1/6}$$

(Milosavljevic et al. 2008 b; ISO 2631 – 5 (2004))

References

Adams, M., Bogduk, N., Burton, K., & Dolan, P. (2002). *The biomechanics of back pain*. China: Churchill Livingstone.

Adams, M. A. (1995). Spine update mechanical testing of the spine; A appraisal of methodology, results, and conclusion. *Spine, 20*(19), 2151 - 2156.

Adams, M. A., & Dolan, P. (1995). Time-dependent changes in the lumbar spine's resistance to bending. *Clinical Biomechanics, 11*(4), 194 - 200.

Adams, M. A., Green, T. P., & Dolan, P. D. (1994). The strength in anterior bending of lumbar intervertebral discs. *Spine, 19*(19), 2197 - 2203.

Adams, M.A., & Hutton, W.C. (1982). Prolapsed intervertebral disc; A hyperflexion injury 1981 Volvo Award in Basic Science. Spine, 7(3), 184 - 191

Adams, M. A., & Hutton, W. C. (1985). Gradual disc prolapse. *Spine, 10*(6), 524 - 531.

Adams, M. A., McNally, D. S., & Dolan, P. (1996). "Stress" distributions inside intervertebral disc. *The Journal of Bone and Joint Surgery, 78*(6), 965 - 972.

Adams, M. A., Freeman, B. J. C., & Morrison, H. P. (2000). Mechanical initiation of intervertebral disc degeneration. *Spine, 25*(13), 1625 - 1636.

Adams, P., & Muir, H. (1976). Qualitative changes with age of proteoglycans of human lumbar discs. *Annals of the Rheumatic Diseases, 35*, 289 - 296.

Aultman, C. D., Scannell, J., & McGill, S. M. (2005). The direction of progressive herniation in porcine spine motion segments is influenced by the orientation of the bending axis. *Clinical Biomechanics (Bristol, Avon), 20*(2), 126-129.

Beer, F. P., Johnston, E. R., & DeWolf, J. T. (2004). *Mechanics of materials* (3rd Edition ed.). Singapore: McGraw Hill.

Bernard, T. R. (1990). Lumbar discography followed by computed tomography; refining the diagnosis of low-back pain. *Spine, 15*(7), 690-707.

Bluthner, R., & Seidel, B. H. (2001). Examination of the myoelectric activity of back muscles during random vibration - methodological approach and first results. *Clinical Biomechanics, 16*(Supplement No. 1), S25 - S30.

Bogduk, N. Twomey T. (1991). *Clinical anatomy of the lumbar spine* (2 nd ed.). Melbourne: Churchill Livingstone.

Bovenzi, M., & Stacchini, I.P. (2002). Low back pain in port machinery operators. *Journal of Sound and Vibration, 253*(1), 3-20.

Bovenzi, M., & Betta, A. (1994). Low-back disorders in agricultural tractor drivers exposed to whole-body vibration and postural stress. *Applied Ergonomics, 25*(4), 231 - 241.

Bovenzi, M., & Hulshof, C. T. J. (1999). An updated review of epidemiologic studies on the relationship between exposure to whole-body vibration and low back pain (1986 - 1997). *Int Arch Occup Environ Health, 72*, 351 - 365.

Brinckmann, P., & Porter, R. W. (1994). A laboratory model of lumbar disc protrusion. *Spine, 19*(2), 228 - 235.

Brinkmann et al. (1998). Quantification of overload injuries. *Clinical Biomechanics, S(2) 36*

Bushberg, J. T., Seibert, J. A., Leidhold, E. M., & Boone, J. M. (2002). *The essential physics of medical imaging*. Philadelphia, PA USA: Lippincott Williams & Wilkins.

Callaghan, J. P. (2005). Cumulative spine loading: From basic science to application. In W. Karwowski, & W. S. Marras (Eds.), *The occupational ergonomics handbook* (). Boca Raton: CRC Press.

Callaghan, J. P., & McGill, S. M. (1995). Frozen storage increases the ultimate compressive load of porcine vertebrae. *Journal of Orthopaedic Research, 13*, 809 - 812.

Callaghan, J. P., & McGill, S. M. (2001). Intervertebral disc herniation: Studies on a porcine model exposed to highly repetitive flexion/extension motion with compressive force. *Clinical Biomechanics, 16*, 28 - 37.

Carragee, E. J., & Kim, D. H. (1997). A prospective analysis of magnetic resonance imaging finding in patients with sciatica and lumbar disc herniation; correlations of outcomes with disc fragments and canal morphology. *Spine, 22*(14), 1650-1660.

Deyo, R. A., Loeser, J. D., & Bigios, S. J. (1990). Herniated lumbar intervertebral disc. *Annals of Internal Medicine, 112*(8), 598 - 603.

Dhillon, N., Bass, E. C., & Lotz, J. C. (2001). Effect of frozen storage on the creep behaviour of human intervertebral discs. *Spine, 26*(8), 883-888.

Drake, J. D. M., Aultman, C. D., McGill, S. M., & Callaghan, J. P. (2005). The influence of static axial torque in combined loading on intervertebral joint failure mechanics using a porcine model. *Clinical Biomechanics, 20*, 1038-1045.

Drake, D. M., & Callaghan, J. P. (2009). Intervertebral neural foramina deformation due to two types of repetitive combined loading. *Clinical Biomechanics, 24*, 1 - 6.

Dupuis, H., Hartung, E., & Haverkamp, M. (1991). Acute effects of transient vertical whole-body vibration. *International Archives of Occupational and Environmental Health, 63*, 261-265.

Dupuis, H., & Zerlett, G. (1987). Whole-body vibration and disorders of the spine. *Int Arch Occup Environ Health, 59*, 323 - 336.

Edwards, W. T., Ordway, N. R., Zheng, Y., McCullen, G., Han, Z., & Yuan, H. A. (2001). Peak stresses observed in the posterior lateral annulus. *Spine, 26*(16), 1753-1759.

Ekstrom, A. S., Kaigle, A., Hult, E., Holm, S., Rostedt, M., & Hansson, T. (1996). Intervertebral disc response to cyclic loading - an animal model. *Proc Instn Mech Engrs, 210*, 249-258.

Etye, D. R., & Muir, H. (1975). The distribution of different molecular species of collagen in fibrous, elastic and hyaline cartilages of the pig. *Biochemical Journal, 151*, 595-602.

Eyre, D. E., & Muir, H. (1976). Types I and II collagens in intervertebral disc; interchanging radial distributions in annulus fibrosus. *Biochemical Journal, 157*, 267 - 270.

Fardon, D. F., & Milette, P. C. (2001). Nomenclature and classification of lumbar disc pathology. *Spine, 26*(5), E93-E113.

Farfan, H. F. (1973). *Mechanical disorders of the low back*. Philadelphia: Lea & Febiger.

Fritz, M. (1998). Three-dimensional biomechanical model for simulating the response of the human body to vibration stress. *Medical & Biological Engineering & Computing, 36*, 686 - 692.

Fritz, M. (2000). Description of the relation between the forces acting in the lumbar spine and whole-body vibrations by means of transfer functions. *Clinical Biomechanics, 15*, 234 - 240.

Galante, J. O. (1967). Tensile properties of the human lumbar annulus fibrosus. *Acta Orthopaedica Scandinavica, Suppliment 100*, 5-91.

Goel, V. K., Monroe, B. T., Gilbertson, L. G., & Brinckmann, P. (1995). Interlaminar shear stresses and laminae separation in a disc: Finite element analysis of the L3-L4 motion segment subjected to axial compressive loads. *Spine, 20*(6), 689 - 698.

Gordon, S. J., Yang K.H., Mayer, P.J. Mace, A.H., Kish, V. L., & Radin, E. L. (1991). Mechanism of disc rupture: A preliminary report. *Spine, 16*(4), 450-456.

Gunning, J. L., Callaghan, J. P., & McGill, S. M. (2001). Spinal posture and prior loading history modulate compressive strength and type of failure in the spine: A biomechanical study using a porcine cervical spine model. *Clinical Biomechanics, 16*, 471 - 480.

Hayes, A. J., Benjamin, M., & Ralphs, J. R. (2001). Extracellular matrix in development of the intervertebral disc. *Matrix Biology, 20*, 107-121.

Hinz, B., Bluethner, R., Memzel, G., & Seidel, H. (1993). Estimation of disc compression during transient whole-body vibration. *Clinical Biomechanics, 9*(4), 263 - 271.

Hirano, N., Tsuji, H., Ohshima, H., Kitano, S., Itoh, T., & Sano, A. (1988). Analysis of rabbit intervertebral disc physiology based on water metabolism II. Changes in normal intervertebral discs under axial vibratory load. *Spine, 13*(11), 1297 - 1302.

International Standards Organization. (2004). *Mechanical vibration and shock - evaluation of human exposure to whole-body vibration - Part5: Method for evaluation of vibration containing multiple shocks* (No. ISO 2631 - 5). Switzerland: International Standard Organization.

Kelsey, J. L., & Hardy, R. J. (1975). Driving of motor vehicles as a risk factor for acute herniated lumbar intervertebral disc. *American Journal of Epidemiology, 102*(1), 63-73.

Kittusamy, N. K., & Buchholz, B. (2004). Whole-body vibration and postural stress among operators of construction equipment: A literature review. *Journal of Safety Research,* (255 - 261)

Kumar, S. (1990). Cumulative load as a risk factor for back pain. Spine, 15, 1311 – 1316.

Li, H., & Wang, Z. (2006). Intervertebral disc biomechanical analysis using the finite element modeling based on medical images. *Computerized Medical Imaging and Graphics: The Official Journal of the Computerized Medical Imaging Society, 30*(6-7), 363-370.

Liu, Y. K., Njus, G., Buckwalter, J. A., & Wakano, K. (1983). Fatigue response of lumbar intervertebral joints under axial cyclic loading. *Spine, 8*, 857 - 865.

Mansfield, N. J. (2005). *Human response to vibration*. United States of America: CRC Press LLC.

Marras, W. S. (2000). Occupational low back disorders causation and control. *Ergonomics, 43*(7), 880 - 902.

Marshall, L. (2008). An investigation of the role of dynamic axial torque on the disc herniation mechanism. Master's Thesis *University of Waterloo.*

Mayton, A. G., Kittusamy, N. K., Ambrose, D. H., Jobes, C. C., & Legault, M. L. (2007). Jarring/jolting exposure and musculoskeletal symptoms among farm equipment operators. *International Journal of Industrial Ergonomics, In Press*

McGill, S. (2007). *Low back disorders: Evidence-based prevention and rehabilitation*. Second Edition. United States of America: Human Kinetics.

McNalley, D. S., & Adams, M. A. (1992). Internal intervertebral disc mechanics as revealed by stress profilometry. *Spine, 17*(1), 65 - 72.

Milosavljevic, S., Carman, A. B., & Rehn, B. (2008a). All-terrain vehicle use in New Zealand agriculture: (part A) exposure to whole body vibration. *Under Review,*

Milosavljevic, S., Bergman, F., & Carman, A.B. Rehn, B. (2008b). All-terrain vehicle use in New Zealand agriculture: (part B) exposure to mechanical shock. *Under Review,*

Milosavljevic, S. (2008). *Personal communication: Details of exposure to vibration*

Moore, K. L., & Dalley, A. F. (1999). *Clinically oriented anatomy* (4th Edition ed.). Canada: Lippincott Williams & Wilkins.

Osti, O. L., Vernon-Roberts, B., & Fraser, R. D. (1990). Annulus tears and intervertebral disc degeneration: An experimental study using an animal model. *Spine, 15*(8), 762-767.

Osti, O. L., Vernon-Roberts, B., Moore, R., & Fraser, R. D. (1992). Annular tears and disc degeneration in the lumbar spine. *The Journal of Bone and Joint Surgery, 74-B*(5), 678-682.

Oxland, T. R., Panjabi, M. M., Southern, E. P., & Duranceau, J. S. (1991). An anatomic basis for spinal instability: A porcine trauma model. *Journal of Orthopaedic Research, 9*(3), 452 - 562.

Panjabi, M. M., Duranceau, J. S., Oxland, T. R., & Bowen, C. E. (1989). Multidirectional instabilities of traumatic cervical spine injuries in a porcine model. *Spine, 14*(10), 1111-1115.

Pankoke, S., Hofmann, J., & Wolfel, H. P. (2001). Determination of vibration-related spinal loads by numerical simulation. *Clinical Biomechanics, 16*(Supplement No. 1), S45 - S56.

Parkinson, R. J., & Callaghan, J. P. (2007) a. Can periods of static loading be used to enhance the resistance of the spine to cumulative compression? *Journal of Biomechanics, 40*, 2944 - 2952.

Parkinson, R. J., & Callaghan, J. P. (2007) b. The role of load magnitude as a modifier of the cumulative load tolerance of porcine cervical spinal units: Progress towards a force weighing approach. *Theoretical Issues in Ergonomics Science, 8*(3), 171 - 184.

Parkinson, R. J., & Callaghan, J. P. (2009). The role of dynamic flexion in spine injury is altered by increasing dynamic load magnitude. *Clinical Biomechanics, 24*, 148 - 154.

Parkinson, R. J., Durkin, J. L., & Callaghan, J. P. (2005). Estimating the compressive strength of the porcine cervical spine. *Spine, 30*(17), E492-E498.

Rostedt, M., Ekstrom, L., Broman, H., & Hansson, T. (1989). Axial stiffness of human lumbar motion segments, force dependence. *Journal of Biomechanics, 31*, 503-509.

Sandover, J. (1983). Dynamic loading as a possible source of low-back disorders. *Spine, 8*(6), 652 - 658.

Sandover, J. (1998). High acceleration events: An introduction and review of expert opinion. *Journal of Sound and Vibration, 4*, 927 - 945.

Sandover, J., & Dupuis, H. (1987). A reanalysis of spinal motion during vibration. *Ergonomics, 30*(6), 975 - 985.

Scannell, J. P. (2007). In vitro and in vivo biomechanical investigation of the clinical practice of disc prolapse prevention and rehabilitation. PHD Thesis, *University of Waterloo.*

Scannell, J. P., & McGill, S. M. (2009). Disc prolapse: Evidence of reversal with repeated extension. *Spine, 34*(4), 344 - 350.

Seidel, H. (1988). Myoelectric reactions to ultra-low frequency and low-frequency whole body vibration. *European Journal of Applied Physiology, 57*, 558 - 562.

Seidel, H., Bluethner, R., & Hinz, B. (1986). Effects of sinusoidal whole-body vibration on the lumbar spine: The stress-strain relationship. *Int Arch Occup Environ Health, 57*, 207-223.

Spengler, D. M., Bigos, S. J., Martin, N. A., Zeh, J., Fisher, L., & Nachemson, A. (1986). Back injuries in industry: A retrospective study. *Spine, 11*(3), 241 - 245.

Stratec Medizintechiniz. (2007). *XCT 2000 manual software version 6.00*. Germany: Stratec Medizintechiniz, GmbH.

Sullivan, S., & McGill, S. M. (1990). Changes in spine length during and after seated whole-body vibration. *Spine, 15*, 1257 - 1260.

Takenaka, Y., Revel, M., Kahan, A., & Amor, B. (1987). Experimental models of disc herniations in rats for study of nucleolytic drugs. *Spine, 12*(6), 556 - 560.

Tampier, C. D. (2006). Progressive disc herniation; an investigation of the mechanism using histochemical and microscopic techniques. *Master's Thesis Dissertation*

Tampier, C. D., Drake, J. D. M., Callaghan, J. P., & McGill, S. M. (2007). Progressive disc herniation: An investigation of the mechanism using radiologic, histochemical, and microscopic dissection techniques on a porcine model. *Spine, 32*(25), 2869 - 2874.

Thompson, R. E., Pearcy, M. J., Downing, K. J. W., Manthey, B.A. Parkinson, I.H., & Fazzalari, N. L. (2000). Disc lesions and the mechanics of the intervertebral joint complex. *Spine, 25*(23), 3026-3035.

Troup, J. D. G. (1978). Driver's back pain and its prevention: A review of the postural, vibratory and muscular factors, together with the problem of transmitted road-shock. *Applied Ergonomics, 9*(4), 207 - 214.

Tsai, K. M., Lin, R. M., & Chang, G. L. (1998). Rate-related fatigue injury of vertebral disc under axial cyclic loading in a porcine body-disc-body unit. *Clinical Biomechanics, 13*(Supplement 1), S32-S39.

Urban, J. P. G., Smith, S., & Fairbanks, J. C. T. (2004). Nutrition of the intervertebral disc. *Spine, 29*, 2700 - 2709.

Verver, M. M., Hoff, J. V., Oomens, C. W. J., Van de Wouw, N., & Wismans, J. S. H. M. (2003). Estimation of spinal loading in vertical vibrations by numerical simulation. *Clinical Biomechanics, 18*, 800 - 811.

Videman, T., Nurminen, M., Troup, J.D.G. (1990). 1990 Volvo award in clinical sciences: Lumbar spinal pathology in cadaveric material in relation to history of back pain, occupation, and physical loading. *Spine, 15*(8), 728-740.

Village, J., Morrison, J. B., & Leong, D. K. N. (1989). Whole-body vibration in underground load-haul-dump vehicles. *Ergonomics, 32*, 1167-1184.

Virtanen, I. M., Kappinen, J., Taimela, S., Ott, J., Barral, Sandra, Kaikkonen, K., Heikkila, O., et al. (2007). Occupational and genetic risk factors associated with intervertebral disc disease. *Spine, 32*(10), 1129-1134.

Waters, T., Rauche, C., Genaidy, A., & Rashed, T. (2007). A new framework for evaluating potential risk of back disorders due to whole body vibration and repeated mechanical shock. *Ergonomics, 50*(3), 379-395.

Webster, B. S., & Snook, S. H. (1994). The cost of 1989 workers' compensation low back pain claims. *Spine, 19*(10), 1111-1116.

Wilkstorm, B. O., Kjellberg, A., & Landstrom, U. (1994). Health effects of long-term occupational exposure to whole-body vibration: A review. *International Journal of Industrial Ergonomics, 14*, 273 - 292.

Yates, J. P., Giangregorio, L., & McGill, S. M. The influence of intervertebral disc shape on the pathway of posterior / posterior lateral partial herniation. *Submitted to Spine November 2008, Under review May 2008.*

Yates, J. P., Giangregorio, L., & McGill, S. M. Disc herniation: Concordance between contrast enhanced computed tomography, plane film discogram and a 'gold standard' dissection technique. *Submitted to Spine May 2009.*

Yingling, V. R., Callaghan, J. P., & McGill, S. M. (1999). The porcine cervical spine as a model of the human lumbar spine: An anatomical, geometric, and functional comparison. *Journal of Spinal Disorders, 12*(5), 415-423.